The influence of hypoxia on RIG-I-mediated melanoma immunotherapy

Dissertation
zur
Erlangung des Doktorgrades (Dr. rer. nat.)
der
Mathematisch-Naturwissenschaftlichen Fakultät
der
Rheinischen Friedrich-Wilhelms-Universität Bonn

vorgelegt von

Christina Engel
aus
Bremen

Bonn 2016

Angefertigt mit der Genehmigung der Mathematisch-Naturwissenschaftlichen Fakultät der Rheinischen Friedrich-Wilhelms-Universität Bonn.

1. Gutachter: Prof. Dr. Gunther Hartmann
2. Gutachter: Prof. Dr. Sven Burgdorf

Tag der Promotion: 30.08.2016

Erscheinungsjahr: 2016

Table of content

1 Summary 1

2 Zusammenfassung 2

3 Introduction 4

3.1 The innate and adaptive immune response 4

3.2 The pattern recognition receptor RIG-I 5

3.3 Immunotherapy of cancer 9

3.4 RIG-I as immunotherapeutic target 13

3.5 Malignant melanoma 14

3.6 Tumor hypoxia and its consequences 15

3.7 Aim of the study 18

4 Material and methods 19

4.1 Material 19

4.1.1 Consumables 19

4.1.2 Equipment 19

4.1.3 Solid chemicals 20

4.1.4 Liquid chemicals 21

4.1.5 Cell culture substances 21

4.1.6 Buffers 22

4.1.7 Recombinant proteins / inhibitors / stimulators 22

4.1.8 Kits 23

4.1.9 Cell lines 23

4.1.10 Fluorescently-labeled antibodies 23

4.1.11 Western blot and immunohistochemistry antibodies 24

4.1.12 Primer sequences 24

4.1.13 Oligonucleotide sequences 25

4.2 Methods 26

4.2.1 Methods for handling cell lines and primary cells 26

4.2.1.1 Cultivation of cell lines 26

4.2.1.2 Seeding of cells and hypoxic incubation 26

4.2.1.3 Stimulation of cells with oligonucleotides or IFNα 27

4.2.1.4 Treatment of cells with different inhibitors or vitamin C 27

4.2.1.5 Isolation of mouse splenocytes and co-culture with melanoma cells 28
4.2.1.6 Detection of hypoxia in cultured cells 28
4.2.1.7 Measurement of reactive oxygen species 29
4.2.1.8 Viability assay and quantification of apoptotic cells 29
4.2.1.9 IFNα/β reporter assay 29
4.2.2 Methods for handling nucleic acids 29
4.2.2.1 In vitro transcription of 3pRNA 29
4.2.2.2 Annealing of siRNAs and 3pGFP2 30
4.2.2.3 RNA extraction from cells using spin columns 30
4.2.2.4 RNA extraction from tumors using trizol reagent 30
4.2.2.5 cDNA synthesis and quantitative PCR 31
4.2.3 Methods for handling proteins 31
4.2.3.1 Protein quantification via Bradford assay 31
4.2.3.2 Western blot analysis 32
4.2.3.3 Flow cytometry 32
4.2.3.4 Enzyme-linked immunosorbent assay (ELISA) 33
4.2.3.5 Multiplex cytokine flow cytometry 33
4.2.4 In vivo methods 33
4.2.4.1 Establishment and treatment of B16 tumors 33
4.2.4.2 Immunohistochemistry 34
4.2.4.3 Ethics statement 34
4.2.5 Statistical analysis 34

5 Results 35

5.1 Hypoxia and EMT in B16F10 melanoma cells 35
5.2 Hypoxia-mediated effects on pattern recognition receptor expression 38
5.3 Hypoxia-mediated effects on RIG-I signaling outcome 41
5.4 Hypoxia-mediated effects on regulatory components of RIG-I signaling 50
5.5 Enhancing RIG-I function under hypoxia and normoxia 53
5.6 EMT and immune activation in vitamin C-supported 3pRNA therapy in vivo 55

6 Discussion 61

6.1 Dissecting IFNα desensitization and differential RIG-I mRNA and protein levels 61
6.2 Differential regulation of RIG-I and MDA5 under hypoxia 64
6.3 Cytokine expression patterns and cellular differentiation 65
6.4 Mechanisms of sustained 3pRNA-dependent immune cell activation 66
6.5 Modulation of regulatory components in hypoxic RIG-I signaling 68

6.6 The two-sided role of ROS 69
6.7 3pRNA-triggered modulation of tumor differentiation, MDSC and NK cells *in vivo* 72
6.8 Evolving combinatorial treatment strategies 74
6.9 Conclusion 76

7 References 78

8 Appendix 89
8.1 Abbreviations 89
8.2 List of figures 92
8.3 List of tables 94

9 Acknowledgments 95

1 Summary

Hypoxia, being the inadequate tissue supply of oxygen, is a characteristic of many solid tumors that has negative implications for the patient's prognosis. Cancer cells adapt to this hostile microenvironment by inducing transcriptomic and translational changes, which ultimately can lead to their epithelial-to-mesenchymal-transition (EMT) and resistance to anti-tumor treatments like radiation-, chemo- and immunotherapy. Thus, it is fundamental to investigate the impact of hypoxia on novel developing therapies, such as the intratumoral activation of the innate pattern recognition receptor retinoic acid-inducible gene I (RIG-I) using 5'-triphosphate RNA (3pRNA) ligands. Stimulation of RIG-I signaling elicits tumor cell death as well as anti-tumoral immunity and has shown promising results in preclinical studies against malignant melanoma. However, the influence of oxygen deprivation on the function of RIG-I has not been investigated. That is why this study aimed at uncovering the effects of hypoxia on the RIG-I signaling pathway and the immunostimulatory potential of 3pRNA in murine melanoma.

As presented here, 3pRNA-induced RIG-I protein upregulation was attenuated upon hypoxic incubation (2% partial oxygen pressure) as compared to normoxia (20% partial oxygen pressure) in different melanoma cell lines, which occurred concomitant to the induction of EMT and downregulation of interferon alpha (IFNα) receptor expression. Interestingly, while IFNα lost its capacity to trigger an immune response under hypoxia, the RIG-I signaling outcome was largely unaffected in B16F10 melanoma cells, as indicated by unaltered induction of IFN-stimulated genes and equal expression of major histocompatibility complex (MHC) class-I and programmed cell death ligand 1 (PDL-1). Besides, cytokine profiles were moderately modulated; exhibiting enhanced 3pRNA-stimulated type-I IFN production. Most importantly, the ability of 3pRNA-treated melanoma cells to activate melanocyte antigen specific CD8+ T-cells and NK cells *in vitro* was not inhibited by oxygen deprivation. Finally, treatment of melanoma cells with vitamin C as ROS scavenger or NFκB inhibitors, to protect cells from EMT, reinstated 3pRNA-induced RIG-I expression in hypoxic cells *in vitro.* Moreover, vitamin C also increased intratumoral proinflammatory cytokine production and anti-tumor efficacy in a subcutaneous melanoma model *in vivo.*

In conclusion, this thesis provides evidence that the immunostimulatory potential of RIG-I activation is preserved under hypoxia and resists attenuation of RIG-I protein upregulation as well as tumor cell IFNα-desensitization. Thus, immunotherapy utilizing 3pRNA proved superior to IFNα by being effective also in hypoxic tumors. Furthermore, adjuvant vitamin C treatment has the potential to aggravate 3pRNA-mediated tumor eradication. These findings essentially contribute to the successful establishment of 3pRNA mono- or combinatorial therapies to the valuable benefit of melanoma patients.

2 Zusammenfassung

Eine unzureichende Versorgung von Zellen mit Sauerstoff (Hypoxie) ist ein häufiges Merkmal solider Tumore und wirkt sich negativ auf die Prognose betroffener Patienten aus. Um sich an die lebensfeindliche Umgebung anzupassen, kommt es bei hypoxischen Krebszellen zu Veränderungen des Transkriptoms und Proteoms, die letztendlich zur epithelialen-zu-mesenchymalen-Transition (EMT) der Zellen, sowie zur Resistenz gegen Bestrahlungs-, Chemo- und Immuntherapie führen können. Daher ist eine Untersuchung der Auswirkungen von Hypoxie auf neue Tumortherapien Voraussetzung für deren erfolgreiche Entwicklung, so auch für die intratumorale Aktivierung des Mustererkennungsrezeptors RIG-I (engl.: *retinoic acid-inducible gene I*) mithilfe seines spezifischen Liganden 5'-triphosphorylierter RNA (3pRNA). Die Stimulierung des RIG-I Signalweges führt zum Tumorzelltod, bei gleichzeitiger Induktion einer anti-tumoralen Immunantwort, und hat vielversprechende Ergebnisse in präklinischen Studien zur Behandlung des malignen Melanoms geliefert. Jedoch wurde der Einfluss von Sauerstoffmangel auf die Funktion von RIG-I bislang nicht untersucht. Daher sollte diese Arbeit die Auswirkungen von Hypoxie auf den RIG-I Signalweg und die immunstimulatorischen Fähigkeiten von 3pRNA in murinen Melanomzellen aufklären.

Die Ergebnisse zeigten eine Verminderung der 3pRNA-induzierten Aufregulation der RIG-I Proteinmenge als Folge der Hypoxie (2% Sauerstoffpartialdruck) im Vergleich zu normoxischen Bedingungen (20% Sauerstoffpartialdruck). Dies ging mit einer EMT und verringerten Expression des Interferon alpha (IFNα) Rezeptors einher. Interessanter Weise blieb die immunaktivierende Fähigkeit von RIG-I hiervon weitgehend unbeeinflusst, was sich durch eine unveränderte Expression IFN-stimulierter Gene, sowie eine gleichbleibende Aufregulation des Haupthistokompatibilitäts-komplexes Klasse-I (engl.: *major histocompatibility complex class-I*, MHC class-I) und des immunregulatorischen Oberflächenmoleküls PDL-1 (engl.: *programmed cell death ligand 1*) auszeichnete. Daneben wurde eine moderate Änderung der 3pRNA-induzierten Zytokin-Produktion beobachtet, die eine Erhöhung der Typ-I IFN Menge beinhaltete. Von besonderer Bedeutung ist die Beobachtung dass 3pRNA-behandelte Melanomzellen auch unter Hypoxie in der Lage waren Antigen-spezfische CD8+ T-Zellen und NK Zellen *in vitro* zu aktivieren – eine Grundvoraussetzung für eine erfolgreiche Immuntherapie. Schließlich konnte durch die Behandlung der Zellen mit dem Antioxidants Vitamin C oder NFκB Inhibitoren zum Schutz vor einer EMT, die 3pRNA-induzierte RIG-I Expression in hypoxischen Zellen wiederhergestellt werden. Darüber hinaus resultierte die zusätzliche Vitamin C Behandlung *in vivo* in einer verstärkten intratumoralen Zytokinproduktion und einer verbesserten anti-tumoralen Wirkung von 3pRNA in einem Model transplantierter, subkutaner Melanome.

Zusammengefasst zeigt diese Arbeit dass die RIG-I-vermittelte Immunaktivierung, entgegen einer verminderten RIG-I Aufregulation und einer Desensibilisierung gegenüber IFNα, auch unter Hypoxie erhalten bleibt. Folglich ist die 3pRNA-basierte Immuntherapie einer Behandlung mit IFNα überlegen, da sie ihre Wirksamkeit in hypoxischen Tumoren behält. Weiterhin kann eine unterstützende Behandlung mit Vitamin C die anti-tumorale Aktivität von 3pRNA verstärken. Diese Erkenntnisse leisten einen unverzichtbaren Beitrag zur erfolgreichen Entwicklung von 3pRNA-Mono- und -Kombinationstherapien und stellen somit einen kostbaren Gewinn für Melanom Patienten dar.

3 Introduction

3.1 The innate and adaptive immune response

To cope with the constant infectious threat of fungi, parasites, bacteria or viruses the human body is equipped with the strong physical barriers of the skin and inner epithelia as well as two finely coordinated cellular defence systems: the innate and adaptive immune responses. Key elements and concepts illustrating the establishment of complex protective immune responses are summarized concisely in the following section.

Upon pathogen invasion through one of the physical barriers, the innate immune system poses the first line of defence. Macrophages and neutrophils provide initial protection by eliminating extracellular pathogens through their active internalisation (phagocytosis). These cells can rapidly detect a wide range of microorganisms with the help of pathogen recognition receptors (PRR) that activate upon detecting evolutionarily conserved microbial structures, so-called pathogen-associated molecular patterns (PAMPs). Consequently, cytokines released from these cells coordinate the function of other immune- and non-immune cells equipped with relevant cytokine receptors. Moreover, secreted chemokines mediate the attraction of additional effector cells from the innate and adaptive immune systems [1]. For example, natural killer (NK) cells disrupt pathogen-infected or tumor cells by releasing the cytotoxic content of their lytic granules following complex signal integration of activating and inhibiting receptors [2]. Other innate immune cells, like dendritic cells (DCs), phagocytose microbial matter at the site of infection and subsequently present their processed foreign peptides in surface-expressed major histocompatibility complexes (MHC). MHC class-II molecules are classically loaded with peptides derived from extracellular pathogens and their expression is largely restricted to immune cells. In contrast, MHC class-I is expressed by all nucleated cells and allows presentation of intracellularly-generated peptides, including those specific for viruses or characteristic for tumor cells (tumor-associated antigens, TAA). Following DC homing to the lymph node, antigen-receptors on $CD4^+$ and $CD8^+$ T-cells recognize antigens bound to MHC class-II and MHC class-I respectively, leading to activation of adaptive immunity. Consequently, $CD8^+$ T-cells (also called cytotoxic T lymphocytes, CTL) disrupt their target cells through the release of cytotoxic molecules similar to NK cells. Whereas $CD4^+$ helper T-cells can either drive the B-cell response, leading to specific antibody production, or assist $CD8^+$ T-cell activation [1,3]. Importantly, in DCs so-called cross-presentation allows loading of peptide antigens derived from extracellular sources also in MHC class-I molecules, enabling cytotoxic $CD8^+$ T-cell activation against extracellular pathogens.

In contrast to innate immune cells, which can be activated by the single event of PRR-binding, adaptive immune cells require a second signal in addition to antigen-recognition. The co-stimulatory molecules (CD80 and CD86) providing this signal for T-cell activation upon their interaction with the DC in the lymph node can be induced by PRR-stimulation within the DC [4,5]. Whereas innate immune cells possess a limited number of germline-encoded PRR, adaptive immune cells utilize a vast variety in their antigen-receptors due to genetic recombination during their development, enabling them to specifically detect virtually any presented peptide.

Importantly, sophisticated mechanisms ensure termination of effector functions to avoid an overshooting immune response and excessive tissue damage. T-cells can express multiple inhibitory receptors, embodying "immune checkpoints" that enable regulation of the extent of their activation. These receptors like programmed cell death protein 1 (PD-1) and cytotoxic T-lymphocyte-associated antigen 4 (CTLA-4) respectively blunt T-cell activity during the effector phase, or outcompete binding of activating receptors during the activation phase in the lymph node. Both pathways result in suppression of T-cell function and induction of immune tolerance [6,7]. Additionally, regulatory T- (Treg) cells can attenuate immune responses by secreting immunomodulatory cytokines. In pathologic situations such as cancer, myeloid-derived suppressor cells (MDSC) can also contribute to immunosuppression and thus prevent efficient clearing of tumor cells [8].

All in all, the concerted actions of the innate and adaptive immune responses, with the indispensable contribution of PRRs to their initial activation, provides the host with rapid and lasting protection against a huge variety of pathogens.

3.2 The pattern recognition receptor RIG-I

The special importance of PRRs was lately underlined by awarding the Nobel Prize in physiology or medicine 2011 to the immunologists Jules A. Hoffmann and Bruce A. Beutler. Hoffmann identified the drosophila Toll-gene as being involved in pathogen sensing and mediating efficient protection from infection, whereupon Beutler discovered a Toll-like receptor (TLR) in mice that is responsible for detection of bacterial lipopolysaccharide (LPS) and consequent activation of innate immunity.

Depending on their localization, three different general classes of PRRs can be distinguished: soluble receptors like mannose-binding lectin as part of the complement system, cytoplasmic receptors and membrane-bound receptors (Figure 1). The latter class includes C-type lectin receptors (CLR), which mainly detect fungal PAMPs and TLRs that recognize a wide variety of PAMPs ranging from lipid-based bacterial cell wall components and microbial proteins, to distinct nucleic acid structures [9]. Until today, respectively 10 and 12 functional TLRs have been identified in humans and mice, which are expressed either at the plasma membrane surface or within the endosomal compartment, thus providing surveillance of bacterial and viral entry routes [10]. In phagocytic cells the

endosomal localization allows instant pathogen detection, as incorporated material is first directed into these intracellular vesicles. Cytosolic PRRs comprise the recently discovered DNA receptor cyclic GMP-AMP synthase (cGAS) as well as the nucleotide-binding domain (NOD)-like receptors (NLR) and retinoic acid-inducible gene I (RIG-I)-like receptors (RLR) [11]. NLRs recognize bacterial peptidoglycan amongst others [12]. Whereas RLRs detect viral nucleic acids in the cytosol, the place of viral replication, thus providing an important contribution to the protection against viral infection [13].

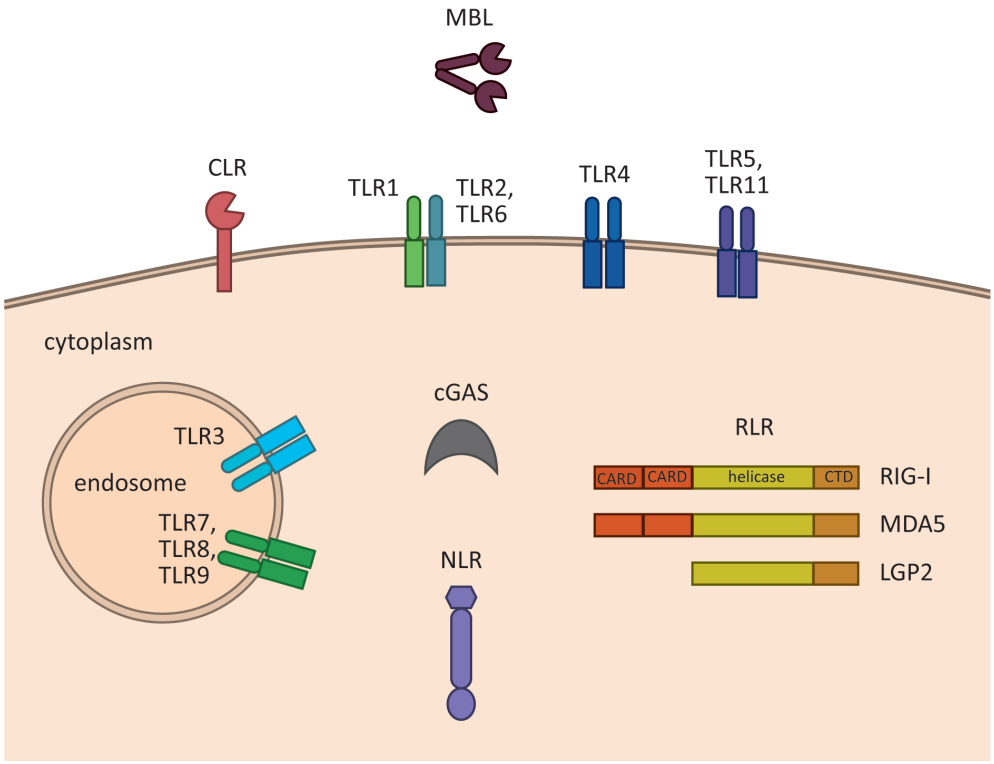

Figure 1: Pattern recognition receptors and their cellular localizations. While mannose-binding lectin (MBL) is a soluble receptor and part of the complement system, the transmembrane C-type lectin receptors (CLR) are situated on the plasma membrane surface. Toll-like receptors (TLR) form homo- or heterodimers at the plasma- or endosomal membranes. Cytosolic receptors comprise cyclic GMP-AMP synthase (cGAS), nucleotide-binding domain (NOD)-like receptors (NLR) and retinoic acid-inducible gene I (RIG-I)-like receptors (RLR). The latter family consists of RIG-I, melanoma differentiation associated factor 5 (MDA5) and laboratory of genetics and physiology 2 (LGP2). The characteristic N-terminal caspase-activation and -recruitment domains (CARD), helicase domains and C-terminal domains (CTD) are shown to indicate structural homologies within the RLR.

The RLR family is composed of the ubiquitously expressed receptors RIG-I, melanoma differentiation associated factor 5 (MDA5) and laboratory of genetics and physiology 2 (LGP2), all of which belong to the family of DExD/H (Asp-Glu-X-Asp/His) box RNA helicases and share a distinct domain structure (Figure 1). Although all RLRs detect virus-derived RNA, RIG-I and MDA5 discriminate their ligands in a length-dependent manner with RIG-I binding short and MDA5 long dsRNA species [14]. Still, both

receptors ultimately activate the same signaling pathway inducing a cellular antiviral state, whereas LGP2 has rather been ascribed a regulatory role that is discussed in detail in section 6.2.

RIG-I, the eponymous receptor of the RLR family, was initially identified in promyelocytic leukemia cells as one of the genes induced by retinoic acid treatment [15]. Yet, its important function in innate immunity remained elusive until 2004 when Yoneyama *et al.* found RIG-I to be involved in the detection of viral nucleic acids [16]. RIG-I has hereafter been identified as the receptor for ssRNA virus genomes like newcastle disease virus, sendai virus, vesicular stomatitis virus, hepatitis C virus and influenza A and B as well as for RNA polymerase III-derived transcripts of DNA viruses [13,17,18]. Much effort has been undertaken to decipher the structural characteristics of the minimal RIG-I ligand and in 2006 two groups independently discovered 5'-triphosphate ends as essential prerequisites for RIG-I-mediated RNA detection [19,20]. Schlee and colleagues further described the minimal RIG-I agonist to be blunt-ended 5'-triphosphate dsRNA of at least 20 base pairs [21]. Yet, it was recently found that 5'-diphosphate ends, as found in reovirus genomes, are also sufficient for RIG-I activation, thus extending the number of RIG-I-detectable viruses [22]. Still, the specificity of RIG-I for di- or triphosphorylated RNA allows the discrimination between self and non-self molecules as eukaryotic 5'-ends of messenger RNA (mRNA) are modified by a cap structure and 2'O-methylation of the terminal nucleotide [23]. Even though the chemical synthesis of RIG-I-activating RNAs is technically possible [24], laboratory research on RIG-I is mostly performed by transfection of *in vitro* transcribed ssRNA containing a 5'-triphosphate moiety (3pRNA) ultimately forming a hairpin structure that also potently activates the receptor.

Binding of the 3pRNA ligand to RIG-I is accomplished by a central, ATPase activity-containing RNA helicase domain and a C-terminal domain (CTD) that are characteristic features of RIG-I, MDA5 and LGP2. Furthermore MDA5 and RIG-I share two N-terminal caspase-activation and -recruitment domains (CARDs), which are liberated upon receptor activation [25]. Since the adaptor protein mitochondrial antiviral signaling protein (MAVS, also known as IPS-1, CARDIF and VISA) contains a CARD as well, homotypic interactions of these domains lead to the formation of large oligomeric complexes of several MAVS and RIG-I molecules [26]. Originally, localization of MAVS at the mitochondrial membrane was thought to be essential for proper RIG-I signalling [27], but according to Dixit *et al*. also peroxisomal MAVS is responsible for the establishment of an early antiviral response [28]. The oligomerization of MAVS provides a scaffold for the recruitment of downstream signaling molecules that ultimately activate members of the inhibitor of nuclear factor-κB (IκB) kinase (IKK) family (Figure 2). Signaling through the canonical IKK complex consisting of IKKα, IKKβ and nuclear factor-κB essential modulator (NEMO) results in the phosphorylation and proteasomal degradation of IκB, thus liberating the transcription factor nuclear factor-κB (NFκB). Additionally, RIG-I activation signals via the non-canonical IKK complex containing IKKε and TANK-binding kinase 1

(TBK1). These protein kinases phosphorylate interferon-regulatory factor 3 (IRF3) and IRF7 that subsequently form homo- or heterodimers. Finally, upon NFκB and IRF3/7 translocation into the nucleus the transcription of type-I interferon (IFN) and inflammatory cytokines is induced, functionally kicking-off the antiviral immune response induced by RLR [16,29]. Moreover, the direct production of antiviral factors via peroxisomal MAVS is mediated by IRF1 [28]. This establishment of an antiviral state is further amplified by a feed-forward loop initiated by autocrine and paracrine IFN signaling. Binding of RIG-I-induced type-I IFN to its cognate receptor activates the janus kinase (Jak) / signal transducer activator of transcription (STAT) pathway, resulting in the expression of hundreds of interferon-stimulated genes (ISG), including RIG-I itself [30].

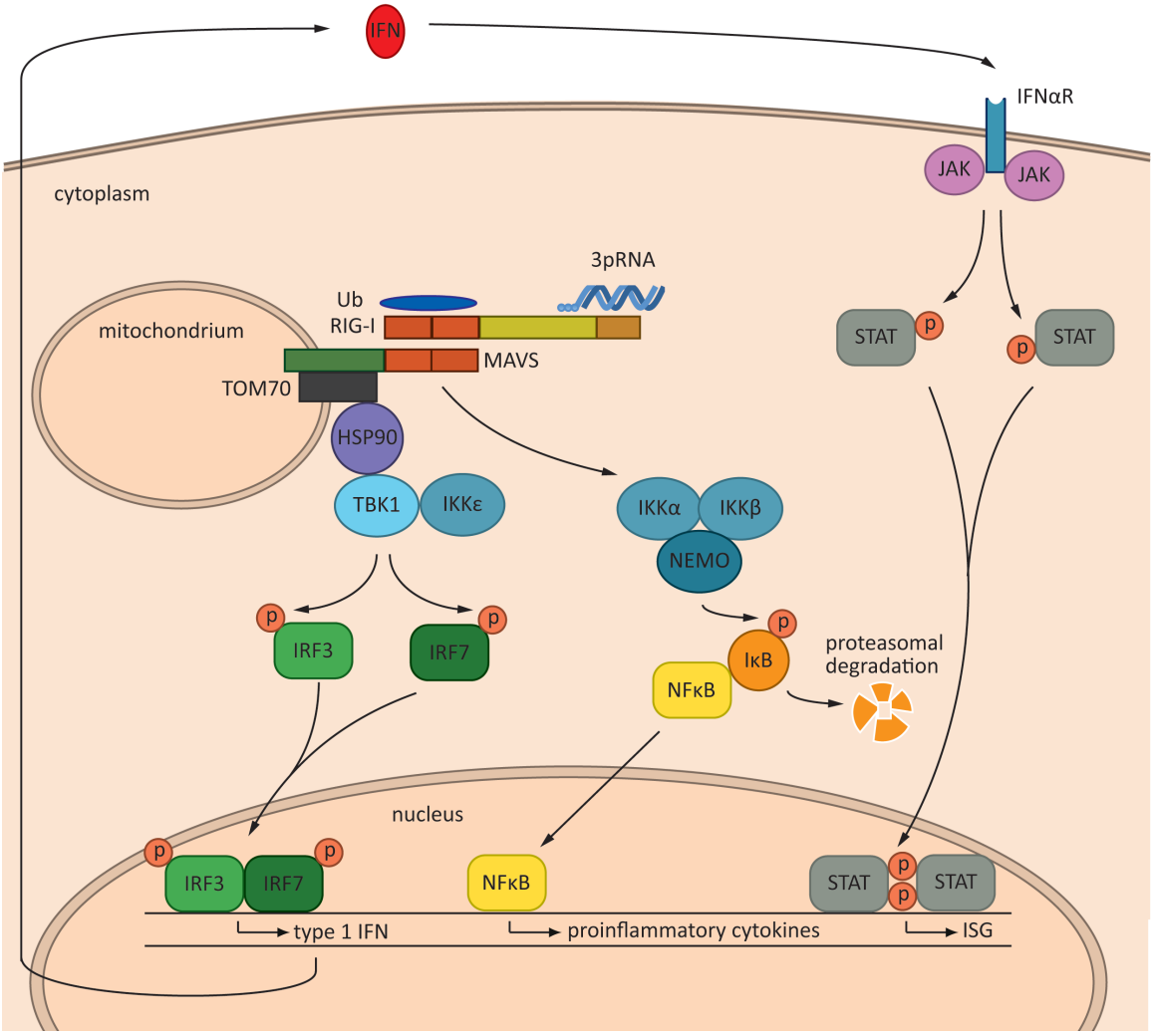

Figure 2: The RIG-I signaling pathway. Upon binding of 5'-triphosphorylated RNA (3pRNA) RIG-I oligomerizes with MAVS and ubiquitin chains (Ub), leading to the activation of IKK complexes. Subsequent phosphorylation events induce nuclear translocation of the transcription factors IRF3/7 and NFκB. Expression of proinflammatory cytokines and type-I interferons (IFN) induces an antiviral state, which is fostered by IFN-induced JAK-STAT forward-signaling and subsequent expression of interferon-stimulated genes (ISG). RIG-I: retinoic acid-inducible gene I; MAVS: mitochondrial antiviral signaling protein; TOM70: translocase of outer membrane 70; HSP90: heat shock protein 90, TBK1: TANK-binding kinase 1; IKK: inhibitor of nuclear factor-κB kinase; IRF: interferon-regulatory factor; NEMO: nuclear factor-κB essential modulator; IκB: inhibitor of nuclear factor-κB; NFκB: nuclear factor-κB; IFNαR: interferon alpha receptor; JAK: janus kinase; STAT: signal transducer activator of transcription.

A functional antiviral immune response not only requires a fast and powerful activation, it also needs an early enough termination to prevent collateral tissue damage and florid autoimmunity. It is hence not surprising that many molecules have been found to be involved in the regulation of the RIG-I signaling pathway. To begin with, post-translational modifications of RIG-I can either enhance its function, like the conjugation of small ubiquitin-like modifier-1 (SUMO), or inhibit the antiviral response such as RIG-I phosphorylation and conjugation of ISG15 [31–34]. Moreover, ubiquitin plays a paramount role in regulation of RIG-I signaling. While lysine 48-linked ubiquitination through the E3 ligase RNF125 (ring-finger protein 125) leads to enhanced proteasomal degradation of RIG-I, the conjugation of lysine 63 (K63)-linked ubiquitin chains to the CARD by TRIM25 (tripartite motif protein 25) is necessary for the interaction of RIG-I with MAVS [35,36]. Additionally, RNF135-mediated K63-linked ubiquitination at the RIG-I C-terminus fosters RIG-I signaling [37]. Finally, unanchored ubiquitin chains activate RIG-I and promote signal transduction by inducing RIG-I oligomerization [38,39].

Besides direct regulatory modifications to the RIG-I protein, functioning of its signaling pathway is influenced by components that facilitate protein-protein interactions, like heat shock protein 90 alpha (HSP90α). This molecular chaperone directly binds RIG-I, thereby protecting the receptor from proteasomal degradation [40]. HSP90 is furthermore involved in the recruitment of TBK1 and IRF3 to mitochondria in collaboration with the mitochondrial import receptor translocase of outer membrane 70 (TOM70). By binding HSP90 as well as MAVS, TOM70 assembles the different signaling proteins (RIG-I, MAVS, TBK1, IRF3), thereby crucially facilitating signal transduction and transcription factor activation [41]. Lastly, Tal and colleagues found RLR signaling to be influenced by reactive oxygen species (ROS) as they observed amplified IFN secretion upon the accumulation of ROS in the absence of autophagy. Moreover, RLR signaling could be enhanced by the generation of mitochondrial ROS independently of autophagy by inhibiting electron transfer within the mitochondrial respiratory chain [42].

In summary, a whole armada of factors is involved in fine-tuning the RIG-I pathway to ensure effective antiviral defence without the devastating effects of an overshooting immune response. Furthermore, such detailed knowledge about RLR signaling and its function in innate immunity sets the stage for utilizing these receptors in cancer immunotherapy as activators of a cancer cell-directed immune response.

3.3 Immunotherapy of cancer

In 2013 cancer immunotherapy was proclaimed breakthrough of the year by one of the most high-ranking scientific journals, *Science*, in recognition of the considerable improvement novel immunotherapies have achieved in the overall survival of end-stage cancer patients, in particular advanced melanoma. The concept of cancer immunotherapy is based on the specific activation of the

innate- or adaptive immune system against tumors or the blockade of immune-inhibiting mechanisms, in order to achieve eradication of the malignant cells and establish the formation of long-lasting immune memory cells. This section provides an overview of already approved immunotherapies and the most promising experimental strategies, as summarized in Figure 3.

One of the most direct ways to boost the immune system, yet in a non-specific manner, is the systemic application of cytokines. Recombinant IFNα and interleukin 2 (IL-2) are approved compounds for cancer therapy and are respectively used for treatment of melanoma, kaposi sarcoma, several haematological cancers, metastatic kidney cancer and metastatic melanoma. The functions of IFNα include maturation and activation of DCs, enhancement of MHC expression as well as the generation of CTL, whereas IL-2 activates NK cells and stimulates growth and differentiation of $CD8^+$ T-cells. The latter was however also found to expand Treg cells [43–45].

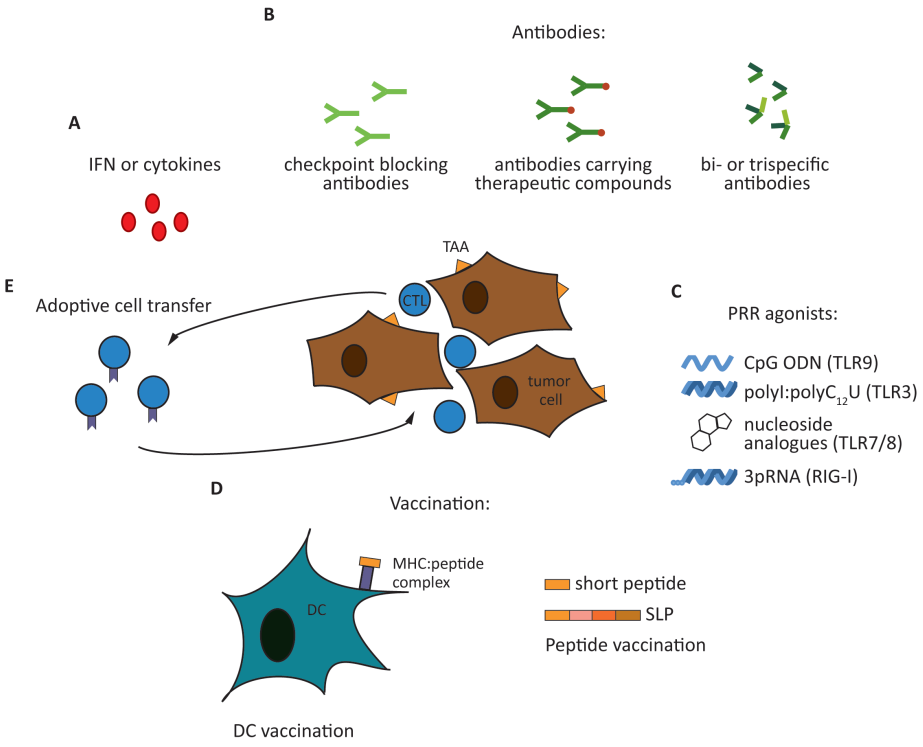

Figure 3: Different cancer immunotherapy approaches. (A) Pre-existing immune responses can be boosted by systemic application of interferons (IFN) or cytokines. (B) Antibody-dependent strategies involve the blockade of immune checkpoints to prevent T-cell exhaustion, antibodies that target tumor-associated antigens (TAA) and carry cytostatic, cytotoxic or radioactive compounds as well as bi- or trispecific antibodies that bridge tumor and immune cells. (C) Currently investigated agonists of pattern recognition receptors (PRR) include 5'-triphosphorylated RNA (3pRNA) activating retinoic-acid inducible gene I (RIG-I), as well as Toll-like receptor (TLR) agonists like CpG-oligodeoxynucleotides (ODN), dsRNA (polyI:polyC$_{12}$U) or nucleoside analogues. (D) Vaccination approaches aim at activating antigen-specific immune effector cells either by administration of short peptides and synthetic long peptides (SLP) consisting of several antigens or by reinfusion of *ex vivo* manipulated dendritic cells (DC) that present TAA-epitopes on major histocompatibility complexes (MHC). (E) Adoptive cell transfer comprises the isolation of immune cells like cytotoxic T-lymphocytes (CTL), their *ex vivo* expansion and genetic manipulation to express tumor-specific receptors and their reinfusion into the patient.

Holding eight U.S. Food and Drug Administration (FDA)-approved compounds the most prosperous group of immunotherapeutics are the therapeutic antibodies. This class comprises antibodies that target tumor-associated antigens and may carry a cytostatic, cytotoxic or radioactive compound, as well as bi- or trispecific antibodies and checkpoint-inhibitors. By combining antigen-binding domains with tumor cell- and effector cell specificity in one molecule, lacking the Fc domain of classical antibodies, bi- and trispecific antibodies enhance the interaction of effector and target cells. This ultimately results in effector cell activation and target cell killing. This technique for example enables targeted NK cell activation by utilizing a CD16 specific domain (bi- or trispecific killer cell engager, BiKE or TriKE) or T-cell activation through incorporation of a CD3 specific domain (bispecific T-cell engager antibody, BiTE) [46,47]. The first licensed BiTE antibody, blinatumomab, is directed against CD19-expressing acute lymphoblastic leukemia cells and was launched in 2014. In contrast to these directly activating therapeutic antibodies, checkpoint-inhibitors enhance T-cell-mediated tumor cell eradication by blocking inhibiting receptor interaction during their priming or effector phase. For the first time overall survival of advanced melanoma patients could be increased from 6.4 months to 10.1 months and 16.8 months, using anti-CTLA-4- and anti-PD-1 antibodies respectively [48,49]. The latter additionally showed promising anti-tumor activity against non-small cell lung cancer and renal cell cancer [50,51]. Until today three checkpoint-inhibiting antibodies, ipilimumab (anti-CTLA-4), nivolumab and pembrolizumab (both anti-PD-1) have been approved and are continuously studied in mono- and combinatorial therapies. For example, nivolumab plus ipilimumab achieved objective responses in 53% of advanced melanoma patients, all with tumor reduction of 80% or more [52]. Unfortunately, the downside of releasing the brakes on the immune system is the risk of immune-related adverse events, such as diarrhea, colitis and rashes, that might have severe impact on the patient's health and quality of life, which should not be neglected.

Active induction of an antigen-specific immune response is the goal of different vaccination strategies, including peptide and DC vaccines. The former technique relies on direct administration of TAA-epitopes that either bind directly to external MHC molecules (short peptides) or are taken up and processed by DCs beforehand (long peptides). As example, synthetic long peptides, possibly containing several antigens, have shown successful induction of T-cell-mediated immunity and anti-cancer efficacy in patients with human papilloma virus positive cervical cancer [53,54]. Alternatively, DC-based vaccination makes use of autologous DCs that are loaded *ex vivo* with TAA and reinfused into the patient together with immunostimulatory intervention. In 2010 the first therapeutic autologous vaccine, sipuleucel-T, was approved for treatment of asymptomatic or minimally symptomatic castration-resistant metastatic prostate cancer. In the corresponding study, treatment with autologous DCs that had been exposed to a chimeric protein of human growth factor GM-CSF (granulocyte macrophage colony-stimulating factor) and prostatic acid phosphatase led to a 4.1

months increase in median survival and a 22.5% reduction of risk of death. In this setting GM-CSF induces the maturation and expansion of DCs, while their presentation of prostatic acid phosphatase-derived peptides activates T-cells exclusively against prostate cancer cells [55].

Although the above-mentioned compounds are the only approved immunotherapies so far, other strategies, like adoptive cell transfer (ACT), have shown encouraging results in clinical trials. This technique implies the isolation of autologous or allogenic immune effector cells that are expanded, activated and possibly genetically manipulated *ex vivo* to increase their number and tumor specificity, to be subsequently re-infused into the patient. Suitable cell types for ACT are cytotoxic lymphocytes like NK cells and CTL. To enhance anti-tumor effector functions isolated cells can be equipped with TAA-specific T-cell receptors or chimeric antigen receptors (CAR). The latter have been initially developed by Steve A. Rosenberg and Zelig Eshhar and consist of an antigen-binding domain of a TAA-specific antibody fused to intracellular signaling domains that render T-cell activation independent of MHC molecules [56]. CAR T-cells have shown to be safe and induce considerable rates of objective, long-lasting clinical responses in trials using CD19-directed CARs against different types of B-cell malignancies characterized by their surface CD19 expression [57,58]. Likewise, CAR T-cells have demonstrated promising safety and efficacy profiles against solid tumors, for example by targeting the diasialoganglioside GD2 on neuroblastoma cells or human epidermal growth factor receptor 2 (HER2) on sarcoma [59,60].

Finally, therapeutic immune activation can be achieved by employing PRRs in different stimulatory settings. Although PRR agonists have demonstrated anti-tumor effects in monotherapy, they are currently predominantly studied as adjuvant molecules [61]. For example TLR3 activation by polyI:polyC$_{12}$U (polyI:polyC dsRNA with a U mismatch every 12th base of the C strand) is tested in breast cancer patients as adjuvant therapy in combination with HER2 vaccination (NCT01355393). Furthermore, imiquimod, a small molecule nucleoside analogue that functions as TLR7/8 agonist, induced rejection of skin metastases in breast cancer patients upon topical administration and is now tested in combination with cyclophosphamide and radiotherapy (NCT01421017) [62]. Lastly, TLR9 can be activated by synthetic oligonucleotides that mimic bacterial unmethylated CpG DNA sequences, like CpG-7909. Yet, this compound has demonstrated varying effects in clinical trials. While inclusion of CpG as adjuvant in a peptide vaccination strategy in metastatic melanoma patients elevated antigen-specific T-cells by 10-fold and enhanced cytokine production upon *in vitro* re-stimulation, another study in melanoma patients exhibited no superior clinical outcome to standard therapies [63,64]. Importantly, these diverse TLR ligands all share the disadvantage that they usually only act on immune cells without having any direct effects on tumor cells.

3.4 RIG-I as immunotherapeutic target

The suitability of RIG-I as immunotherapeutic target is based on its ubiquitous expression, including tumor cells, as well as a number of signaling effects that collectively result in stimulation of anti-tumor immunity and induction of tumor cell death. These qualities have also been studied *in vivo* by intratumoral injection of RIG-I ligands complexed with a polymer-based transfection reagent (in vivo-jetPEI®). Since this compound is not yet approved for human application, efficient delivery poses the current limitations to RIG-I-targeted immunotherapy. Thus, efforts are ongoing to find the optimal delivery tool that protects the ligand from degradation, is non-toxic and allows specific tumor targeting to reach the primary tumor and metastases upon intravenous application.

Besch and colleagues first described that activation of RIG-I triggers mitochondrial apoptosis in melanoma cells. Importantly, this apoptotic effect is restricted to malignant cells, as non-malignant cells are largely protected by their endogenous expression of Bcl-xL [65]. The induction of tumor cell death, which can provide the immune system with an important source of tumor antigens, was furthermore described in human ovarian cancer and pancreatic cancer cells [5,66]. In addition, RIG-I-mediated cell death is considered to be immunogenic. This refers to the release of danger signals like HMGB1 (high mobility group protein B1) or the translocation of calreticulin to the outer cell membrane that may facilitate antigen uptake by DCs [5]. Duewell *et al.* demonstrated that IFN produced by 3pRNA-treated tumor cells activates DCs, which then effectively cross-present TAA to naive $CD8^+$ T-cells. Moreover, RIG-I activation sensitizes tumor cells for CTL-mediated killing by enhancing surface expression of MHC class-I and Fas [5].

While RIG-I ligands were shown to induce systemic activation of B-cells, $CD4^+$ and $CD8^+$ T-cells as well as NK and NKT cells *in vivo*, anti-tumoral effects seem to be mediated by different immune cell types depending on the tumor model. This likely results from tumor type-specific variations in the expression of MHC class-I and activating NK cell ligands as well as the availability of TAA. Utilizing a B16 melanoma lung metastasis model Poeck *et al.* demonstrated that anti-tumor activity relies on NK but not $CD8^+$ T-cells [67]. In contrast, in a pancreatic cancer model the therapeutic efficacy of RIG-I ligands was solely dependent on $CD8^+$ T-cells, whereas NK cells were dispensable [68]. Moreover, RIG-I therapy might benefit from an IFNα-dependent reduction of MDSC frequency and their suppressive function as shown for TLR9 activation, as well as from reduced attraction of Treg cells owing to an IFN-dependent blockade of intratumoral CCL22 (C-C motif chemokine 22) expression [69,70].

Besides these intrinsic anti-cancer properties, RIG-I ligands carry the inherent possibility to be equipped with a RNA-interference (RNAi) functionality, thus enabling simultaneous knockdown of oncogenes or anti-apoptotic proteins for example. The effective induction of anti-tumor immunity by such dual-functional 3p-siRNAs was shown by Poeck and colleagues in a B16 melanoma lung

metastasis model and meanwhile this concept has been adapted for TGFβ (transforming growth factor β) silencing in pancreatic cancer [67,68].

In summary, the ubiquitous expression of RIG-I together with the tumoricidal and immunostimulatory properties of RIG-I agonists renders 3pRNA a promising candidate for future tumor immunotherapy, for example of malignant melanoma.

3.5 Malignant melanoma

Malignant melanoma, a malignancy of pigmented cells, metastasizes quickly and overall patient survival rates are very low. Still, this tumor has a high intrinsic immunogenicity, mediated by a strongly expressed unique set of differentiation antigens. Although melanoma makes up only 2% of all skin cancers, the incidence rates rapidly increased over the past 30 years (from 11.2 new cases per 100,000 in 1982 to 22.9 per 100,000 in 2012 [71]) and it accounts for the vast majority of skin cancer deaths. Treatment options and survival chances are closely related to the metastatic potential of melanoma, which is demonstrated by a 5-year relative survival rate of 98% for local disease that declines to 63% for regional and 16% for distant stage disease [72]. Thus, an early detection and surgical resection of this malignancy is still most beneficial for prognosis.

In 40-60% of advanced melanoma activating mutations in the BRAF kinase (serine/threonine-protein kinase B-raf) can be found, that constantly drive the successive oncogenic MAPK (mitogen-activated protein kinase) pathway [73]. Hence, targeted therapy utilizing V600E-mutated BRAF- or MEK (MAPK kinase) inhibitors, such as vemurafenib, dabrafenib and trametinib, can potently improve overall- and progression-free survival of mutation-positive melanoma patients [74–76]. Still, tumor cells frequently develop resistance and the group of therapy responders is limited.

The recent development of immune checkpoint-inhibitors has further significantly extended the overall survival of advanced melanoma patients. In accumulated data of multiple ipilimumab-trials, three-year survival rates of advanced melanoma patients were 22% and median overall survival added up to 11.4 months [77]. Of note, immune checkpoint-inhibition might come along with severe adverse effects. Yet, these have been shown to be generally manageable with temporary immunosuppression. Moreover, PD-1-directed antibodies appeared to have improved toxicity profiles as compared to CTLA-4 blockade [78].

Since a large proportion of melanoma patients still does not benefit long-term from these new checkpoint-inhibiting and targeted therapies, combinatorial approaches need to be further developed to maximize benefit. This will most likely involve the combined use of immunotherapies from different classes, or a combination of classic interventions with immunotherapies [79]. In general, targeted RIG-I activation by 3pRNA in the tumor microenvironment can focus the attention of the

immune system to the tumor site, possibly maximizing local efficacy and reducing systemic side effects.

3.6 Tumor hypoxia and its consequences

During the development of a therapy that functions directly on tumor cells, like RIG-I-mediated immunotherapy, different stress factors found within the tumor microenvironment have to be considered as they may alter drug function or -efficacy. These include nutrient deprivation, pH variations, necrotic neighboring cells or tumor hypoxia. The latter is the inadequate tissue supply with oxygen that compromises biologic functions [80]. Throughout the body the partial oxygen pressure (pO_2) differs substantially from the 21% of the inspired air and varies greatly between tissues reaching 13% in arterial blood, 10% in kidney and 4% in muscle for example [81]. Yet, normal tissues are well adapted to the local oxygen conditions they reside in. In inflamed tissue oxygen availability is often further reduced due to increased oxygen consumption by infiltrating immune cells and blood vessels that are clogged with phagocytes. This can induce suppression of immune functions and hypoxia might thus serve as a physiologic brake, limiting cytotoxic action of immune effector cells and protecting healthy tissue against excessive damage and autoimmunity. Importantly, pO_2-values found in tumors are often even lower than in the healthy tissue they are derived from resulting in tumor hypoxia (Figure 4). As demonstrated by a study of Lartigau and colleagues hypoxia is also commonly found in malignant melanoma. Utilizing a needle probe technique they detected a median pO_2 of 1.6% in tumors and 0.9% in skin metastases as compared to 5% in surrounding “normal” tissue [82]. This can be caused by rapid tumor cell proliferation exceeding vascular growth, leading to increased diffusion distances, structural and functional abnormality of vessels and disturbed microcirculation [83].

As a reaction to oxygen deprivation cells can activate the transcription factors NFκB and hypoxia-inducible factor (HIF), which can induce the expression of hundreds of genes, including glycolytic enzymes, glucose transporters, angiogenic molecules, survival and growth factors as well as heat shock proteins [80,84,85]. Thereby the cellular metabolism is shifted towards anaerobic glycolysis and neovascularization is induced, the latter being largely dependent on vascular endothelial growth factor (VEGF)-mediated proliferation and migration of endothelial cells [86]. Beyond that, hypoxia is associated with resistance to radiation and chemotherapy, epithelial-to-mesenchymal transition (EMT) and escape of immune surveillance, all of which will be elucidated below. Together, these modulations allow cells to adapt to the hostile environment or to facilitate their escape by enhancing tumor cell spread and tumor tissue-invasion.

Indeed, the phenomenon of tumor hypoxia was originally discovered as a factor mediating resistance to radiation therapy. As early as in the 1950s Gray *et al.* observed that the concentration

of oxygen dissolved in tissues at the time of irradiation influences treatment outcome [87]. That is because ionizing radiation causes the formation of radicals in the DNA either by direct ionization or by reaction with hydroxyl radicals and other ROS produced from radiolysis of water [88].

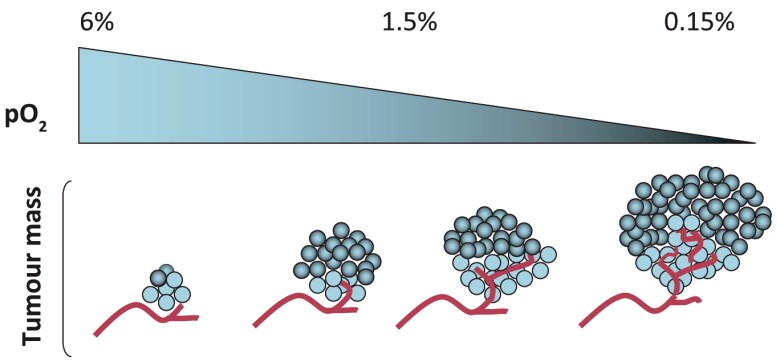

Figure 4: Correlation of tumor growth and hypoxia. With increasing tumor size, vascularization becomes more and more insufficient resulting in a decrease of the partial oxygen pressure (pO_2). When pO_2-values fall below those of the surrounding healthy tissue and biologic functions of cells are compromised, the tumor is considered hypoxic. Adapted from Brahimi-Horn and Pouyssegur [89].

Importantly, hypoxia also plays a role in resistance to chemotherapy. While the abnormal structure and function of blood vessels can prevent efficient drug delivery into the tumor, hypoxia-mediated slowing of proliferation limits the effectiveness of drugs that target highly proliferative cells [81]. Moreover, oxygen deprivation enhances genetic instability, for example through the enrichment of DNA mismatch repair deficient cells, that might affect genes involved in drug uptake, -metabolism and -export, thus accelerating the development of therapy resistant clones [81,90].

Besides its impediment of classical therapies, hypoxia is known to induce EMT in tumor cells including murine melanoma cells [91]. This reversible dedifferentiation of resident epithelial-like cells into motile mesenchymal-like cells plays an important physiological role in embryo formation, organ development, wound healing and tissue regeneration [92]. As example, keratinocytes in wounds undergo partial EMT to gain the ability to move and attach to new substrates and thus facilitate wound re-epithelialization [93]. During tumor development EMT is induced by a number of events, including hypoxia-mediated formation of ROS and NFκB activation [94,95]. Transition into the mesenchymal phenotype provides cancer cells with an enhanced migratory capacity, increased invasiveness and protection against apoptosis. Moreover, this kind of phenotypic plasticity can contribute to cancer cell resistance to chemo-, immuno- and targeted therapies [96]. Thus, EMT is not only a consequence of tumor formation owing to environmental changes like the occurrence of hypoxia, but at the same time it is a stimulant of tumor spread and often is associated with cancer immune escape. Exemplarily for the relationship between EMT and immune escape is a study by

Landsberg and colleagues who showed that immune evasion of melanoma cells can be mediated by reversible loss of melanocytic antigens during tumor necrosis factor alpha (TNFα)-induced switch between a differentiated and dedifferentiated phenotype. As a result T-cell recognition is prevented and melanoma cells acquire resistance to adoptive cell transfer therapy [97].

However, EMT is only one among many different mechanisms of hypoxic tumor cells to evade immune attack. Importantly, hypoxia induces suppression of immune functions. This is indicated for example by impaired survival and proliferation of $CD4^+$ T-cells as well as loss of IFNγ-production by Th1 $CD4^+$ T-cells, an effect mediated by increased expression of immunoinhibitory IL-10 [98,99]. Additionally, differentiation and maturation of DCs upon TLR stimulation is repressed, as well as their homing to lymph nodes, thereby preventing T-cell priming [100]. Still, what functions as a 'friend' in the setting of inflammation may act as a 'foe' in the fight against cancer. Moreover, hypoxic tumor cells can evolve additional immunosuppressive mechanisms. Amongst others, tumor cell susceptibility to NK- or CTL-mediated lysis is impaired by hypoxia-induced autophagy in breast cancer and lung cancer cells respectively, an effect that can be prevented by inhibiting autophagy [101,102]. As shown by Barsoum *et al.* resistance to CTL-mediated lysis is further aggravated by the HIF-dependent upregulation of PDL-1 expression on cancer cells, thus enforcing T-cell apoptosis via the PD-1 receptor in response to hypoxia [103]. Blocking HIF accumulation by activating nitric oxide signaling instead represses PDL-1 upregulation and resistance to T-cell attack. Diminished nitric oxide signaling upon oxygen deprivation is also involved in shedding of cell stress-induced MHC class-I chain-related (MIC) molecules on human prostate cancer cells, which prevents the binding of activating receptors on NK and cytotoxic T-cells [104]. Nitric oxide mimetics and autophagy inhibitors therefore represent encouraging tools to counteract hypoxia-related tumor immune escape. All in all, these studies clearly demonstrate that without learning the effect of hypoxia on RIG-I signaling, we will never get 3pRNA-mediated cancer immunotherapy to work right.

3.7 Aim of the study

Knowing that hypoxia contributes to tumor immune escape on different levels and based on the observation that IFNα receptor (IFNαR) expression and IFNα signaling are diminished upon oxygen deprivation [105], the starting hypothesis of this thesis assumed a negative influence of hypoxia on RIG-I function and thus on 3pRNA-mediated tumor immunotherapy.

To test this hypothesis, effects of oxygen deprivation on the RIG-I expression itself were investigated in a set of murine melanoma cell lines and primary tissue cells. Moreover, the influence of hypoxia on different regulatory components that play crucial roles in signal transduction from RIG-I to the effector transcription factors were additionally analysed. Finally, functional repercussions of the hypoxia-mediated effects on RIG-I signaling outcome were investigated. In particular anti-melanoma antigen-specific T- and NK cell responses were studied in different settings.

The gained insights were then used for the identification of measures that might enhance the RIG-I response under hypoxia and result in beneficial treatment outcome in an *in vivo* model of transplantable murine melanoma.

4 Material and methods

4.1 Material

4.1.1 Consumables

Blotting paper	GE Healthcare	Chalfont St Giles, GB
Cell culture flasks (75 cm^2)	Sarstedt	Nümbrecht
Cell strainer (70 µm, nylon)	Corning	Amsterdam, Netherlands
Centrifuge tubes (15 ml, 50 ml)	Greiner Bio-One	Frickenhausen
Cluster tubes	Corning	Amsterdam, Netherlands
Cryo tubes	Greiner Bio-One	Frickenhausen
ELISA plates	Thermo Scientific	Rochester
Lumitrac 200 96-well white immunology plate	Greiner Bio-One	Frickenhausen
Microlances (30 G, 0.3 x 13 mm)	BD Biosciences	Franklin Lakes, NJ, USA
Micropipette tips	Greiner Bio-One	Frickenhausen
Micropipette tips, RNase free	Corning	Amsterdam, Netherlands
Micropipette tips, with filter	Corning	Amsterdam, Netherlands
Microplates (flat- / round bottom)	Greiner Bio-One	Frickenhausen
Neubauer chamber	VWR International	Darmstadt
Nitrocellulose membrane (0.2 µm, 0.45 µm)	GE Healthcare	Buckinghamshire, GB
PCR tubes (0.2 ml)	Biozym Scientific	Hessisch Oldendorf
Petri dishes (10 cm)	Sarstedt	Nümbrecht
Pipettes (5 ml, 10 ml, 25 ml)	Greiner Bio-One	Frickenhausen
qPCR plates	Sarstedt	Nümbrecht
Quick spin oligo columns (mini)	Roche	Basel, Switzerland
Reagent reservoirs	Brand	Wertheim
Scalpels	Pfm medical	Cologne
Spin columns	Centic Biotec	Heidelberg
Syringes (5 ml)	BD Biosciences	Franklin Lakes, NJ, USA
Syringes Inject-F (1 ml)	B. Braun	Melsungen
Test tubes (0.5 ml, 1.5 ml, 2 ml)	Sarstedt	Nümbrecht
Tissue culture test plates (12 well, 48 well, 96 well)	TPP Techno Plastic Products	Trasadingen, Switzerland
Zirconia beads (1 mm diameter)	Biospec Products	Bartlesville, OK, USA

4.1.2 Equipment

ABI 7900HT	Applied Biosystems	Waltham, MA, USA
Balance, electronic	Sartorius	Göttingen
Blotting equipment	BioRad	Hercules, CA, USA
Centrifuge 5810R	Eppendorf	Hamburg
EnVision Multilabel plate reader	Perkin Elmer	Waltham, MA, USA
Epoch Microplate Spectrophotometer	BioTek	Winooski, VT, USA

FACS Canto	BD Biosciences	Franklin Lakes, NJ, USA
FACS LSR II	BD Biosciences	Franklin Lakes, NJ, USA
Homogenizer	Bertin Technologies	Montigny le Bretonneux, France
Hypoxia incubator	Life Technologies	Carlsbad, CA, USA
Immunofluorescence microscope	Leica Biosystems	Wetzlar
Magnetic stirrer	Velp Scientifica	Usmate, Italy
Microcentrifuge 5415R	Eppendorf	Hamburg
Micropipettes	Eppendorf / Rainin	Hamburg
Microscope Nicon Eclipse TS100	Nikon	Düsseldorf
Microtome RM2255	Leica Biosystems	Wetzlar
Multichannel pipette	VWR International	Darmstadt
NanoDrop	Peqlab	Darmstadt
Odyssey Fc Imaging System	LI-COR Biotechnology	Lincoln, NE, USA
pH meter	Hanna instruments	Vöhringen
Pipetting aid	Integra Biosciences	Konstanz
Power supply	Labnet International	Edison, NJ, USA
SDS-gel electrophoresis equipment	BioRad	Hercules, CA, USA
Shaker	NeoLab	Heidelberg
Sterile bench	Thermo Scientific	Waltham, MA, USA
Thermocycler	Analytik Jena	Jena
Thermomixer	Eppendorf	Hamburg
Vortex mixer	Velp Scientifica	Usmate, Italy
Water jacketed CO_2 incubator	Panasonic Biomedical Sales Europe	Etten Leur, The Netherlands
Water bath	Julabo	Seelbach
X-ray film developing machine	CAWO	Schrobenhausen

4.1.3 Solid chemicals

Actinomycin D	AppliChem	Darmstadt
Albumin fraction V	Roth	Karlsruhe
Ammonium persulfate	Roth	Karlsruhe
Bromphenolblue (BPB)	Roth	Karlsruhe
Calcium chloride ($CaCl_2$)	Roth	Karlsruhe
Disodium hydrogen phosphate (Na_2HPO_4)	Roth	Karlsruhe
Dithiotreitol (DTT)	Roth	Karlsruhe
Glycine	Roth	Karlsruhe
L-ascorbic acid	Sigma-Aldrich	St. Louis, MO, USA
Milk powder	Roth	Karlsruhe
Ponceau S	Roth	Karlsruhe
Potassium chloride (KCl)	Roth	Karlsruhe
Potassium dihydrogen phosphate (KH_2PO_4)	Roth	Karlsruhe
Sodium azide	Roth	Karlsruhe
Sodium carbonate (Na_2CO_3)	Roth	Karlsruhe
Sodium chloride (NaCl)	Roth	Karlsruhe
Sodium deoxycholate	Sigma-Aldrich	St. Louis, MO, USA
Sodium dodecylsulphate (SDS)	Applichem	Darmstadt

Sodium hydrogen carbonate ($NaHCO_3$)	Roth	Karlsruhe
Tris	Roth	Karlsruhe

4.1.4 Liquid chemicals

Acetic acid	Roth	Karlsruhe
Ampuva (sterile, deionized H_2O)	B. Braun	Melsungen
Antibody diluent for IHC	Dako	Hamburg
Chloroform	Roth	Karlsruhe
Developer for x-ray films	AGFA	Mortsel, Belgium
ECL western blotting substrate	Thermo Scientific	Waltham, MA, USA
ELISA substrate solutions (H_2O_2, tetramethylbenzidine)	BD Biosciences	Franklin Lakes, NJ, USA
Ethanol	Roth	Karlsruhe
FACS Flow	BD Biosciences	Franklin Lakes, NJ, USA
Glycerin	Roth	Karlsruhe
Hydrogen peroxide	Roth	Karlsruhe
In vivo-jetPEI®	Polyplus	Illkirch, France
Isopropanol	Roth	Karlsruhe
Lipofectamine™ RNAiMAX	Invitrogen	Waltham, MA, USA
Lipofectamine™2000	Invitrogen	Waltham, MA, USA
Pascorbin®	Pascoe pharmazeutische Präparate	Gießen
Rapid fixer for x-ray films	AGFA	Mortsel, Belgium
RLT lysis buffer	Quiagen	Hilden
Roti-Quant Bradford reagent	Roth	Karlsruhe
Rotiphorese Gel 30, 37.5:1	Roth	Karlsruhe
RW1 RNA wash buffer	Quiagen	Hilden
Sulfuric acid	Roth	Karlsruhe
TEMED	Roth	Karlsruhe
Triton-X-100	Roth	Karlsruhe
Trizol reagent	Ambion	Waltham, MA, USA
Tween-20	Roth	Karlsruhe
Zinc fixative	BD Biosciences	Franklin Lakes, NJ, USA
Zymo RNA wash buffer	Zymo research	Irvine, CA, USA

4.1.5 Cell culture substances

Dimethylsulfoxide (DMSO)	Roth	Karlsruhe
Dulbecco's modified eagles medium (DMEM)	Gibco	Carlsbad, CA, USA
Dulbecco's phosphate buffered saline (DPBS)	Gibco	Carlsbad, CA, USA
Fetal calve serum (FCS)	Gibco	Carlsbad, CA, USA
Hepes	Gibco	Carlsbad, CA, USA
L-Glutamine	Gibco	Carlsbad, CA, USA
Lysis buffer (10×) for erythrocytes	BD Biosciences	Franklin Lakes, NJ, USA
Non-essential amino acids (NEAA)	Gibco	Carlsbad, CA, USA
OptiMEM	Gibco	Carlsbad, CA, USA
Penicillin-streptomycin	Gibco	Carlsbad, CA, USA

RPMI 1640 medium	Gibco	Carlsbad, CA, USA
Sodium pyruvate	Gibco	Carlsbad, CA, USA
Trypan blue	Sigma-Aldrich	St. Louis, MO, USA
Trypsin/EDTA	Gibco	Carlsbad, CA, USA

4.1.6 Buffers

Annealing buffer (10×)	250 mM tris-/HCl; 250 mM NaCl; pH 7.4
Blocking buffer (western blot)	5% (w/v) milk powder in TBST or PBST
Electrophoresis buffer	24 mM tris; 192 mM glycine; 0.1% (w/v) SDS
ELISA blocking buffer (CXCL10)	2% (v/v) FCS in PBS
ELISA blocking buffer (IL-6)	10% (v/v) FCS in PBS
ELISA coating buffer (IL-6)	100 mM $NaHCO_3$; 33.6 mM Na_2CO_3 in PBS; pH 9.5
ELISA wash buffer	0.05% (v/v) Tween20 in PBS
FACS buffer	2% FCS; 2 mM EDTA; 0.05% NaN_3 in PBS
Fixation buffer (FACS)	3.7% formaldehyde in PBS
Laemmli buffer (2×)	0.2 M tris/HCl pH 6.8; 4% (w/v) SDS; 20% (v/v) glycerol; 20 mM DTT; 0.05% (w/v) bromphenolblue
Luciferin	20 mM tricine; 2.7 mM $MgSO_4*7H_2O$; 0.1 mM EDTA pH 8.0; 33 mM DTT; 0.5 mM ATP; 0.3 mM acetyl CoA; 0.03 g luciferin; 5 mM NaOH; 0,3 mM $(MgCO_3)_4Mg(OH)_2*5H_2O$
Lysis buffer for cell fractionation	50 mM tris; 0.5% (v/v) triton-X-100; 138 mM NaCl; 10% (v/v) glycerol; 5 mM EDTA; 1× protease-; 1× phosphatase inhibitor mix
MACS buffer	2% FCS; 2 mM EDTA in PBS
Permeabilization buffer (FACS)	0.5% saponin in FACS buffer
Phosphate buffered saline (PBS)	140 mM NaCl; 8 mM Na_2HPO_4; 1.5 mM KH_2PO_4; 2.5 mM KCl
Ponceau staining solution	0.1% (w/v) ponceau; 3% (v/v) acetic acid
RIPA buffer	50 mM tris pH 8.0; 150 mM NaCl; 1% (v/v) triton-X-100; 0.5% (w/v) sodium deoxycholate; 0.1% (w/v) SDS, 1× protease inhibitor mix
SAP buffer	0.2% saponin; 50 mM tris/HCl pH 7.8; 15 mM $MgSO_4$; 4 mM EGTA; 10% glycerol
Transfer buffer	24 mM tris; 192 mM glycine; 20% (v/v) ethanol
Tris buffered saline with tween (TBST)	10 mM tris; 150 mM NaCl; 0.1% (v/v) Tween 20; pH 7.6

4.1.7 Recombinant proteins / inhibitors / stimulators

Actinomycin D	AppliChem	Darmstadt
BAY11-7082	InvivoGen	San Diego, CA, USA
BMS-345541	Sigma-Aldrich	St. Louis, MO, USA
Helenalin	Merck Millipore	Darmstadt
IFNα	Miltenyi Biotec	Bergisch-Gladbach
Ionomycin	Sigma-Aldrich	St. Louis, MO, USA
MG132	Selleck Chemicals	München
PMA	Sigma-Aldrich	St. Louis, MO, USA
Protease inhibitor tablets	Roche	Basel, Switzerland

4.1.8 Kits

Annexin V-FITC Apoptosis Detection Kit	Enzo Life Sciences	Farmingdale, NY, USA
CellTiter-Blue® cell viability assay	Promega	Madison, WI, USA
Dako REAL™ Detection System	Dako	Hamburg
FlowCytomix™ Th1/Th2/Th17/Th22 13plex	eBioscience	San Diego, CA, USA
Hypoxyprobe™-1 Kit	Hypoxyprobe Inc.	Burlington, MA, USA
Mouse CXCL10 ELISA Set	R&D Systems	Minneapolis, MN, USA
Mouse IL-6 ELISA Set BD OptEIA™	BD Biosciences	Franklin Lakes, NJ, USA
SuperScript® VILO™ cDNA Synthesis Kit	Invitrogen	Waltham, MA, USA
Total ROS/Superoxide Detection Kit	Enzo Life Sciences	Farmingdale, NY, USA
TranscriptAid T7 High Yield Transcription Kit	Thermo Scientific	Waltham, MA, USA

4.1.9 Cell lines

B16F10	Murine melanoma cell line	Kindly provided by Thomas Tüting[*]
HCmel17	Murine melanoma cell line	Kindly provided by Thomas Tüting
HCmel23	Murine melanoma cell line	Kindly provided by Thomas Tüting
HCmel3	Murine melanoma cell line	Kindly provided by Thomas Tüting
Kera 308	Murine epidermal keratinocyte cell line	CLS cell lines service, Eppelheim
LL171	Mouse IFN type-I reporter cell line	Kindly provided by Andrea Ablasser[†]
Melan-A	Murine melanocyte cell line	Kindly provided by Thomas Tüting

4.1.10 Fluorescently-labeled antibodies

α -CD11b-PE/Cy7 (M1/70)	eBioscience	San Diego, CA, USA
α -CD11c-FITC (N418)	eBioscience	San Diego, CA, USA
α -CD3-APC (145-2C11)	BioLegend	San Diego, CA, USA
α -CD4-APC/Cy7 (GK1.5)	BioLegend	San Diego, CA, USA
α -CD45-APC/Cy7 (104)	BioLegend	San Diego, CA, USA
α -CD49b-eFluor450 (DX5)	eBioscience	San Diego, CA, USA
α -CD49b-PE/Cy7 (DX5)	eBioscience	San Diego, CA, USA
α -CD69-eFluor450 (H1.2F3)	eBioscience	San Diego, CA, USA
α -CD69-PE/Cy7 (H1.2F3)	eBioscience	San Diego, CA, USA
α -CD8-PerCP/Cy5.5 (53-6.7)	BioLegend	San Diego, CA, USA
α -Gr-1-pacific blue (RB6-8C5)	BioLegend	San Diego, CA, USA
α -IFNαR-PE (MAR1-5A3)	BioLegend	San Diego, CA, USA
α -MHC-I-APC (AF6-88.5.5.3)	eBioscience	San Diego, CA, USA
α -mouse-Alexa488, goat Ig	Invitrogen	Waltham, MA, USA
α -NK1.1-PE (PK136)	eBioscience	San Diego, CA, USA
α -PD-1-APC (RMP1-30)	BioLegend	San Diego, CA, USA
α -PDL-1-PE (MIH5)	eBioscience	San Diego, CA, USA

[*] University Clinic for Dermatology and Venerology, University Hospital Magdeburg, Magdeburg
[†] Global Health Institut, École polytechnique fédérale de Lausanne, Lausanne, Switzerland

4.1.11 Western blot and immunohistochemistry antibodies

α -actin-HRP, mouse IgG (C4)	Santa Cruz	Dallas, TX, USA
α -CXCL10, rabbit IgG	PeproTech	Hamburg
α -goat-HRP, donkey IgG	Santa Cruz	Dallas, TX, USA
α -gp100, goat Ig	Novus Biologicals	Cambridge, UK
α -histone 3, rabbit IgG	Cell Signaling	Danvers, USA
α -Hsp90α, mouse IgG (D7a)	Abcam	Cambridge, UK
α -Hsp90β, mouse IgG2a (H9010)	Invitrogen	Waltham, MA, USA
α -K63 ubiquitin, rabbit IgG (D7A11)	Cell Signaling	Danvers, USA
α -MAVS, rabbit IgG	Thermo Scientific	Waltham, MA, USA
α -mouse-HRP, goat IgG	Imgenex	San Diego, CA, USA
α -p65, rabbit IgG (D14E12)	Cell Signaling	Danvers, USA
α -PMP70, rabbit Ig	Thermo Scientific	Waltham, MA, USA
α -rabbit-HRP, bovine IgG	Santa Cruz	Dallas, TX, USA
α -RIG-I, mouse Ig	Santa Cruz	Dallas, TX, USA
α -TOM70, rabbit IgG	ProteinTech	Manchester , UK
α -tubulin, rabbit IgG	Cell Signaling	Danvers, USA
α -vimentin, rabbit IgG (D12H3)	Cell Signaling	Danvers, USA

4.1.12 Primer sequences

Actin	5’-GGATGCAGAAGGAGATTACTG-3’ 5’-CCACCGATCCACACAGAGTA-3’	Metabion	Planegg/ Steinkirchen
RIG-I	5’-GAAGATTCTGGACCCCACCTA-3’ 5’-TGAATGTACTGCACCTCCTCA-3’	Invitrogen	Waltham, MA, USA
TBP	5’-CTTCACCAATGACTCCTATGACC-3’ 5’-ACAGCCAAGATTCACGGTAGA-3’	Integrated DNA Technologies	Coralville, IA, USA
Viperin	5’-TTGGGCAAGCTTGTGAGATT-3’ 5’-GATAGCAAGAATGTCCAAATACTCC-3’	Invitrogen	Waltham, MA, USA
CXCL10	5’-CTCATCCTGCTGGGTCTGAG-3’ 5’-CCTATGGCCCTCATTCTCAC-3’	Invitrogen	Waltham, MA, USA
IFIT1	5’-CAAGGCAGGTTTCTGAGGAG-3’ 5’-GACCTGGTCACCATCAGCAT-3’	Invitrogen	Waltham, MA, USA
gp100	5’-ACACAGTCCAGGGGAACTTG-3’ 5’-AACCACAGAGGGTCCAGATG-3’	Integrated DNA Technologies	Coralville, IA, USA
Tyrosinase	5’-ATAGGTGCATTGGCTTCTGG-3’ 5’-TCTTCACCATGCTTTTGTGG-3’	Integrated DNA Technologies	Coralville, IA, USA
TRP2	5’-ACTCCTTCCTGAATGGGACC-3’ 5’-GCATCTGTGGAAGGGTTGTT-3’	Integrated DNA Technologies	Coralville, IA, USA
Gr-1	5’-AGGAGGGAGCTGCTAGGTTT-3’ 5’-CTGCACACAGTAGGACCACA-3’	Invitrogen	Waltham, MA, USA

4.1.13 Oligonucleotide sequences

3p-siNrf2 sense	5’-(ppp)GCGGCGCUCAACUUGCAUUAAUUCdTdT-3’	Axolabs	Kulmbach
3pGFP2 antisense	5’-AAGAUGAACUUCAGGGUCAGCGUC-3’	‡	
3pGFP2 sense	5’-(ppp)GACGCUGACCCUGAAGUUCAUCUU-3’	‡	
IVT4 DNA template	5’-TTGTAATACGACTCACTATAGGGACGCTGACCCA GAAGATCTACTAGAAATAGTAGATCTTCTGGGTCAGC GTCCC-3’	Invitrogen	Waltham, MA, USA
IVT4 promoter	5’-CAGTAATAGGACTCACTATAG-3’	Invitrogen	Waltham, MA, USA
polyA	$(A)_n$	Sigma-Aldrich	St. Louis, MO, USA
polyCA	$(CA)_{10}$	Biomers	Ulm
polyI:C	5’-$(I)_n$-3’ 3’-$(C)_n$-5’	InvivoGen	San Diego, CA, USA
siNrf2 antisense	5’-GAAUUAAUGCAAGUUGAGCdTdT-3’	Biomers	Ulm
siNrf2 sense	5’-GCUCAACUUGCAUUAAUUCdTdT-3’	Biomers	Ulm

‡ Synthesized and kindly provided by Marion Goldeck, Institute for Clinical Chemistry and Clinical Pharmacology, University Hospital Bonn, Bonn [24]

4.2 Methods

4.2.1 Methods for handling cell lines and primary cells

4.2.1.1 Cultivation of cell lines

All cell lines used for preparation of this thesis are listed in section 4.1.9. Cells were grown in Petri dishes or tissue culture flasks using appropriate culture media as indicated in Table 1 and were kept in a humidified incubator at 37°C, 5% CO_2 and 20% O_2. In order to split cells they were rinsed with PBS and incubated with 1 ml trypsin/EDTA until cells were detached. In case keratinocytes resisted trypsin treatment, they were mechanically unhitched using a cell scraper. Subsequently cells were resuspended in culture medium and the required proportion (Table 1) was transferred into a new culture dish containing fresh medium.

Cell line	Medium with additives	Splitting ratio
B16F10	RPMI + 10% FCS + 100 IU/ml penicillin and 100 µg/ml streptomycin (PS)	1:30, 2×/week
HCmel17	RPMI + FCS + PS + 1× L-glutamine + NEAA + 2 mM HEPES + 0,0075‰ β-Mercaptoethanol	1:4, 2×/week
HCmel23	RPMI + FCS + PS	1:10, 2×/week
HCmel3	RPMI + FCS + PS	1:3, 1×/week
Kera 308	DMEM + FCS + PS	1:2, 1×/week
LL171	DMEM + FCS + PS + 1 mM sodium pyruvate	1:10, 2×/week
Melan-A	RPMI + FCS + PS + 200 nM PMA	1:5, 2×/week

Table 1: Cultivation of cell lines. Additives include fetal calve serum (FCS), penicillin and streptomycin (PS), non-essential amino acids (NEAA), 4-(2-hydroxyethyl)-1-piperazineethanesulfonic acid (HEPES) and phorbol 12-myristate 13-acetate (PMA).

4.2.1.2 Seeding of cells and hypoxic incubation

Cells were harvested with trypsin as described above and the amount of living cells was determined using a Neubauer chamber and trypan blue staining. Depending on the assay cells were seeded in differently sized tissue culture test plates according to Table 2. To ensure proper attachment of the cells before onset of treatment, they were incubated at 37°C, 5% CO_2 and 20% O_2 over night. An oxygen concentration of 20% was considered as normoxic. Hypoxic conditions were implemented by keeping cells for at least 24 h in a humidified incubator at 37°C, 5% CO_2 and 2% O_2 or 0.2% O_2. The reduction of oxygen was achieved by inflating the incubator with nitrogen.

Size	Cell line	Cells/well	Medium/well (µl)
96 well	B16F10, HCmel3, HCmel17, HCmel23, Kera 308, Melan-A LL171	20,000 5,000	100
48 well	B16F10, HCmel3	50,000	350
12 well	B16F10 HCmel3 HCmel17 HCmel23 Kera 308 Melan-A	200,000 380,000 110,000 140,000 450,000 340,000	1,000

Table 2: Cell numbers according to cell line and sizes of tissue culture test plates.

4.2.1.3 Stimulation of cells with oligonucleotides or IFNα

Transfection of oligonucleotides in eukaryotic cells was performed using Lipofectamine, a reagent based on cationic lipids that neutralize the negative charge of nucleic acids, thus facilitating their uptake. While siRNA-experiments were performed with Lipofectamine RNAiMAX, Lipofectamine2000 was used for transfection of *in vitro*-transcribed 3pRNA, polyI:C RNA and the respective controls. According to well size nucleic acids and Lipofectamine were separately mixed with the transfection medium OptiMEM and incubated at room temperature (RT) for 5 min (Table 3 and Table 4). After combining both preparations the resulting transfection mix was incubated at RT for 20 min and subsequently added to the medium in the test plates. Cells were incubated with the transfection mix for 24 h under hypoxic or normoxic conditions if not indicated otherwise.

Alternatively, cells were stimulated with recombinant murine IFNα by direct addition into the culture medium. If not indicated otherwise a final concentration of 1000 IU/ml was used and identical time spans as for RNA stimulations were applied.

Size	RNA/well (ng)	Lipofectamine2000/well (µl)	OptiMEM/reaction (µl)
96 well	20	0.5	25
48 well	64	1.5	35
12 well	250	4	100

Table 3: Composition of transfection mixes using Lipofectamine2000

Size	RNA/well (nM)	Lipofectamine RNAiMAX/well (µl)	OptiMEM/reaction (µl)
96 well	10	0.2	10

Table 4: Composition of transfection mixes using Lipofectamine RNAiMAX

4.2.1.4 Treatment of cells with different inhibitors or vitamin C

The inhibition of proteasomal degradation was performed by treatment of cells with 5 µM MG132 during the time of 3pRNA transfection.

For the assessment of mRNA stability cells were transfected with 3pRNA for 4 h, afterwards transcription was blocked using 5 µg/ml actinomycin D. Cells were lysed 2 h, 4 h and 6 h later using 87 µl RLT buffer.

As a means to prevent hypoxia-induced EMT cells were treated with L-ascorbic acid (vitamin C) or different NFκB inhibitors. The former was used at concentrations of 25 µM or 200 µM and was applied 24 h prior to the onset of hypoxic incubation. The NFκB inhibitors BAY, BMS and Helenalin were added at the start of hypoxia using concentrations of 8 µM, 5 µM and 1 µM, respectively. Vitamin C and NFκB inhibitor treatment continued during hypoxic incubation and 3pRNA stimulation.

4.2.1.5 Isolation of mouse splenocytes and co-culture with melanoma cells

Spleens were retrieved from sacrificed mice, sieved through 70 µm cell strainer and collected in MACS buffer to obtain single cell suspensions. Following a centrifugation at 1400 rpm for 7 min at 4°C, erythrocytes were eliminated from the cell pellet by incubation in 5 ml 1× lysis buffer for 10 min at 37°C. Afterwards splenocytes were washed by addition of 20 ml RPMI and centrifugation as above. The pellet was resuspended in 5 ml RPMI and the amount of cells was determined using trypan blue and a Neubauer chamber.

For co-culture experiments melanoma cells were seeded in 48-well plates, pre-incubated under normoxia or hypoxia and stimulated with 3pRNA or IFNα for 6 h. After removal of the transfection mix and washing with PBS, freshly isolated splenocytes from T-cell receptor (TCR) transgenic Pmel-1 mice were added at 5×10^5 cells per well in 1 ml medium. As control, splenocytes without melanoma cells were activated using 5 µg/ml $gp100_{25\text{-}33}$ peptide (kindly provided by J. W. Drijfhout[§]) or 50 ng/ml phorbol 12-myristate 13-acetate (PMA) and 1 µg/ml Ionomycin. Cells were co-cultured for 18 h under normoxic or hypoxic conditions.

4.2.1.6 Detection of hypoxia in cultured cells

The hypoxic status of melanoma cells was verified using the Hypoxyprobe-1 Kit. Therefore B16F10 cells were seeded in 96-well plates and incubated under hypoxic or normoxic atmosphere for 22 h. Subsequently, pimonidazole was added to give a final concentration of 100 µM and incubation was continued for 2 h. In hypoxic but not normoxic cells pimonidazole is reductively activated, whereupon the reaction intermediate forms covalent adducts with thiol groups of proteins. These adducts can be detected using a specific primary- and a fluorescently labeled secondary antibody. The staining procedure was performed analogously to section 4.2.3.3. Briefly, cells were harvested, washed with FACS buffer, fixed with 3.7% paraformaldehyde in PBS for 15 min at RT and washed again with FACS buffer as well as permeabilization buffer. Afterwards, 30 µl of primary antibody, diluted 1:30 in permeabilization buffer, were added and incubated at RT for 30 min. Cells were washed twice using permeabilization buffer and subsequently incubated with α-mouse-Alexa488 1:200 in 30 µl as above. Following two wash steps with FACS buffer cells were analyzed using a LSRII.

[§] Department of Immunohematology and Bloodtransfusion, Leiden University Medical Center, Leiden, The Netherlands

4.2.1.7 Measurement of reactive oxygen species

Detection of cellular ROS production was performed using the Total ROS/Superoxide Detection Kit. Therefore cells in 12-well plates were washed with PBS and incubated with 200 µl detection reagent in wash buffer (1:5000) for 60 min at 37°C under hypoxia or normoxia. The non-fluorescent, cell-permeable detection dye meanwhile penetrated the cell membrane and reacted directly with ROS to form a fluorescent product. Afterwards cells were scraped off and fluorescence intensity was analyzed by flow cytometry using a LSRII.

4.2.1.8 Viability assay and quantification of apoptotic cells

To assess the viability of melanoma cells a CellTiter-Blue assay was performed, which is based on the reduction reaction of resazurin into a fluorescent product by metabolically active cells. Therefore, the transfection mix was removed from cells in 96-well plates and replaced by 100 µl medium plus 20 µl CellTiter-Blue reagent. Cells were kept in the incubator for approximately 1 h and fluorescence intensity was measured using an EnVision multilabel plate reader (excitation: 560 nm, emission: 590 nm).

The Annexin V-FITC Apoptosis Detection Kit was used to quantify dying cells. Firstly, cells were harvested using trypsin, transferred into a round-bottom microplate, centrifuged (400 × g, 4°C, 3 min) and washed with PBS. Subsequently, the pellet was resuspended in 30 µl 1× binding buffer containing anti-Annexin V-FITC antibody 1:40 and incubated at RT for 10 min. Following a wash step, cells were resuspended in 190 µl binding buffer and supplied with 10 µl propidium iodide directly before measuring the fluorescence at a LSRII flow cytometer.

4.2.1.9 IFNα/β reporter assay

LL171 cells stably expressing luciferase under the control of an ISG promoter were seeded in 96-well plates and treated with a serial dilution of recombinant mouse IFNα or diluted supernatant of stimulated melanoma cells. Following a 6 h incubation at 37°C and 5% CO_2 LL171 cells were washed with PBS and lysed for 15 min using 40 µl SAP-buffer. 25 µl of the lysate were mixed with an equal volume of luciferin in a white Lumitrac 96-well plate and IFN-induced luciferase-mediated bioluminescence was immediately measured with an EnVision multilabel plate reader. The sample concentration of IFNα/β could then be calculated with the help of the standard curve.

4.2.2 Methods for handling nucleic acids

4.2.2.1 In vitro *transcription of 3pRNA*

The RIG-I ligand 3pRNA was generated by *in vitro* transcription using IVT4 T7-promotor and DNA template strands as depicted in 4.1.13. First, 3.4 nmol of both oligonucleotides were annealed in a

final volume of 170 µl 1× annealing buffer. The hybridization was performed in a thermocycler with 95°C for 3 min and stepwise cooling of -1°C every 30 sec to 20°C. For the transcription reaction a TranscriptAid T7 High Yield Transcription Kit was utilized. Therefore, 100 µg of annealed template DNA were mixed with the nucleotides ATP, CTP, GTP and UTP (final concentration of 10 mM each), 100 µl enzyme mix, 1× reaction buffer and H_2O to give a final volume of 1 ml. Following an incubation of 7 h at 37°C, 100 IU DNase I were added and the incubation was continued for 15 min. Finally, the DNase reaction was stopped by adding EDTA to a final concentration of 42 mM and heating to 65°C for 10 min. Separation of 3pRNA from nucleotides was performed using mini quick spin oligo columns. After preparation of the columns by centrifugation at 1000 × g for 2 min, 60 µl of the reaction mix were applied to each column. The 3pRNA was eluted by spinning at 1000 × g for 4 min and pooled afterwards. The concentration of RNA was determined by applying 2 µl to a NanoDrop and measuring the absorption at 260 nm wavelength.

4.2.2.2 Annealing of siRNAs and 3pGFP2

Hybridization of sense and antisense strands to obtain double-stranded RNAs was performed in a final volume of 150 µl, containing 1 µM of each strand and 1× annealing buffer. The annealing was carried out in a thermocycler with 72°C for 5 min and stepwise cooling of -0.1°C per second to 18°C.

4.2.2.3 RNA extraction from cells using spin columns

Cells were either harvested using trypsin and collected in test tubes or directly lysed in 12-well tissue culture test plates. Lysis was performed by resuspension of cells in 350 µl RLT buffer and freezing at -80°C for at least 5 min. Prior to loading onto spin columns 350 µl of 70% ethanol were added. Columns were placed in 2 ml test tubes and centrifuged for 1 min at 10,000 rpm. Subsequently, two wash steps were performed using 350 µl RW1 and Zymo RNA wash buffer respectively. Finally, the spin columns were placed in new test tubes and RNA was eluted by addition of 40 µl H_2O, incubation for 2 min and centrifugation as above. The RNA concentration was determined by applying 2 µl to a NanoDrop and measuring the absorption at a wavelength of 260 nm.

4.2.2.4 RNA extraction from tumors using trizol reagent

Cryo-conserved tissue samples were homogenized in 1 ml trizol using zirconia beads and a Precellys homogenizer (2 × 30 sec, 6500 rpm). After incubation at RT for 5 min, 200 µl chloroform were added, the sample was mixed for 15 sec and incubated for 3 min at RT. Centrifugation at 12,000 × g and 4°C for 15 min allowed phase separation of RNA (aqueous upper phase) from DNA (organic lower phase) and proteins (interphase). The aqueous phase was transferred into a new test tube and mixed with 500 µl 100% isopropanol. Following 10 min incubation at RT the sample was centrifuged as above for 10 min. The supernatant was removed and the RNA pellet was washed using 1 ml of 75% ethanol (centrifugation: 7500 × g, 4°C, 5 min). Residual ethanol was eliminated by air-drying for 5 min and the

RNA was dissolved in 100 µl H_2O. RNA concentration was determined as described in 4.2.2.3. For reliable measurements the RNA solution was diluted with H_2O until a concentration of maximal 1000 ng/µl was achieved.

4.2.2.5 cDNA synthesis and quantitative PCR

Complementary DNA (cDNA) was synthesized using the SuperScript® VILO™ cDNA Synthesis Kit. For one reaction 3.5 µl RNA (= 300 ng) were mixed with 1 µl 5× reaction buffer and 0.5 µl enzyme mix in PCR tubes. Using a thermocycler the sample passed through the following temperature protocol: 25°C for 10 min, 42°C for 60 min, 85°C for 5 min and cooling to 4°C.

Quantitative polymerase chain reaction (qPCR) was performed using the fluorescent double-stranded DNA-binding dye Sybr GreenER. The fluorescent signal of Sybr Green is recorded after each amplification step and is proportional to the DNA concentration in the sample. Newly designed primers were initially tested for efficiency and specificity by amplification of a standard curve of cDNA. These results were further used to identify an appropriate cDNA dilution. One qPCR reaction mix contained primers at a final concentration of 0.33 µM each, 10 µl Sybr GreenER Master Mix and H_2O to give a final volume of 18 µl. This was combined with 2 µl of diluted cDNA in a qPCR plate. The PCR reaction was performed on an ABI 7900 HT using the following thermal profile: 50°C for 2 min, 95°C for 10 min and 40 cycles of 95°C for 15 sec and 60°C for 1 min. Additionally, a dissociation curve was recorded to exclude target-unspecific amplification or primer dimerization. For comparative analysis target mRNA expression was normalized to a housekeeping gene according to $2^{(CtR-CtT)}$ with Ct = cycle threshold, R = reference and T = target. For cell culture experiments normalized target mRNA expression of each sample is shown relative to the value of 3pRNA-treated normoxic cells if not indicated otherwise.

4.2.3 Methods for handling proteins

4.2.3.1 Protein quantification via Bradford assay

The total amount of protein in a cell lysate was determined using Roti-Quant dye according to a method by Bradford [106]. Therefore a 1:2 serial dilution of bovine serum albumin (BSA) ranging from 800 µg/ml to 25 µg/ml was prepared in H_2O. Additionally, lysates were appropriately diluted in H_2O. 5 µl of sample or standard were mixed with 200 µl 1× Roti-Quant in a flat-bottom microplate and agitated for 10 min at RT. Finally, light absorbance at 562 nm was measured using an Epoch microplate spectrophotometer. The sample concentration could then be calculated with the help of the standard curve.

4.2.3.2 Western blot analysis

Cells were harvested from 12-well plates using trypsin and lysed with 10-30 µl RIPA buffer. Following 30 min incubation at 4°C lysates were cleared by centrifugation (13,000 × g at 4°C for 15 min). Alternatively, cells were lysed in cell fractionation buffer for 15 min at 4°C and centrifuged at 13,000 × g and 4°C for 15 min to obtain cytosolic proteins in the supernatant. For extraction of nuclear proteins the resulting pellet was resuspended in cell fractionation buffer containing 0.5% (v/v) SDS, DNA was destroyed using ultrasound and the lysate was cleared by centrifugation. 20-40 µg of total cell protein were mixed with an equal volume of Laemmli buffer and denatured at 95°C for 5 min. SDS polyacrylamide gel electrophoresis was performed in electrophoresis buffer at 30 mA per gel for 1.5 h. Afterwards proteins were transferred onto a nitrocellulose membrane in transfer buffer at 450 mA for 1.5 h. Successful transfer was confirmed by ponceau staining. Membranes were then blocked with 5% milk in TBST or PBST for 1 h at RT and incubated with the respective antibodies at 4°C over night or for 72 h (RIG-I) (Table 5). Horseradish peroxidase (HRP)-coupled secondary antibodies α-rabbit, α-goat and α-mouse were used 1:5000 and were incubated for 1 h at RT. As loading control actin was detected using α-actin-HRP antibody 1:5000 in 0.5% BSA in PBST. After incubation with a 1:1 mixture of ECL western blotting substrates for 1 min, membranes were exposed to x-ray films, which were mechanically developed. Alternatively, chemiluminescence was detected using an Odyssey Fc imaging system. The band intensity was quantified with ImageJ 1.440 software (Wayne Rasband, National Institute of Health) and target expression was normalized to reference protein expression.

Antibody	Dilution	Antibody	Dilution
α-gp100	1:500	α-p65	1:1000
α-histone 3	1:2000	α-PMP70	1:500
α-HSP90α	1:1000	α-RIG-I	1:100
α-HSP90β	1:100	α-TOM70	1:1000
α-K63-ubiquitin	1:1000	α-tubulin	1:1000
α-MAVS	1:2000	α-vimentin	1:1000
α-MDA5	1:1000		

Table 5: Dilutions of primary antibodies for western blot application.

4.2.3.3 Flow cytometry

Briefly, cells were harvested, transferred into round-bottom microplates, centrifuged (400 × g, 4°C, 3 min) and washed with FACS buffer. For determination of surface protein expression cells were stained on ice for 30 min using the following antibodies 1:200 in 30 µl FACS buffer: α-CD11b-PE/Cy7, α-CD11c-FITC, α-CD3-APC, α-CD4-APC/Cy7, α-CD45-APC/Cy7, α-CD49b-eFluor450, α-CD69-pacific blue, α-CD69-PE/Cy7, α-CD8-PerCP/Cy5.5, α-Gr-1-pacific blue, α-IFNαR-PE, α-MHC-I-APC, α-NK1.1-PE, α-PD-1-APC, α-PDL-1-PE and α-PDL-2-PE. Finally, 100 µl FACS buffer were added and samples

centrifuged as above. For preservation cells were optionally fixed by treatment with 3.7% paraformaldehyde in PBS for 15 min at RT and subsequently washed with FACS buffer. Thereafter, cells were resuspended in FACS buffer and fluorescence was measured using the flow cytometers LSRII or Canto.

4.2.3.4 Enzyme-linked immunosorbent assay (ELISA)

For quantification of the cytokines CXCL10 and IL-6 supernatants of stimulated cells were collected 24 h after transfection and analyzed using ELISA kits according to the manufacturer's protocol. Briefly, ELISA plates were coated with the respective capture antibody in 50 µl PBS or coating buffer and incubated at RT or 4°C over night. In-between each incubation step wells were washed at least three times using ELISA wash buffer. Unspecific binding sites were then blocked by 1 h incubation in 150 µl or 50 µl of the respective ELISA buffer. Samples and standards were diluted in 50 µl ELISA buffer and incubated for 2 h at RT. Afterwards biotinylated detection antibody and streptavidin-HRP were added, either successively in 50 µl ELISA buffer each or simultaneously, and incubated at RT for 2 h plus 20 min or 1 h, respectively. Finally, 50 µl of a 1:1 mix of the substrate solutions were added to allow HRP-mediated substrate oxidation into the blue-colored product. The reaction was stopped using 50 µl 1 M H_2SO_4 and absorbance at 450 nm (reference: 570 nm) was measured using an Epoch microplate spectrophotometer. The sample cytokine concentration could then be calculated with the help of the standard curve.

4.2.3.5 Multiplex cytokine flow cytometry

Supernatants of stimulated cells were collected 24 h after transfection and analyzed for expression of 13 cytokines (IL13, IL-1α, IL-22, IL-2, IL-5, IL-21, IL-6, IL-10, IL-27, IFNγ, TNFα, IL-4, IL-7) using a FlowCytomix Kit as described in the manual. Briefly, the sample was mixed with antibody-coated beads, each specific for one of the analytes. Biotin-conjugated antibodies with the same specificity were added and subsequently bound by streptavidin-PE to allow detection of the cytokine. Flow cytometry was used to measure PE fluorescence, which is proportional to the amount of analyte, and to identify the analyte with the help of different bead sizes and intensities of an internal fluorescent dye.

4.2.4 In vivo methods

4.2.4.1 Establishment and treatment of B16 tumors

Female, 10 weeks old C57BL/6 mice (Janvier Labs, Saint Berthevin Cedex, France) were inoculated with 1×10^5 B16F10 cells in 50 µl PBS subcutaneously into the left flank. Treatment protocols of vitamin C and 3pRNA application are indicated. For the immunohistochemical analysis of CXCL10

animals were treated four times with vitamin C followed by a single 3pRNA dose the day before killing. mRNA expression and FACS analyses were performed after repeated treatment comprising daily application of vitamin C and threefold 3pRNA administration within 10 days. Vitamin C (Pascorbin®) was injected intraperitoneally using 30 mg/mouse. For delivery of 3pRNA the oligonucleotide was first diluted in H_2O and the transfection reagent JetPEI was mixed with 10% glucose (0,16 µl JetPEI per 1 µg RNA) and incubated for 5 min at RT. The JetPEI preparation was then added to the 3pRNA dilution in a 1:1 ratio and incubated for approximately 30 min. A final dose of 20 µg 3pRNA per mouse in 50 µl was administered into the tumor. Tumor size was measured daily using calipers and mice were sacrificed when the tumor diameter reached 15 mm. Tumor samples were removed and fixed for 24 h in zinc buffer for immunohistochemistry or were frozen in liquid nitrogen for RNA extraction and qPCR analysis. Furthermore, tumors and draining lymph nodes were processed into single cell suspensions using 70 µm cell strainer for flow cytometric analysis.

4.2.4.2 Immunohistochemistry

Fixed tissue samples were bedded in paraffin and cut into 4 µm slices using a microtome. After blocking with 5% BSA in PBS for 1 h, immunohistochemistry was performed with α-CXCL10 antibody using 1 µg/ml in 200 µl antibody diluent over night. The secondary antibody as well as detection reagents were components of the Dako REAL Detection System Kit. Accordingly, slices were successively incubated with biotin-coupled α-rabbit antibody 1:300 in 200 µl antibody diluent for 1 h and streptavidin-alkaline phosphatase for 30 min. Finally, RED chromagen was added until red staining was visible. The sections were further stained with haematoxylin and eosin (H&E) for 15 sec and sealed afterwards. Pictures were taken with a DMLB immunofluorescence microscope.

4.2.4.3 Ethics statement

All mice were bred and housed in individually ventilated cages in the House for Experimental Therapy (HET) of the University Hospital in Bonn. All mouse experiments were performed according to ethical protocols approved by the local and regional ethical committees.

4.2.5 Statistical analysis

If not indicated otherwise data represent mean and SEM of at least three independent experiments. Statistical differences between groups were determined by unpaired, two-tailed student's t test with confidence intervals of 95% using GraphPad Prism 6 (GraphPad Software, La Jolla, CA, USA). * ($p < 0,05$), ** ($p < 0,01$), *** ($p < 0,001$), **** ($p < 0,0001$), ns: not significant.

5 Results

At the latest since the development of effective immune checkpoint-inhibitors, immunotherapy is considered one of the most promising treatment strategies against cancer. Among the huge variety of immunotherapy approaches currently investigated and developed, the targeted activation of the innate immune receptor RIG-I by its 3pRNA ligand is unique in the way that it can concurrently activate anti-tumor immunity and act in a tumoricidal manner. 3pRNA therapy is currently tested in preclinical studies and is approaching its clinical trial phase. As part of research into effective tumor immunotherapy, the local tumor microenvironment has drawn increasing attention as it can profoundly influence local immune responses. The major environmental factor being investigated here is hypoxia, as it is a characteristic feature of most solid tumors that contributes to metabolic changes, genomic instability and angiogenesis [107]. Hypoxia also induces EMT in cancer cells, thereby favoring tumor dissemination and metastasis formation, but also providing an escape mechanism from T-cell-mediated immune attack [97]. Since hypoxia also negatively affects chemo- and irradiation therapy, it has become an established negative prognostic marker. Although knowledge on the devastating effects of hypoxia on anti-tumor immune responses is increasing, the impact of oxygen deprivation on the functioning of tumor-intrinsic innate PRR like RIG-I and the outcome of RIG-I-mediated immunotherapy are still unknown. This thesis delivers insights into hypoxia-induced effects on the expression of cytosolic PRRs as well as into the influence of hypoxia on RIG-I signaling outcome and its involved regulatory components. The attained findings were ultimately used to test measures to enhance RIG-I function under hypoxia *in vitro* and steps were undertaken to translate these results to the *in vivo* therapeutic setting.

5.1 Hypoxia and EMT in B16F10 melanoma cells

Throughout this thesis comparisons have been made between normoxic cells incubated at 20% oxygen and hypoxic cells, which were kept at 2% oxygen. To ensure that the chosen conditions of oxygen concentration and pre-incubation time induced intracellular hypoxia, B16F10 cells were analyzed for hypoxia-dependent pimonidazole-adducts. Figure 5 demonstrates that a 24-hour incubation at 2% oxygen resulted in an entirely pimonidazole-positive population confirming the hypoxic status of the cells.

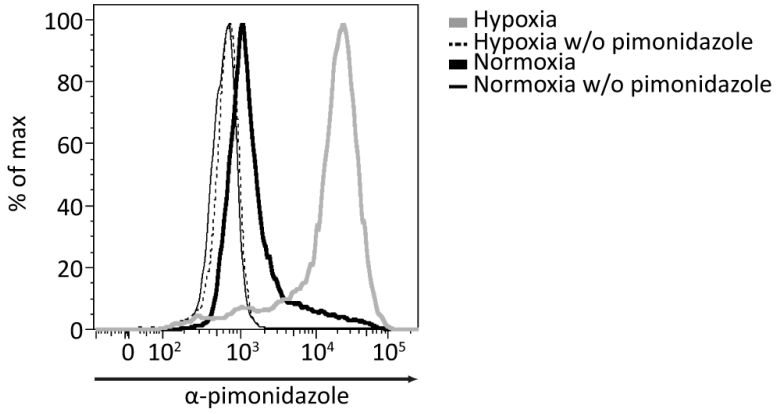

Figure 5: Hypoxia in B16F10 cells. Hypoxia-dependent pimonidazole-adducts were detected using flow cytometry after 24 h at 20% or 2% oxygen. A representative histogram of three independent experiments is shown. w/o: without, max: maximum.

Although hypoxia-induced EMT is a widely accepted phenomenon, vast variations on investigated cell types and oxygen concentrations can be found in the literature. Since the chosen setting of oxygen deprivation induced a hypoxic status of the cells while being reasonably well tolerated, B16F10 cells were tested under these specific conditions for a selection of EMT markers. Firstly, the transfer of normoxic melanoma cells to an oxygen concentration of 2% led to a time-dependent increase in the production of ROS as shown in Figure 6A. Furthermore, cellular fractionation into cytosolic and nuclear components with subsequent western analysis revealed an enhanced translocation of the NFκB subunit p65 into the nucleus upon 24 hours of hypoxia (Figure 6B). Both, ROS production and activation of NFκB, have been associated with EMT [94,95]. Additionally, a more direct representation of dedifferentiation was provided by protein expression analysis of the intermediate filament vimentin, representing a mesenchymal marker, and the melanocyte differentiation antigen gp100. Following a 24-hour incubation under hypoxic conditions vimentin expression in B16F10 cells was increased, whereas gp100 was extensively downregulated, firmly indicating melanoma cell dedifferentiation by the hypoxia regimen used (Figure 6C,D).

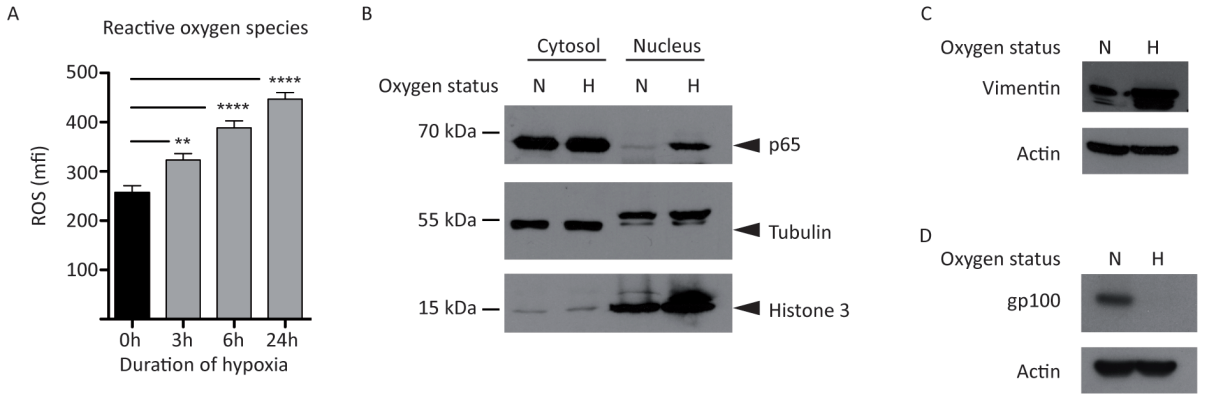

Figure 6: Hypoxia induces epithelial-to-mesenchymal transition (EMT) via reactive oxygen species (ROS)-production and NFκB activation. (A) Time-dependent ROS production upon transfer of B16F10 cells to hypoxia was detected by flow cytometry using a ROS-reactive dye. Mean and +SEM of three independent experiments are shown. (B) Nuclear translocation of p65 after 24 h of hypoxia as determined by western blot. Tubulin and histone 3 represent controls for cellular fractionation. Representative blots of three independent experiments are shown. (C-D) Expression of vimentin (C) and gp100 (D) in B16F10 cells upon 24 h of hypoxia. Actin is shown as loading control. Representative blots of three independent experiments are depicted. Statistical analysis was performed using student's t test. ** ($p < 0.01$), **** ($p < 0.0001$). N: normoxia, H: hypoxia, mfi: mean fluorescence intensity, h: hours.

Bhattacharya *et al.* recently provided evidence for hypoxia-elicited robust downregulation of the IFNαR in human melanoma cells [105]. Therefore, the expression of IFNαR was investigated additionally, using the here established hypoxia regimen on B16F10 cells. As shown in Figure 7, oxygen deprivation led to a 50% reduction of IFNαR expression, which might have implications for cellular IFN sensitivity and the IFN-dependent feed-forward loop important for efficient RIG-I signaling.

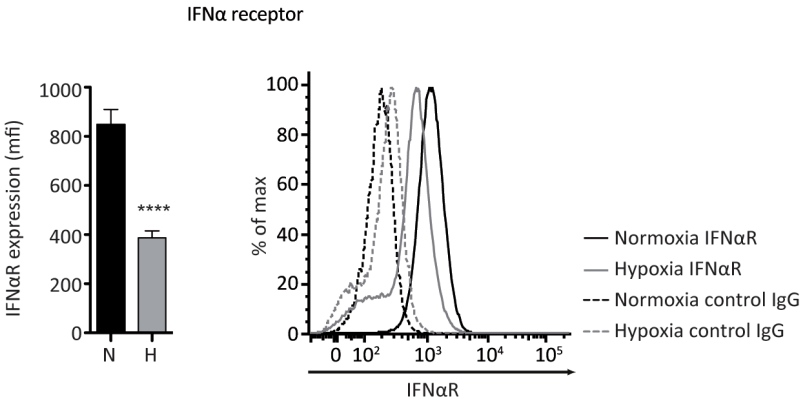

Figure 7: Reduced interferon α receptor (IFNαR) expression under hypoxia. IFNαR expression in B16F10 cells was determined by flow cytometry after 24 h of hypoxia. *Left panel:* Mean and +SEM of four independent experiments. *Right panel*: A representative histogram is depicted. Statistical analysis was performed using student's t test. **** ($p < 0.0001$). N: normoxia, H: hypoxia, mfi: mean fluorescence intensity, max: maximum, IgG: immunoglobulin G.

Taken together these results validate the suitability of the experimental setup for the investigation of intracellular hypoxia, and confirm ROS- and NFκB-dependent EMT coinciding with reduced IFNαR expression in hypoxic B16F10 cells. Of note, EMT and IFNα desensitization might ultimately influence

the outcome of studies testing RIG-I function in the hypoxia setting by alterations of transcriptomes and proteomes or hampered feed-forward signaling as discussed below.

5.2 Hypoxia-mediated effects on pattern recognition receptor expression

To uncover the effects of hypoxia on 3pRNA-induced RIG-I activation, the expression of the receptor itself was initially investigated. The observed reduction of IFNαR expression in hypoxic cells was thereby suggestive of likewise decreased RIG-I expression, given that an IFN-dependent feed-forward loop leads to a strong upregulation of the receptor after 3pRNA transfection (Figure 8). Since hypoxia is only one of several environmental stress factors that can be encountered within a tumor, the influence of hypoxia on RIG-I upregulation was compared to starvation (0% FCS) and necrotic cell co-incubation (Figure 8A). While the latter factors did not have an impact on the RIG-I response, oxygen deprivation strongly reduced 3pRNA-stimulated receptor expression. Shortening the RIG-I signaling pathway by direct treatment with recombinant IFNα likewise resulted in hypoxia-mediated attenuation of RIG-I protein upregulation (Figure 8B). The comparison of 3pRNA and IFNα is of particular interest as the latter is already approved for the treatment of malignant melanoma and other solid tumors. These results indicate hypoxia to influence ISG upregulation that might result in decreased RIG-I signaling and diminished 3pRNA-mediated anti-tumor immunity.

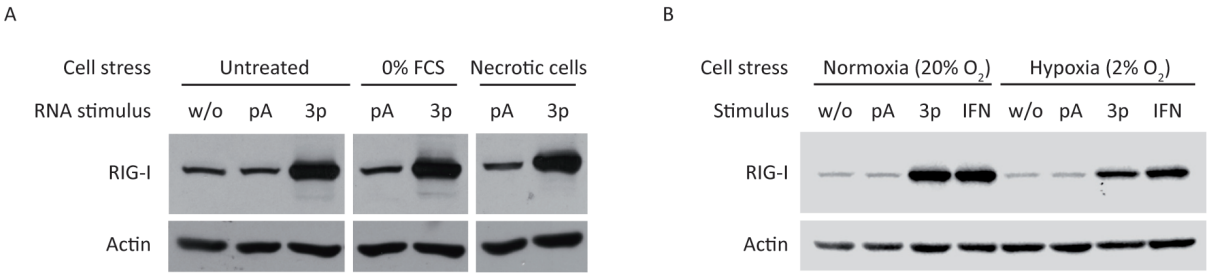

Figure 8: Hypoxia attenuates RIG-I protein upregulation. (A-B) B16F10 cells were exposed to 0% FCS or co-culture with necrotic B16F10 cells (A) or were incubated at 2% oxygen for 24 h (B) and subsequently stimulated with the indicated oligonucleotides or IFNα. RIG-I expression was determined by western blot 24 h after stimulation. Actin served as loading control. Representative blots of two and three independent experiments are shown respectively. w/o: without treatment, pA: poly-A, 3p: 3pRNA, FCS: fetal calve serum, IFN: recombinant IFNα.

The reduced upregulation of RIG-I was independent of its basal expression level, as unstimulated cells showed equal RIG-I amounts on average (Figure 9, time point 0 h). Moreover, the observed difference was not due to a delay of the RIG-I response, because prolongation of stimulation time from 24 hours to 48 hours did not equalize hypoxic and normoxic RIG-I expression (Figure 9).

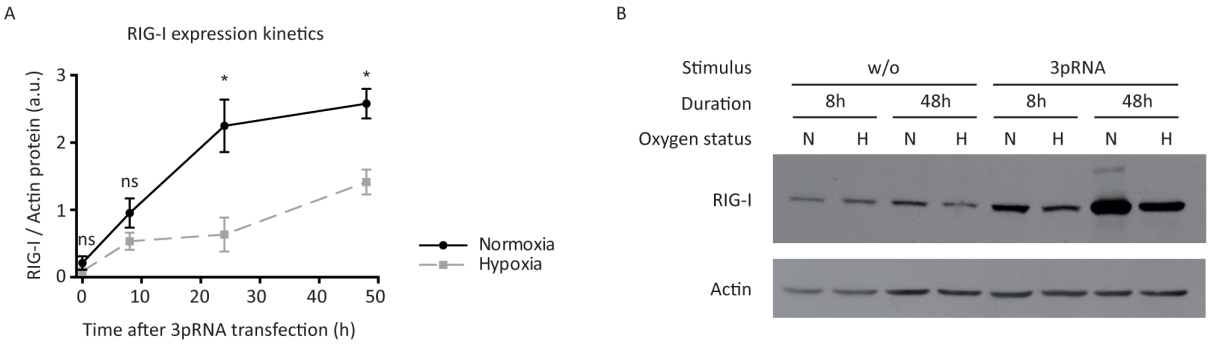

Figure 9: RIG-I expression kinetics upon 3pRNA stimulation. (A-B) RIG-I expression was detected by western blot following a 24 h hypoxic pre-incubation and 3pRNA stimulation for the indicated time spans. (A) Quantified RIG-I expression normalized to actin as mean and +/-SEM of three independent experiments. (B) A representative western blot illustrating RIG-I expression 8 h and 48 h after 3pRNA transfection. Statistical analysis was performed using student's t test. * ($p < 0.05$). ns: not significant, w/o: without treatment, N: normoxia, H: hypoxia, h: hours, a.u: arbitrary units.

Since hypoxia is not defined as one specific pO_2-value, but rather describes a range of oxygen concentrations between anoxia (0% O_2) and the physiologic tissue-pO_2, 3pRNA-induced RIG-I protein upregulation was additionally investigated using the near-anoxia oxygen concentration of 0.2%. Interestingly, this further reduction of oxygen supply did not result in stronger inhibition of RIG-I responsiveness, therefore indicating an uncompromising event upon oxygen deprivation rather than a dose-dependent effect (Figure 10).

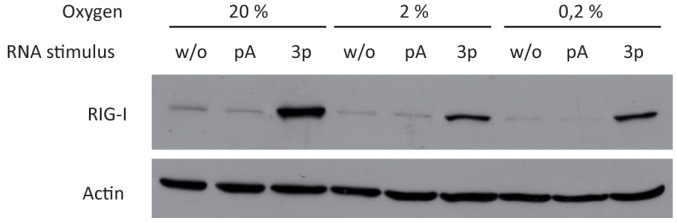

Figure 10: Attenuation of RIG-I upregulation is not aggravated by increased hypoxia. B16F10 cells were pre-incubated under normoxic (20%) or hypoxic (2% and 0.2%) conditions and transfected with the indicated oligonucleotides. RIG-I expression was determined 24 h later. Actin served as loading control. A representative blot is shown. w/o: without treatment, pA: poly-A, 3p: 3pRNA,

As RIG-I activation was achieved by 3pRNA transfection, it had to be verified whether the blunted RIG-I upregulation was caused by deteriorated transfection efficiency under hypoxia. This was ruled out by transfection of B16F10 cells with fluorescein amidite (Fam)-labeled 3pRNA, which showed equal cellular fluorescence intensities under normoxia and hypoxia (Figure 11).

Having observed a hypoxia-mediated inhibition of RIG-I protein induction, consequently the influence of oxygen deprivation on the receptor's mRNA expression was investigated. Surprisingly, 3pRNA-triggered RIG-I mRNA upregulation took place equally well under normoxia and hypoxia. Importantly, IFNα substantially lost its potential to stimulate RIG-I mRNA expression following

oxygen deprivation (Figure 12A). Taking into account that hypoxia equally attenuates RIG-I protein upregulation, but differentially acts on RIG-I mRNA expression induced by 3pRNA or IFNα, these results suggest at least partly independent mechanisms for regulation of IFNα- and 3pRNA-induced RIG-I responsiveness under hypoxia.

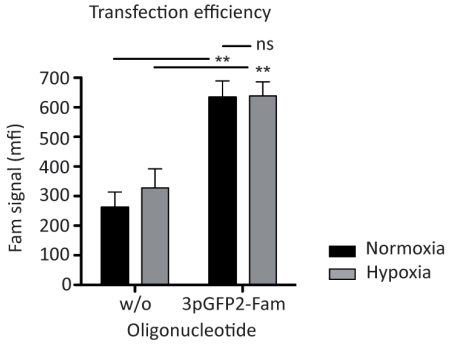

Figure 11: Transfection efficiency is not affected by hypoxia. Normoxic and hypoxic B16F10 cells were transfected with a Fam-labeled 3pRNA. Transfection efficiency was determined by flow cytometry 5 h later. Mean and +SEM of two independent experiments are shown. Statistical analysis was performed using student's t test. ** ($p < 0.01$). ns: not significant, w/o: without treatment, Fam: fluorescein amidite, mfi: mean fluorescence intensity, 3pGFP2: 3pRNA

Possibly, posttranscriptional regulation might explain the observation of unaffected mRNA levels and yet reduced RIG-I protein expression. One potential mechanism of posttranscriptional regulation is the degradation of mRNA. Using actinomycin D as transcription inhibitor, the time dependent decay of RIG-I mRNA was tested under normoxia and hypoxia. While degradation of RIG-I mRNA occurred less rapidly following 3pRNA transfection as compared to unstimulated cells, no difference in mRNA stability was detectable between both oxygen conditions (Figure 12B). Accordingly, it is unlikely that enhanced mRNA degradation is the ultimate cause for reduced RIG-I protein amounts under hypoxia.

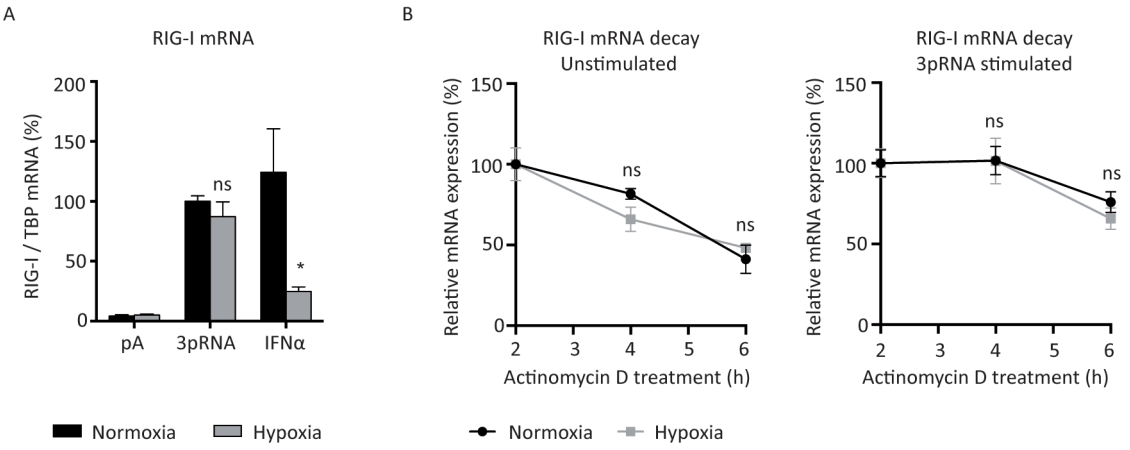

Figure 12: Hypoxia differentially influences 3pRNA- or IFNα-induced RIG-I mRNA expression. (A) Expression of RIG-I mRNA in B16F10 cells was determined 6 h after stimulation with the indicated oligonucleotides or IFNα and is shown relative to TBP. Mean and +SEM of three independent experiments, each normalized to 3pRNA treatment under normoxia, are shown. (B) Expression of RIG-I mRNA was quantified 2 h, 4 h and 6 h after transcription blockade with actinomycin D in unstimulated (*left*) or 3pRNA-treated (*right*) cells. Values were normalized to actin and are shown relative to the 2 h time point for each oxygen condition. Mean and +/-SEM of one or three biological replicates, each consisting of two technical replicates, are depicted respectively. Statistical analysis was performed using student's *t*-test. * ($p < 0.05$), ns: not significant, pA: poly-A, h: hours.

To verify whether the reduction of receptor upregulation caused by hypoxia might also apply to another RIG-I like receptor family member, the expression of MDA5 was analyzed. Although MDA5 differs from RIG-I in terms of ligand specificity, it employs the same downstream signaling complexes to elicit an immune response and also initiates an IFN-mediated feed-forward loop [108,109]. While treatment of melanoma cells with 3pRNA, poly-I:C or IFNα each led to a profound increase of MDA5 protein expression under normoxic conditions, this was practically lost under hypoxia (Figure 13). Attenuation of the MDA5 responsiveness by oxygen deprivation appeared to be even more severe than for RIG-I, since 3pRNA or IFNα treatment was still able to enhance RIG-I expression over basal levels, which was not the case for MDA5.

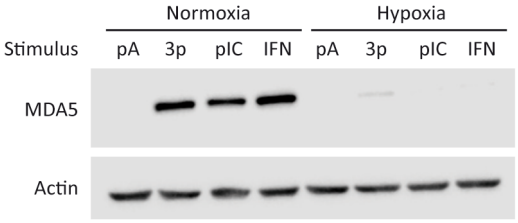

Figure 13: Hypoxia prevents MDA5 protein upregulation upon stimulation. B16F10 cells were incubated at 2% oxygen for 24 h and subsequently stimulated with the indicated oligonucleotides or IFNα. MDA5 expression was determined 24 h later. Actin served as loading control. A representative blot of three independent experiments is shown. pA: poly-A, 3p: 3pRNA, pIC: poly-I:C.

In summary these results show for the first time that hypoxia attenuates RLR protein upregulation triggered by ligand transfection as well as IFNα treatment. Importantly, the inhibitory effect of oxygen deprivation is less severe for RIG-I expression than for MDA5. The desensitization of hypoxic melanoma cells to IFNα, shown on RIG-I mRNA and protein level, relates well to the diminished IFNαR expression at 2% oxygen. On the other hand, the attenuated 3pRNA-induced RIG-I protein responsiveness does not derive from transcriptional effects and seems to be independent of hampered IFN signaling.

5.3 Hypoxia-mediated effects on RIG-I signaling outcome

The discovery of the inhibiting impact of hypoxia on 3pRNA-induced RIG-I expression gave rise to the question whether also RIG-I signaling outcome might be negatively affected. Concerning 3pRNA-based cancer immunotherapy, the influence of hypoxia on RIG-I-mediated tumoricidal effects as well as cytokine production and lymphocyte activation is of outmost interest and is described in the following section.

The analysis of cell death via flow cytometry indicated mild induction of apoptosis through transfection of 3pRNA in normoxic B16F10 cells (Figure 14). This related well to the low dose of

3pRNA used throughout this thesis, as the main focus was to investigate different aspects of RIG-I signaling in living cells. Importantly, while the hypoxic incubation itself induced noticeable apoptosis as compared to normoxic untreated cells, the pro-apoptotic potential of 3pRNA was preserved under oxygen deprivation (Figure 14). These results suggest that the attenuation of 3pRNA-induced RIG-I protein expression is not necessarily reflected in reduced tumoricidal activity of 3pRNA.

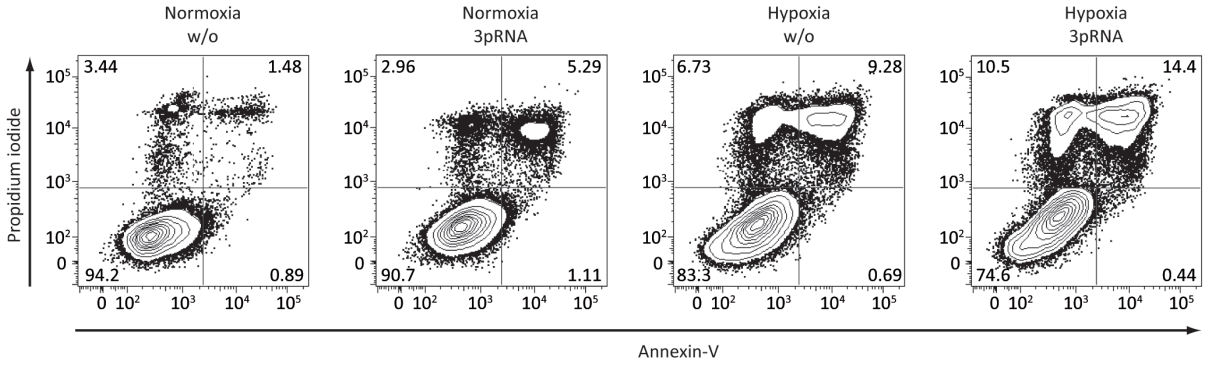

Figure 14: Hypoxia does not influence 3pRNA-induced apoptosis. B16F10 cells were incubated under hypoxic atmosphere for 24 h and subsequently stimulated with 3pRNA. Apoptosis was measured 24 h later using Annexin-V and propidium iodide detection by flow cytometry. Representative plots of three experiments are shown. w/o: without treatment

Interferon-stimulated genes and pro-inflammatory cytokines are commonly used as surrogate markers for functional activation of the RIG-I signaling pathway and represent major players in the establishment of an early immune response upon 3pRNA-sensing by RIG-I. To determine the influence of hypoxia on RIG-I signaling the mRNA expression of a selection of ISGs and cytokines was assessed below. Furthermore, since recombinant IFNα had turned out to be likewise ineffective in inducing RIG-I under hypoxia, 3pRNA-dependent RIG-I signaling outcome was compared to IFNα treatment in melanoma cells. As shown in Figure 15A hypoxia caused an almost complete loss of IFNα-induced mRNA upregulation of IFIT1 (interferon-induced protein with tetratricopeptide repeats 1), CXCL10 (interferon-dependent lymphocyte-attracting chemokine) and viperin, which was comparable to the reduction of IFNα-stimulated RIG-I expression (Figure 12A). In contrast, 3pRNA-mediated mRNA induction of all target genes was not significantly altered by oxygen deprivation. Furthermore, mRNA stability of IFIT1 and CXCL10 following 3pRNA transfection was equal under normoxia and hypoxia (Figure 15B). These results again demonstrate a superior function of 3pRNA-based RIG-I activation to direct IFNα stimulation in a hypoxic environment and suggest that 3pRNA-triggered RIG-I signaling outcome resists hypoxia-mediated IFNα desensitization.

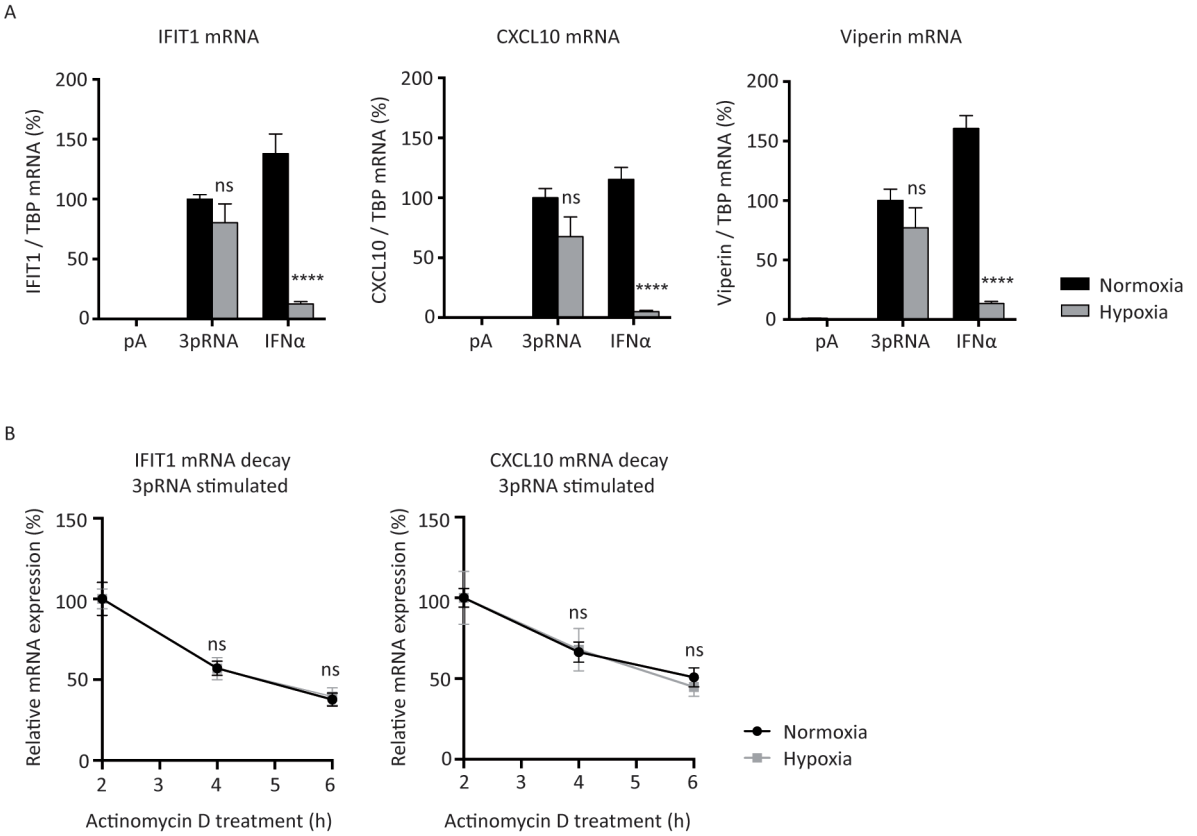

Figure 15: 3pRNA- and IFNα-induced interferon-stimulated gene (ISG) mRNA expression and -stability. (A) Expression of IFIT1, CXCL10 and viperin mRNA in hypoxic B16F10 cells was determined 6 h after stimulation with the indicated oligonucleotides or IFNα and is shown relative to TBP. Mean and +SEM of three independent experiments, each normalized to 3pRNA treatment under normoxia, are shown. (B) Expression of IFIT1 and CXCL10 mRNA was quantified 2 h, 4 h and 6 h after transcription blockade with actinomycin D in 3pRNA-treated cells. Values were normalized to actin and are shown relative to the 2 h time point for each oxygen condition. Mean and +/-SEM of two independent experiments are depicted. Statistical analysis was performed using student's *t*-test. * ($p < 0.05$), ns: not significant, pA: poly-A, h: hours. Experiments depicted in (A) were performed by Dorottya Horváth.

Expanding the investigation of 3pRNA-induced cytokine expression by the quantification of secreted type-I IFN, TNFα, CXCL10 and IL-6 finally revealed functional modulation of the 3pRNA-induced RIG-I response under oxygen deprivation. Interestingly, hypoxia caused a significant increase of the 3pRNA-triggered production of type-I IFN and TNFα (Figure 16A-B). On the other hand 3pRNA-induced CXCL10 protein secretion was reduced, an effect not observed on the mRNA expression level (Figure 16C). Lastly, the amount of IL-6 was not affected by hypoxia (Figure 16D). Altogether, oxygen deprivation influenced translation or secretion of cytokines that was not necessarily reflected by their mRNA expression. These results indicate a modulation of RIG-I signaling under hypoxia rather than an inhibition, and might suggest interplay between hypoxia- and EMT-mediated influencing of translation.

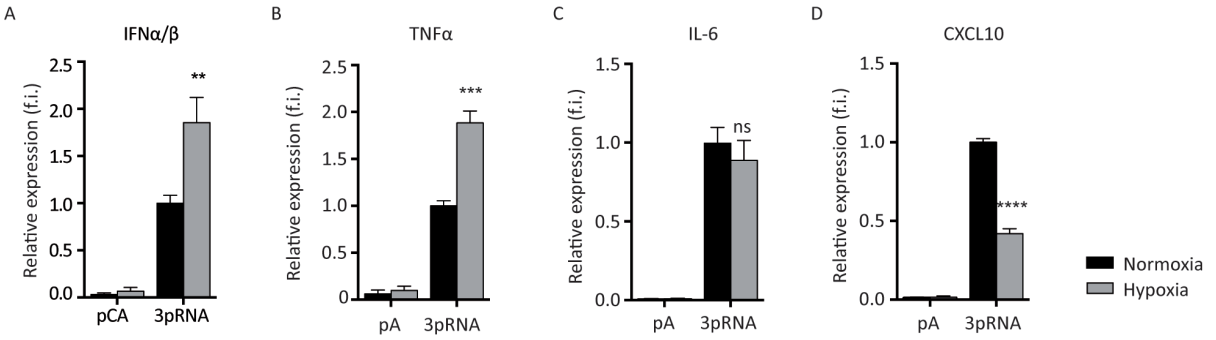

Figure 16: Hypoxia modulates the 3pRNA-induced cytokine pattern. (A-D) Normoxic or hypoxic B16F10 cells were stimulated with the indicated oligonucleotides for 24 h. (A) Type-I IFN in the supernatant was quantified using a cellular reporter assay. (B) TNFα secretion was determined by multiplex flow cytometry-based cytokine analysis. (C) IL-6 and (D) CXCL10 amounts were measured using ELISA. Diagrams depict mean and +SEM of three independent experiments, each normalized to 3pRNA treatment under normoxia. Statistical analysis was performed using student's *t*-test. ** ($p < 0.01$), *** ($p < 0.001$), **** ($p < 0.0001$). ns: not significant, pA: poly-A, pCA: poly-CA, f.i.: fold induction.

To investigate whether the hypoxia-mediated suppression of RIG-I upregulation and modulation of cytokine secretion is a general phenomenon or is restricted to certain cell types, a comparison of different cell lines and primary cells was conducted. Firstly, a panel of three melanoma cell lines was tested for RIG-I-, CXCL10- and IL-6 expression after 3pRNA stimulation under hypoxia. The investigated cell lines HCmel23, HCmel17 and HCmel3 were all derived from the HGF-Cdk4^{R24C} model of spontaneous autochthonous melanoma and closely mirror the histopathology and immune-ignorance of spontaneous human cutaneous melanoma [110]. In concordance with B16F10 melanoma cells all three cell lines displayed a suppressed 3pRNA-induced RIG-I protein upregulation under hypoxic conditions (Figure 17A-C, left panel). Moreover, cytokine production by HCmel23 and HCmel17 resembled the pattern of B16F10 cells with a reduction of CXCL10 and unaffected IL-6 (Figure 17A-B, middle and right panel). In HCmel3 cells CXCL10 showed a trend towards hypoxia-mediated decrease, but also a significant suppression of IL-6 (Figure 17C, middle and right panel). As conclusion, despite variations in the extent, the attenuation of 3pRNA-induced RIG-I response and the modulation of cytokine expression under hypoxia could generally be recapitulated in a set of syngeneic mouse melanoma cell lines.

As representatives for non-malignant cells of the same tissue the murine melanocyte cell line Melan-A and the murine epidermal keratinocyte cell line Kera 308 were tested for RIG-I responsiveness under hypoxia. In contrast to melanoma, these cell lines did not show a reduction in RIG-I protein expression upon 3pRNA stimulation at 2% pO_2 (Figure 18A-B, left panel). While the CXCL10 production was equally suppressed in malignant and non-malignant cells, only the latter exhibited significantly reduced amounts of IL-6 (Figure 18A-B, middle and right panel).

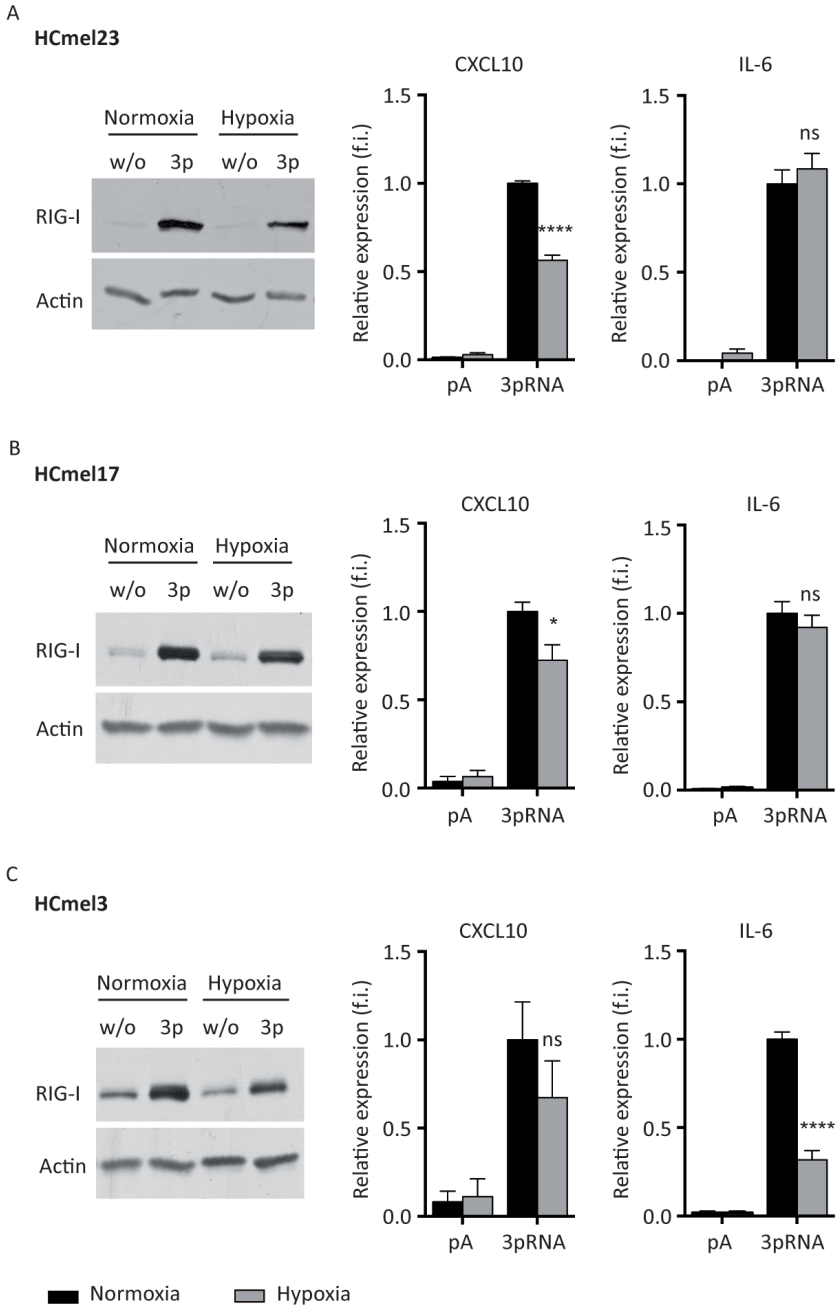

Figure 17: Hypoxia influences the 3pRNA-triggered RIG-I response in various melanoma cell lines. (A-C) Normoxic or hypoxic murine melanoma cells HCmel23 (A), HCmel17 (B) and HCmel3 (C) were stimulated with the indicated oligonucleotides for 24 h. *Left panel*: RIG-I expression as determined by western blot. Actin is shown as loading control. Representative blots of three independent experiments are depicted. *Middle and right panel*: CXCL10 and IL-6 were measured using ELISA. Diagrams show mean and +SEM of three independent experiments, each normalized to 3pRNA treatment under normoxia. Statistical analysis was performed using student's *t*-test. * ($p < 0.05$), **** ($p < 0.0001$). ns: not significant, w/o: without treatment, 3p: 3pRNA, pA: poly-A, f.i.: fold induction.

A third class of cell types that would inevitably encounter the hypoxic tumor microenvironment upon 3pRNA therapy is immune cells. Interestingly, in primary murine splenocytes hypoxia did not have any effect on 3pRNA-induced RIG-I upregulation or IL-6 production, whereas CXCL10 was significantly reduced (Figure 19). Of note, the difference between basal- and 3pRNA-induced RIG-I expression was low, with an increase of approximately 2-fold in contrast to a 10-fold increment for B16F10 cells.

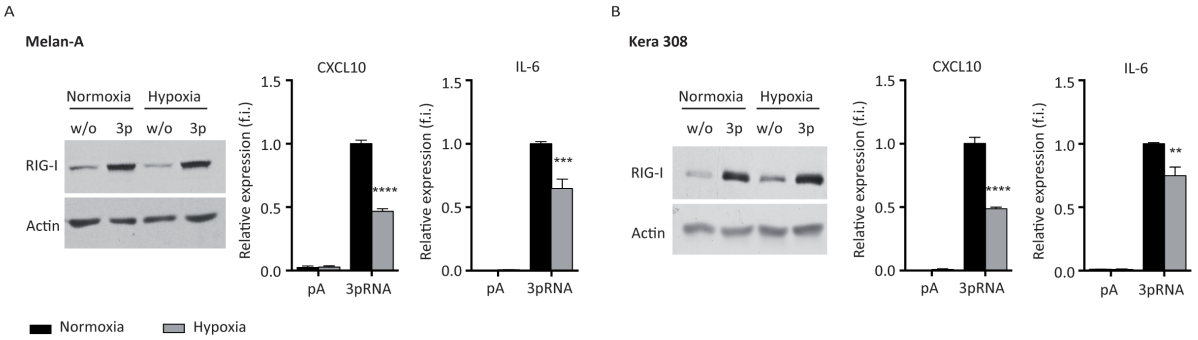

Figure 18: Hypoxia-mediated effects on the 3pRNA-induced RIG-I response in non-malignant cells. (A-B) Normoxic or hypoxic cells of the murine melanocyte cell line Melan-A (A) and of the murine epidermal keratinocyte cell line Kera 308 (B) were stimulated with the indicated oligonucleotides for 24 h. *Left panel*: Western blots showing RIG-I expression and actin as loading control. A representative blot of three independent experiments is depicted. *Middle and right panel:* CXCL10 and IL-6 amounts as mean and +SEM of three independent experiments, each normalized to 3pRNA treatment under normoxia. Statistical analysis was performed using student's *t*-test. ** ($p < 0.01$), *** ($p < 0.001$), **** ($p < 0.0001$). w/o: without treatment, 3p: 3pRNA, pA: poly-A, f.i.: fold induction.

In summary, the here investigated cell types, namely malignant melanoma cell lines, non-malignant melanocyte and keratinocyte cell lines as well as primary splenocytes, all showed that hypoxia had an inhibitory effect on 3pRNA-triggered CXCL10 production, whereas the influence on IL-6 varied between cell types and cell lines. Still, reduction of RIG-I protein upregulation was restricted to malignant melanoma cells and was absent in the investigated non-malignant cell types.

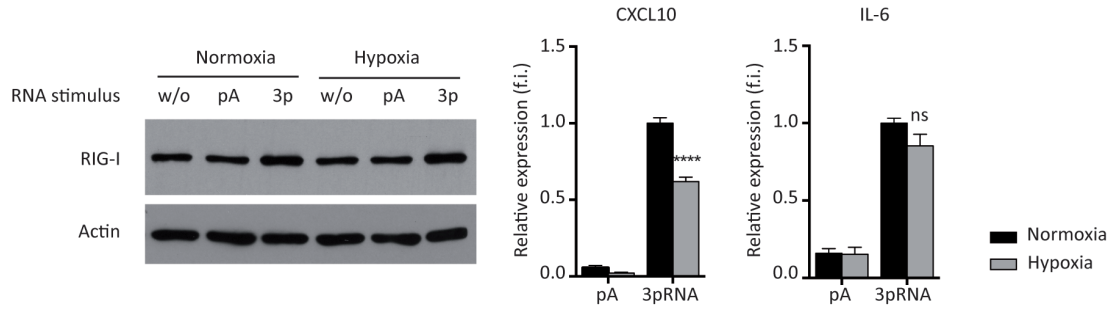

Figure 19: Hypoxia-mediated effects on the 3pRNA-induced RIG-I response in murine splenocytes. Normoxic or hypoxic mouse splenocytes were stimulated with the indicated oligonucleotides for 24 h. *Left panel*: Western blot of RIG-I expression and actin as loading control. A representative blot of three independent experiments is shown. *Middle and right panel:* CXCL10 and IL-6 amounts are depicted as mean and +SEM of three independent experiments, each normalized to 3pRNA treatment under normoxia. Statistical analysis was performed using student's *t*-test. **** ($p < 0.0001$). ns: not significant, w/o: without treatment, 3p: 3pRNA, pA: poly-A, f.i.: fold induction.

Apart from the induction of cytokines and type-I IFN, an important function of 3pRNA-mediated RIG-I activation is the upregulation of MHC class-I on the cell surface. This allows enhanced melanocyte differentiation antigen presentation to cytotoxic T-cells, enabling their activation via MHC class-I – T-cell receptor/CD8 receptor interaction. The RIG-I-induced MHC class-I upregulation thus spurs cytotoxic T-cell effector function, and thereby bridges innate and adaptive immunity. A comparison

of 3pRNA- and IFNα treatment of B16F10 cells showed a strong increase of MHC class-I expression triggered by both components under normoxia. Interestingly, oxygen deprivation almost completely abrogated IFNα-induced MHC class-I upregulation, while its 3pRNA-triggered expression was not affected on average (Figure 20A). Similar results were obtained for the analysis of PDL-1 expression on B16F10 cells, upregulation of which has been found to be an additional indicator of RIG-I activation in our lab. This immune checkpoint molecule confers inhibition of T-cell proliferation and cytokine production upon interaction with its corresponding receptor PD-1 on lymphocytes [111]. Importantly, activation of RIG-I by 3pRNA strongly upregulated PDL-1 as compared to control-RNA transfection (Figure 20B). In concordance with MHC class-I, hypoxia did not alter PDL-1 upregulation upon 3pRNA stimulation, whereas its IFNα-induced expression was clearly diminished (Figure 20B). Furthermore, analysis of the respective receptor PD-1 on splenocytes upon PMA/ionomycin activation revealed equal expression under normoxic and hypoxic conditions (Figure 20C), indicating the existence of a fully intact PD-1/PDL-1 inhibitory axis under hypoxia. In brief summary, hypoxia strongly suppressed IFNα-mediated MHC class-I and PDL-1 expression on B16F10 cells, whereas upregulation of both molecules by 3pRNA treatment was not reduced. These results again indicate functional immune activation by RIG-I under hypoxia and suggest that tumor antigen presentation by MHC class-I on melanoma cells is still working. Yet, since also PDL-1 and PD-1 expression are maintained upon oxygen deprivation, the inhibiting impact of this immune checkpoint likely is preserved as well. This opens up a new avenue of research into anti-PD-1/PDL-1 – 3pRNA combinations, to further release the brakes on anti-tumor immunity.

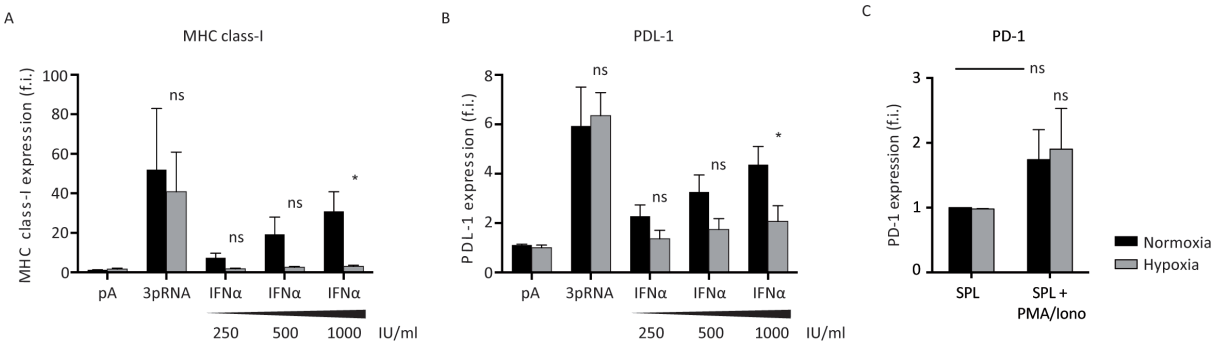

Figure 20: Hypoxia abrogates IFNα- but not 3pRNA-induced MHC class-I and PDL-1 expression. (A-B) Normoxic or hypoxic B16F10 cells were stimulated with the indicated oligonucleotides or IFNα. Expression of MHC class-I (A) and PDL-1 (B) was determined 24 h later by flow cytometry. Mean and +SEM of four to seven independent experiments, each normalized to normoxic, untreated cells, are depicted. (C) Pmel-1 splenocytes were left untreated or activated with PMA/ionomycin for 18 h and expression of PD-1 was analyzed by flow cytometry. Diagrams show mean and +SEM of three independent experiments, each normalized to normoxic, unstimulated conditions. Statistical analysis was performed using student's *t*-test. * ($p < 0.05$). ns: not significant, pA: poly-A, 3p: 3pRNA, SPL: splenocytes, PMA: phorbol 12-myristate 13-acetate, Iono: ionomycin, f.i.: fold induction.

The different parameters of RIG-I signaling outcome investigated above are supposed to eventually contribute to the activation of T- and NK cells to induce tumor specific cell killing. Since oxygen deprivation was found to modulate the 3pRNA-induced cytokine profile, the question was whether immune cells might react differently to stimulated melanoma cells. A co-culture protocol of 3pRNA-transfected melanoma cells together with $gp100_{25-33}$ antigen-specific Pmel-1 splenocytes was applied, to uncover the hypoxia-mediated effects on their mutual interaction (Figure 21A). Compared to control-RNA-transfected cells, 3pRNA-treated B16F10 cells were indeed capable of activating CD8+ T-cells and NK cells as indicated by upregulation of the activation marker CD69 (Figure 21B-C). Furthermore, incubation at hypoxic atmosphere resulted in slightly, but not significantly, lower responses to 3pRNA-transfected melanoma cells. In contrast, treatment of B16F10 cells with IFNα induced only minimal, if any, detectable activation of CD8+ T-cells and NK cells, even when applying high doses of IFNα under normoxic conditions (up to 5000 IU/mL).

Importantly, comparable results could be obtained when the co-culture procedure was performed using HCmel3 melanoma cells together with Pmel-1 splenocytes (Figure 21D-E). Notably, the general ability of T- or NK cells to become activated was not influenced by the employed hypoxia-regimen, since different control incubations did not show an altered CD69 expression under hypoxia (Figure 22). These results indicate no influence of oxygen deprivation on the immune cell activating potential of 3pRNA-treated melanoma cells. This is especially remarkable when taking into account that hypoxia-induced EMT in B16F10 and HCmel3 cells leads to a near-complete loss of melanoma differentiation antigen gp100 expression (Figure 6 and data not shown), the cognate antigen for Pmel-1 T-cells.

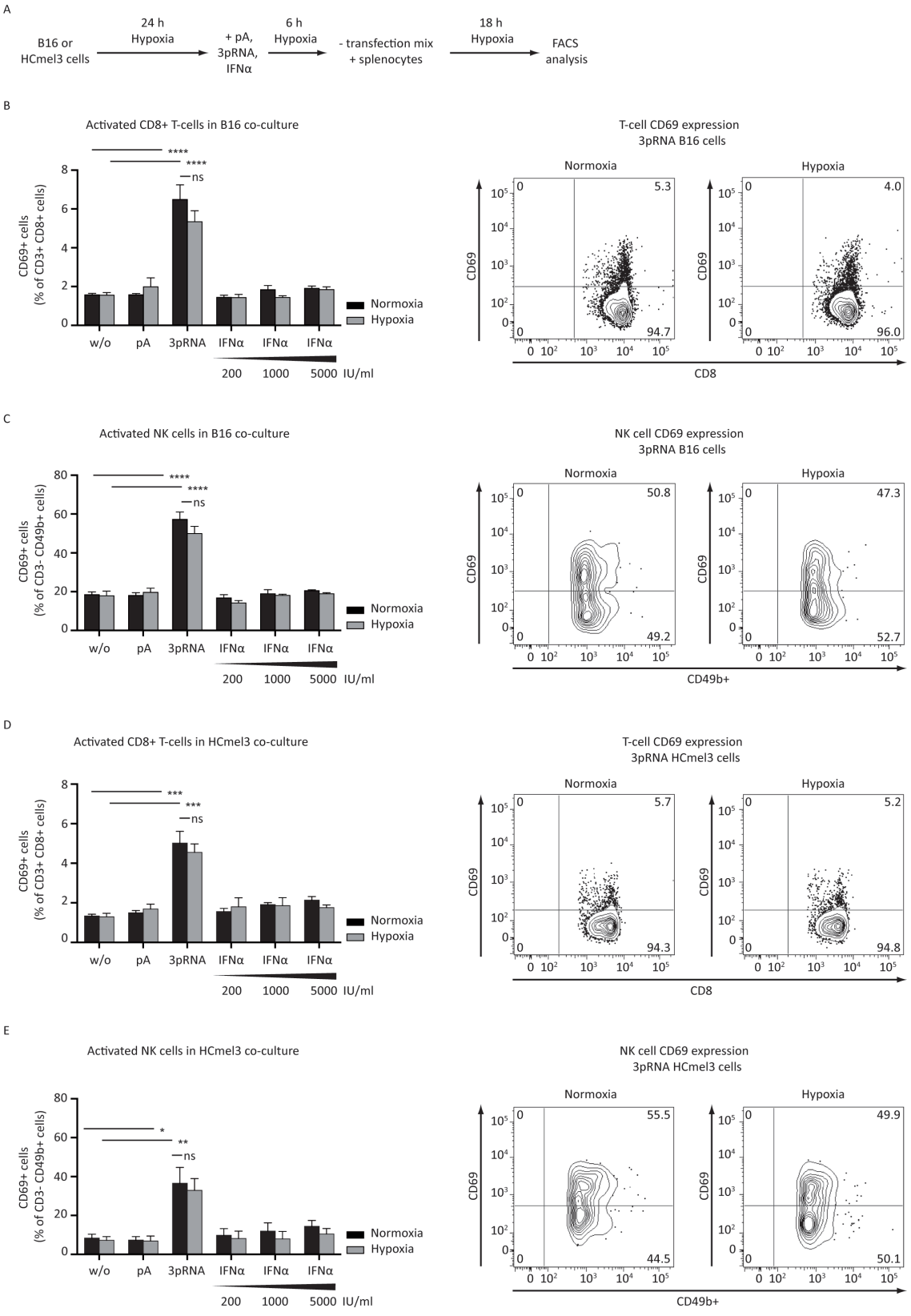

Figure 21: *In vitro* CD8+ T- and NK cell activation through 3pRNA-treated melanoma cells remains fully functional under hypoxia. (A) Schematic representation of the co-culture protocol of melanoma cells and Pmel-1 splenocytes. (B-E) Activation of immune cells was determined by flow cytometric analysis of CD69 expression. *Left panels:* Mean and +SEM of three to nine independent experiments. *Right panels:* Representative flow cytometry plots of co-cultures with 3pRNA-stimulated melanoma cells. (B) Activated CD8+ T-cells in B16F10 co-culture. (C) Activated NK cells in B16F10 co-culture. (D) Activated CD8+ T-cells in HCmel3 co-culture. (E) Activated NK cells in HCmel3 co-culture. Statistical analysis was performed using student's *t*-test. * ($p < 0.05$), ** ($p < 0.01$), *** ($p < 0.001$), **** ($p < 0.0001$). ns: not significant, w/o: without treatment, pA: poly-A.

Altogether, the investigation of RIG-I signaling outcome revealed a sustained immune stimulatory function of 3pRNA treatment under hypoxia. While protein expression or release of type-I interferon and different cytokines was modulated upon oxygen deprivation, MHC class-I and PDL-1 expression as well as T- and NK cell activation worked equally well under normoxia and hypoxia. Moreover, 3pRNA proved to be superior to IFNα treatment concerning all investigated immune-related functions, indicating RIG-I activation resists IFNαR-downregulation and IFNα-desensitization under hypoxia.

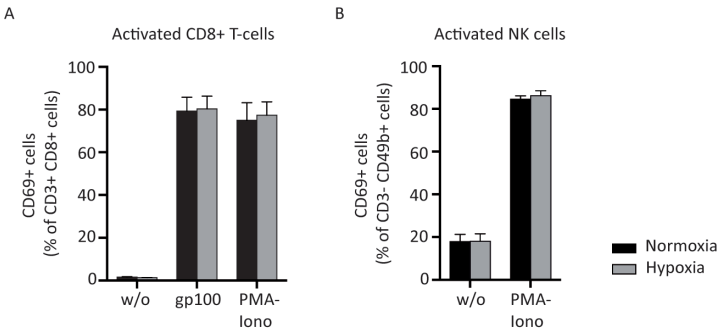

Figure 22: Hypoxia does not affect the capability of cytotoxic effector cells to become activated. (A-B) Pmel-1 splenocytes were activated with $gp100_{25-33}$ peptide or with PMA/ionomycin for 18 h under normoxic or hypoxic conditions. Activation of CD8+ T-cells (A) and activation of NK cells (B) was assessed by flow cytometric analysis of CD69 expression. Mean and +SEM of five to seven independent experiments are shown. w/o: without treatment, PMA: phorbol 12-myristate 13-acetate, iono: ionomycin.

5.4 Hypoxia-mediated effects on regulatory components of RIG-I signaling

To exert its manifold anti-viral effector functions the RIG-I signaling pathway is composed of various interacting proteins and tight regulation is necessary for its proper function. Since on the one hand 3pRNA-induced RIG-I protein upregulation was attenuated by hypoxia, but on the other hand the functional RIG-I response was upheld, the influence of hypoxia on regulatory components of RIG-I signaling required more detailed investigation. Therefore the following section presents the effects of oxygen deprivation on some of the most important molecules and mechanisms that control signal transmission from RIG-I to transcription factors of pro-inflammatory proteins.

Interestingly, the molecular chaperone HSP90 forms a link between hypoxia and RIG-I-signaling as its expression is upregulated by HIF activation and it is involved in the recruitment of TBK1/IRF3 to mitochondria [41,112]. Importantly, HSP90 also protects RIG-I against degradation [40]. Therefore, a possible hypoxia-induced change in HSP90 expression can also affect RIG-I protein levels or signaling outcome. Nevertheless a 24-hour incubation of B16F10 cells at 2% oxygen did neither alter the protein expression of the isoform HSP90α nor of HSP90β (Figure 23).

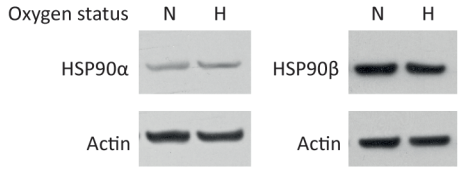

Figure 23: HSP90 expression is not affected by hypoxia. Expression of HSP90α (*left panel*) and HSP90β (*right panel*) in B16F10 cells was determined by western blot upon 24 h of hypoxia. Representative blots of three independent experiments are shown. Actin served as loading control. N: normoxia, H: hypoxia

To alternatively test the possibility that the reduced RIG-I upregulation after 3pRNA stimulation under hypoxia resulted from enhanced proteasomal degradation, RIG-I expression was determined upon proteasome inhibition. Surprisingly, MG132 treatment of B16F10 cells caused a reduction of 3pRNA-triggered RIG-I expression predominantly under hypoxic atmosphere (Figure 24A). This indicates enhanced proteasomal degradation is not responsible for attenuated RIG-I protein upregulation. Instead one might speculate that degradation of another component is required to maintain the remaining RIG-I expression upon oxygen deprivation.

The component that is typically associated with protein degradation is the 8 kDa protein ubiquitin, which additionally plays a role in signal transduction in signaling cascades. Lysine 63 (K63)-linked ubiquitin chains for example are conjugated to RIG-I and are necessary for the interaction of RIG-I with MAVS [36]. As seen in Figure 24B a whole cell protein analysis of K63-ubiquitin-conjugates by western blot did not show differences between normoxic and hypoxic B16F10 cells, neither with and without 3pRNA treatment nor with and without proteasome inhibition using MG132. Thus, enhanced K63-ubiquitination cannot be made responsible for fostering signal transmission from RIG-I to transcription factors and thereby compensating for reduced RIG-I expression under hypoxia.

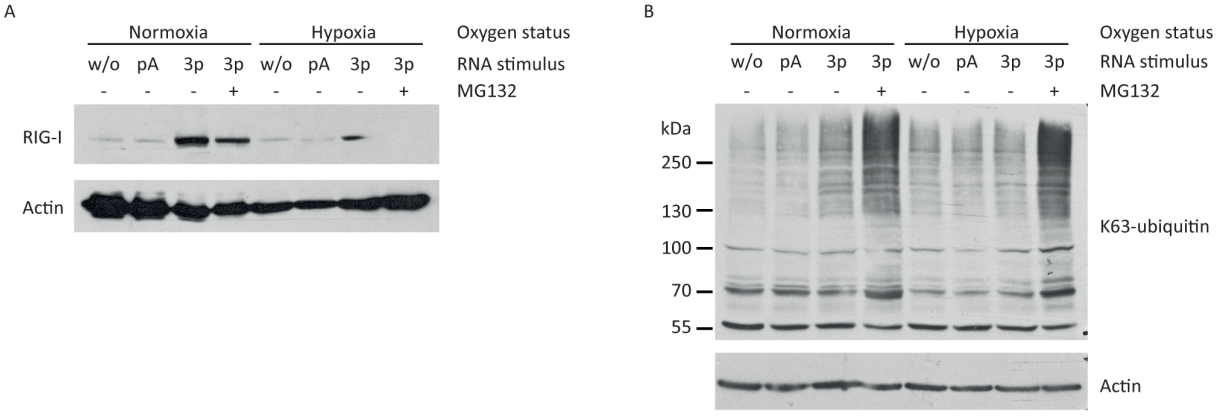

Figure 24: Effects of hypoxia on K63-ubiquitin expression and RIG-I expression upon proteasome inhibition. (A-B) Normoxic or hypoxic B16F10 cells were transfected with the indicated oligonucleotides for 24 h and simultaneously treated with the proteasome inhibitor MG132 where indicated. RIG-I (A) and K63-ubiquitin expression (B) were determined by western blot. Representative blots of three and two independent experiments are depicted respectively. Actin is shown as loading control. w/o: without treatment, pA: poly-A, 3p: 3pRNA, K63: lysine 63.

Lastly, three other important RIG-I signaling components were tested for differential protein expression under hypoxia and normoxia: MAVS, which represents the central signaling adaptor protein of the RIG-I pathway by providing a scaffold for the assembly of RIG-I and a variety of effector molecules at mitochondria. Secondly, the mitochondrial import receptor subunit TOM70, which is required for the HSP90-dependent recruitment of TBK1 and IRF3 to the mitochondrial signaling complex [41]. And lastly, the peroxisomal membrane protein PMP70 was analyzed as indicator of peroxisome abundance, because MAVS also locates to these organelles [28]. As shown in Figure 25A PMP70 expression was slightly reduced by hypoxia independent of RNA transfection, which is in concordance with Walter *et al.* [113]. However, this did not coincide with loss of MAVS protein, instead the overall MAVS expression was not changed (Figure 25B). Interestingly, TOM70 detection revealed an additional 55 kDa product exclusively in hypoxic samples, whereas the expression of the 70 kDa protein was equal to normoxic conditions (Figure 25B).

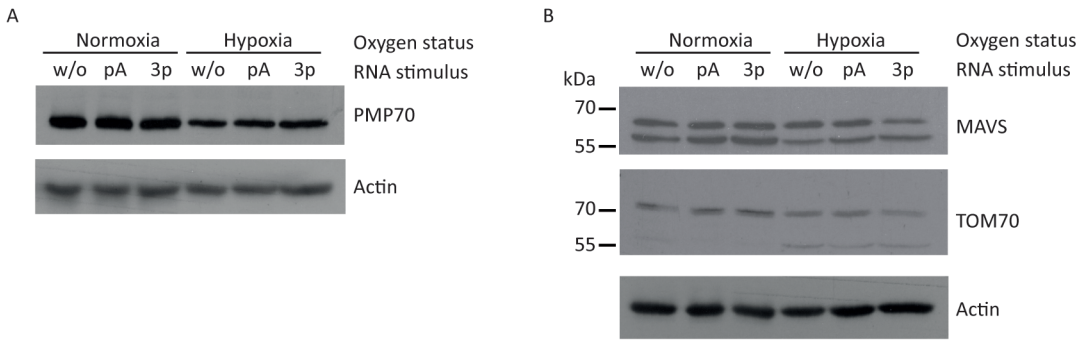

Figure 25: Influence of hypoxia on the protein expression of RIG-I signaling components. (A-B) Normoxic or hypoxic B16F10 cells were transfected with the indicated oligonucleotides for 24 h. Expression of PMP70 (A) and MAVS and TOM70 (B) were determined by western blot. TOM70 was detected after stripping MAVS-specific antibodies. Actin is shown as loading control. Representative blots of three independent experiments are depicted. w/o: without treatment, pA: poly-A, 3p: 3pRNA

Altogether, these data show that hypoxia-mediated reduced RIG-I upregulation is not caused by enhanced RIG-I degradation through the proteasome. Further, attenuated RIG-I expression is not compensated by changes in K63-ubiquitination or HSP90, MAVS and TOM70 protein expression, which can maintain functional RIG-I signaling outcome. Instead it remains unclear whether a different distribution of MAVS between mitochondria and peroxisomes or the additional 55 kDa protein detected by TOM70 antibody exert effects on 3pRNA-induced RIG-I signaling. Taking into account that RIG-I mRNA expression and the functional RIG-I response was not hampered by hypoxia argues for specific changes in translational regulation, posttranslational modifications or miRNA functions that lead to reduced RIG-I protein upregulation. Importantly, all of these play a role in EMT, which is induced by oxygen deprivation in the here-investigated melanoma cells.

5.5 Enhancing RIG-I function under hypoxia and normoxia

Having discovered an attenuation of 3pRNA-induced RIG-I protein upregulation under hypoxia that coincided with EMT, the resulting question was whether counteracting EMT could restore RIG-I expression and thus enhances its immune-activating function. Since the increased production of ROS as well as enhanced NFκB activation can be held responsible for hypoxia-induced EMT, ROS scavenging and NFκB-inhibition were tested for their effects on RIG-I expression. L-ascorbic acid (vitamin C) was utilized as ROS scavenger, which exhibited an approximate 50% reduction of ROS production by B16F10 cells under hypoxic conditions (Figure 26A). To investigate the effects of vitamin C or NFκB inhibition on the differentiation status of hypoxic melanoma cells, the expression of gp100 was analyzed (Figure 26B). Interestingly, 3pRNA transfection alone led to a small increase in gp100 expression under oxygen deprivation. While the addition of vitamin C to the cells 24 hours prior to onset of hypoxia had only marginal effects, prevention of NFκB activation by applying the IκB phosphorylation inhibitor BAY during hypoxic incubation potently reinstated gp100 expression.

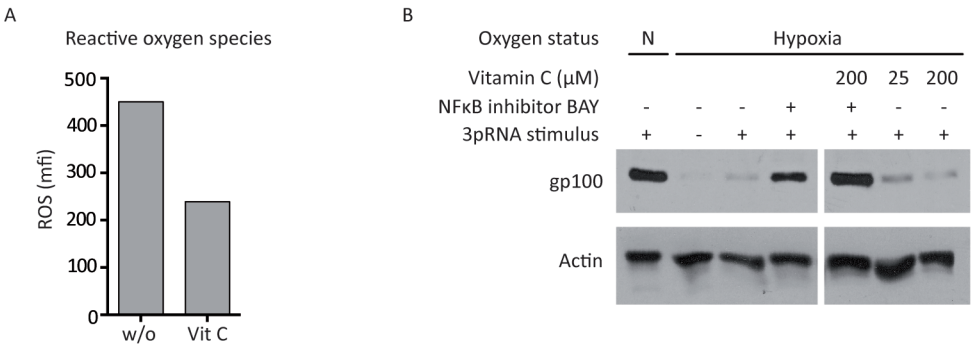

Figure 26: Rescue of melanocyte differentiation antigen expression under hypoxia. (A) During a 24 h incubation under hypoxia B16F10 cells were treated with 200 μM vitamin C. ROS production was determined by flow cytometry using a ROS reactive dye. Results of one performed experiment are shown. (B) gp100 differentiation antigen expression was detected by western blot following vitamin C or NFκB inhibitor treatment under hypoxia. Actin served as loading control. A representative blot of three independent experiments is shown. w/o: without treatment, Vit C: vitamin C, ROS: reactive oxygen species, N: normoxia, mfi: mean fluorescence intensity.

In contrast, ROS scavenging via vitamin C and NFκB inhibition by BAY both significantly restored 3pRNA-induced RIG-I protein expression under hypoxia as seen in Figure 27A. Likewise, two additional NFκB inhibitors, namely BMS (an IKKα-complex blocker) and helenalin (a p65 inhibitor) were also able to re-establish RIG-I responsiveness under hypoxia (Figure 27B), while none of the treatments exerted an effect under normoxic conditions. Figure 27C summarizes the quantification of RIG-I expression upon 3pRNA transfection, indicating that vitamin C was comparably effective as NFκB inhibitors in restoring RIG-I upregulation. Taken together, although the effects on gp100 expression varied, ROS scavengers or NFκB inhibitors open up a possibility to rescue RIG-I protein expression in response to 3pRNA stimulation under hypoxia.

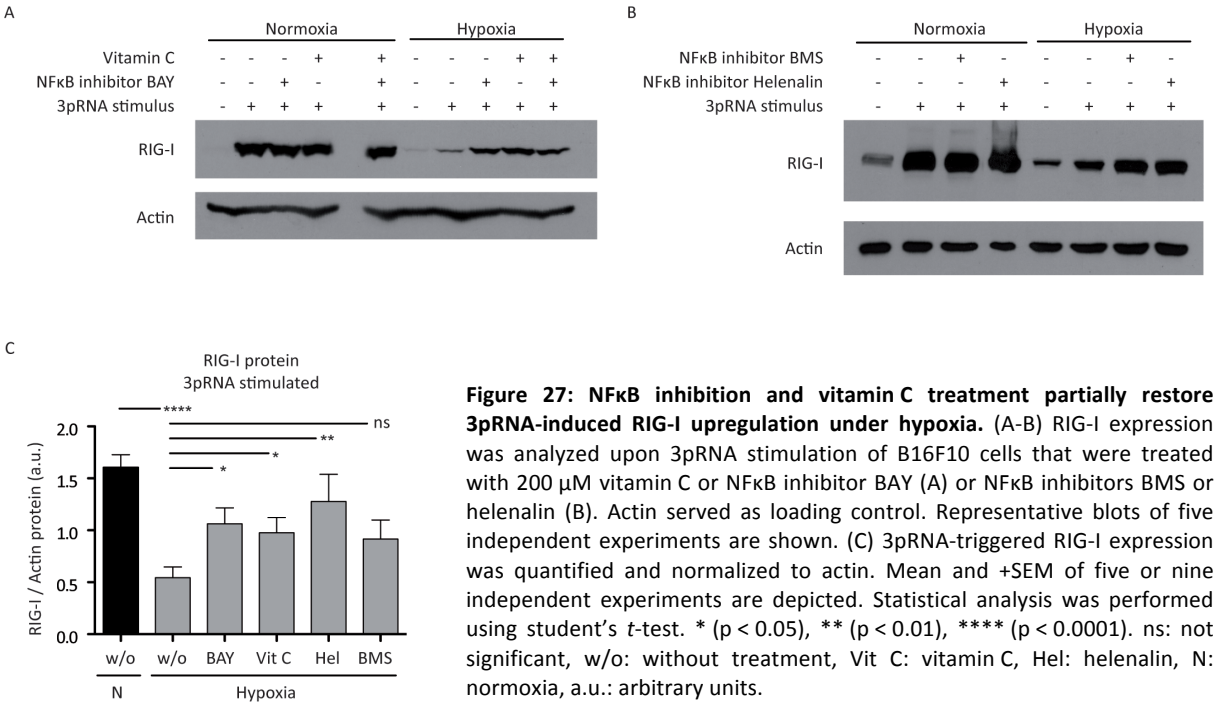

Figure 27: NFκB inhibition and vitamin C treatment partially restore 3pRNA-induced RIG-I upregulation under hypoxia. (A-B) RIG-I expression was analyzed upon 3pRNA stimulation of B16F10 cells that were treated with 200 µM vitamin C or NFκB inhibitor BAY (A) or NFκB inhibitors BMS or helenalin (B). Actin served as loading control. Representative blots of five independent experiments are shown. (C) 3pRNA-triggered RIG-I expression was quantified and normalized to actin. Mean and +SEM of five or nine independent experiments are depicted. Statistical analysis was performed using student's *t*-test. * ($p < 0.05$), ** ($p < 0.01$), **** ($p < 0.0001$). ns: not significant, w/o: without treatment, Vit C: vitamin C, Hel: helenalin, N: normoxia, a.u.: arbitrary units.

At this point it is important to refer to the heterogeneous role of ROS in RIG-I signaling. In contrast to hypoxia-induced ROS, which contribute to EMT and therefore supposedly correlate with an attenuation of RIG-I expression, intrinsic NADPH oxidase (NOX2)-produced ROS and ROS accumulated through dysfunctional autophagy have been shown to be required for proper RIG-I signaling or its amplification respectively [42,114]. Importantly, ROS accumulation can also be achieved by siRNA-mediated suppression of the anti-oxidative transcription factor nuclear factor erythroid 2-related factor 2 (Nrf2). Thus, it seemed worth additionally investigating a method to boost RIG-I function that was intrinsically linked to the 3pRNA agent as 3p-siNrf2. Such dual-functional RNA that combines RIG-I activating capacity and ROS induction via Nrf2 silencing, would deliver both functions to the same cell, whereas vitamin C treatment might not reach all 3pRNA-stimulated cells in sufficient amounts. The superior function of the 3p-siRNA combination over 3pRNA alone was demonstrated *in vitro* in B16F10 cells in terms of enhanced CXCL10 production and augmented tumor cell apoptosis (Figure 28A-B). As 3pRNA-induced RIG-I mRNA expression was not further enhanced by the siRNA function (Figure 28C), the superior performance of 3p-siNrf2 was shown to be independent of Nrf2 knockdown-related direct RIG-I upregulation. Despite these promising *in vitro* results, preliminary data investigating the therapeutic potential of 3p-siNrf2 in a transplantable B16 tumor model, showed the strongest effect when extra ROS were induced through the additional application of depigmenting-agent monobenzone (data not shown). Since further elaboration was beyond the scope of this thesis, studies were focused on the ability of vitamin C to enhance RIG-I expression under hypoxia.

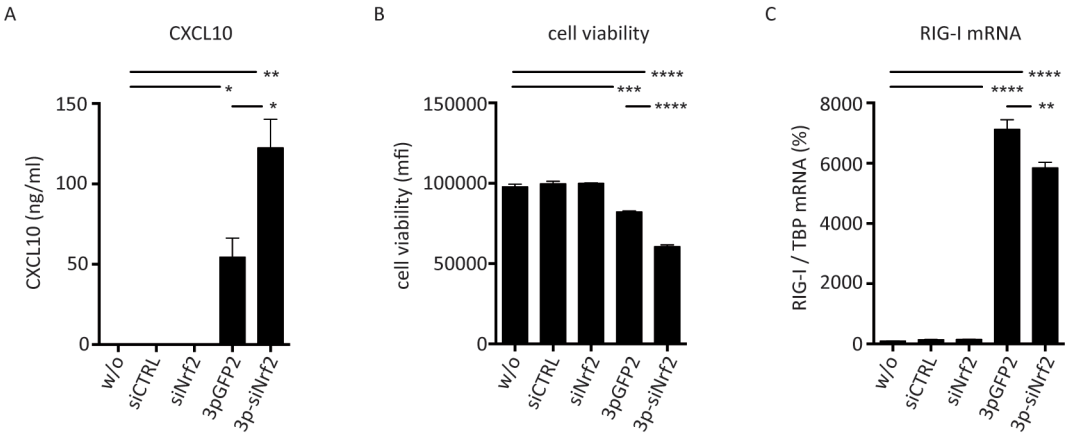

Figure 28: Superior cytokine release and tumor cell toxicity of bi-functional 3p-siNrf2 over 3pRNA alone. (A-C) B16F10 cells were transfected with the indicated oligonucleotides for 24 h. (A) CXCL10 amounts were quantified in the supernatant using ELISA. (B) Cell viability was measured using CellTiter-Blue assay. (C) RIG-I mRNA expression was determined by RT-qPCR and normalized to TBP. Results are shown relative to untreated cells. Mean and +SEM of technical triplicates are shown. Statistical analysis was performed using student's *t*-test. * ($p < 0.05$), ** ($p < 0.01$), *** ($p < 0.001$), **** ($p < 0.0001$). w/o: without treatment, siCTRL: control siRNA, siNrf2: Nrf2-specific siRNA, 3pGFP2: 3pRNA without target, 3p-siNrf2: Nrf2-specific siRNA with 3p-function. Experiments were performed by Christian Hagen.

In conclusion, accumulation of ROS by downregulation of anti-oxidative proteins can act in favor of RIG-I-mediated anti-viral or anti-tumoral effects under normoxia, whereas under hypoxic conditions ROS scavenging protects against attenuation of RIG-I expression.

5.6 EMT and immune activation in vitamin C-supported 3pRNA therapy *in vivo*

Since the induction of EMT is one of the major impacts of hypoxia on tumor cells, the main focus of this work remained to counteract EMT and thus investigate a potential means to enhance RIG-I function *in vivo*. In contrast to a prolonged inhibition of NFκB *in vivo*, application of systemic vitamin C has little side effects and is already in use for the treatment of different indications in humans. That is why ROS scavenging via vitamin C was chosen for tests in combination with therapeutic 3pRNA-mediated immunotherapy in a transplantable B16 mouse model. Investigation of intratumoral RIG-I levels showed a weak basal expression in untreated as well as vitamin C-treated mice, which was considerably boosted in the 3pRNA-treated group. Yet, additional administration of vitamin C did not further enhance RIG-I protein expression (Figure 29). Of note, this analysis included whole tumor lysates consisting of normoxic and hypoxic areas, whereas *in vitro* experiments compared two distinct setups of 20% versus 2% oxygen.

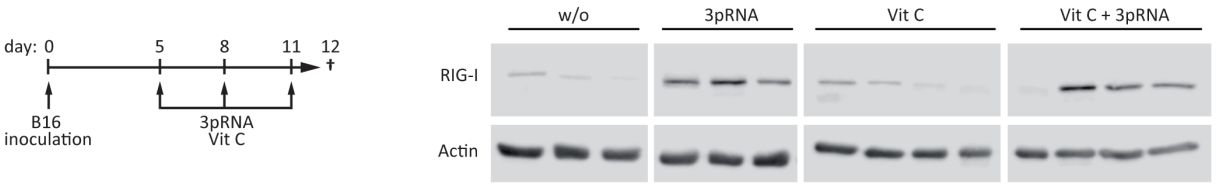

Figure 29: 3pRNA therapy enhances RIG-I expression in B16 tumors. Established subcutaneous tumors were treated with 3pRNA (i.t.) and vitamin C (i.p.) as indicated and RIG-I expression was determined in tumor lysates. Actin served as loading control. Three to four mice per group are shown.

Immunohistochemistry studies further revealed profoundly induced CXCL10 production in tumors upon intratumoral 3pRNA transfection as indicated by Figure 30A. Importantly, addition of vitamin C to 3pRNA therapy further augmented the expression of the immunostimulatory cytokine, while vitamin C alone did not induce CXCL10 expression. Similar results were obtained when CXCL10 mRNA was quantified in tumor biopsies (Figure 30B).

The tumors were additionally analyzed for expression of melanoma differentiation markers to assess the influence of vitamin C on EMT *in vivo*. In concordance with gp100 protein expression in hypoxic B16F10 cells (Figure 26B), tumors also exhibited significantly increased gp100 mRNA expression upon 3pRNA therapy, either with or without vitamin C treatment (Figure 31A). Likewise, the mRNA expression of tyrosinase-related protein-2 (TRP2) was upregulated by 3pRNA alone and in combination with vitamin C (Figure 31B). The combinatorial approach furthermore led to a slight but significant enhancement of tyrosinase expression as compared to untreated tumors (Figure 31C).

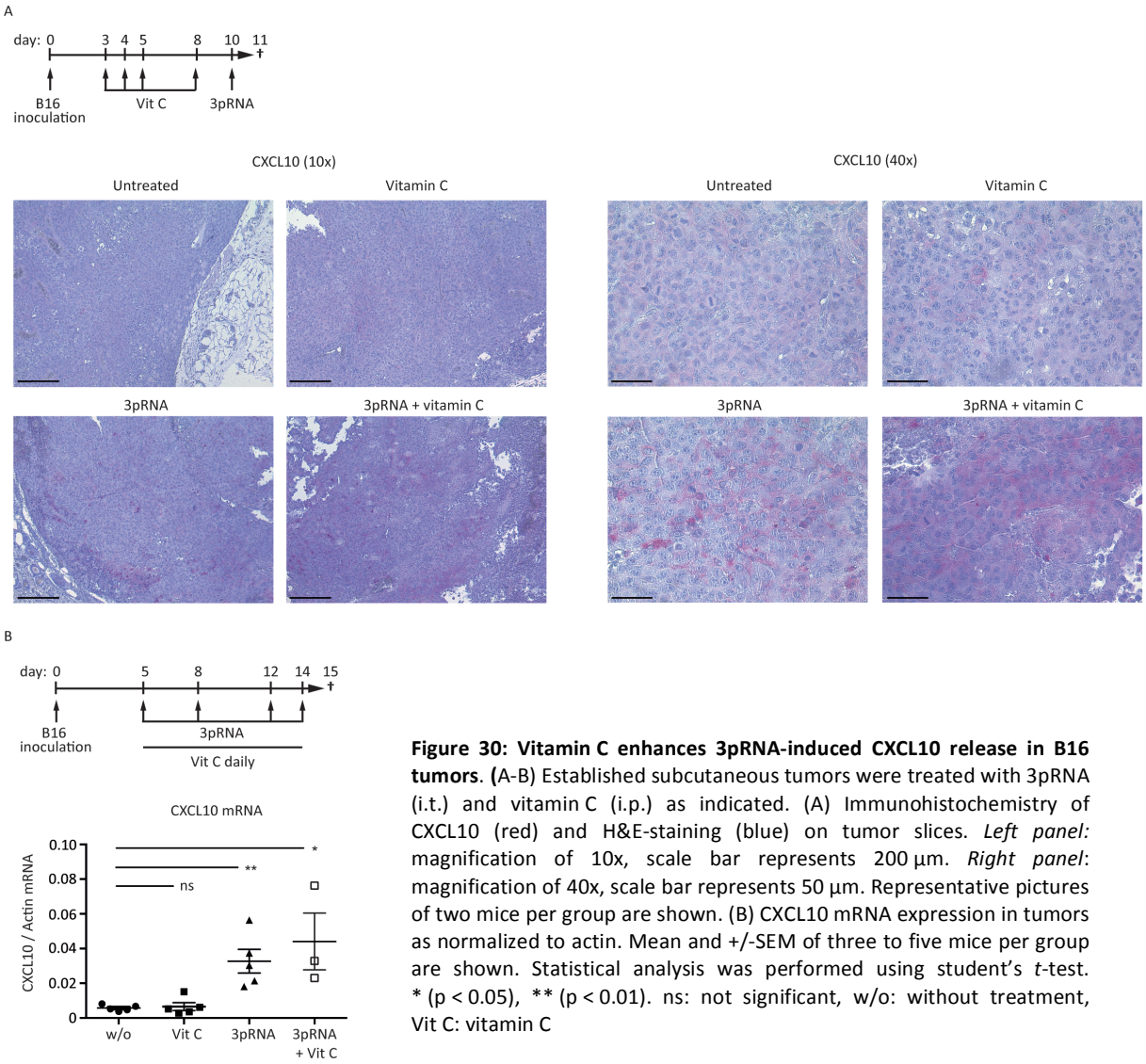

Figure 30: Vitamin C enhances 3pRNA-induced CXCL10 release in B16 tumors. **(**A-B) Established subcutaneous tumors were treated with 3pRNA (i.t.) and vitamin C (i.p.) as indicated. (A) Immunohistochemistry of CXCL10 (red) and H&E-staining (blue) on tumor slices. *Left panel:* magnification of 10x, scale bar represents 200 µm. *Right panel*: magnification of 40x, scale bar represents 50 µm. Representative pictures of two mice per group are shown. (B) CXCL10 mRNA expression in tumors as normalized to actin. Mean and +/-SEM of three to five mice per group are shown. Statistical analysis was performed using student's *t*-test. * ($p < 0.05$), ** ($p < 0.01$). ns: not significant, w/o: without treatment, Vit C: vitamin C

Altogether, these results indicate the transition of melanoma cells into a more differentiated state by 3pRNA treatment *in vivo*. Although vitamin C did not significantly enhance differentiation, it supported the formation of a pro-inflammatory tumor microenvironment by enhancing 3pRNA-mediated CXCL10 production, thus potentially facilitating immune cell responses.

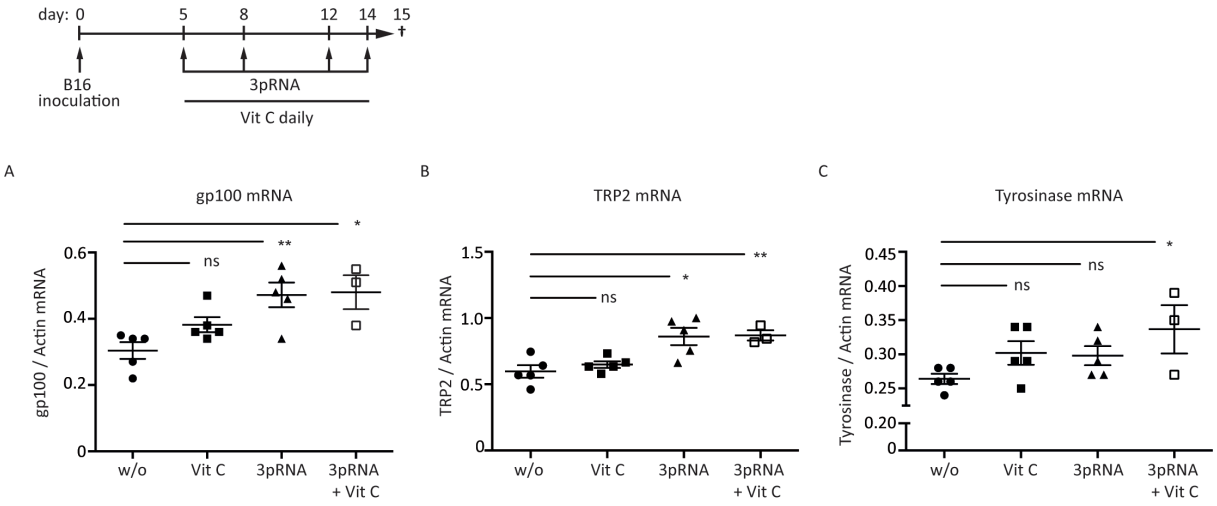

Figure 31: Differentiation antigen expression in vitamin C- and 3pRNA-treated B16 tumors. (A-C) Established subcutaneous tumors were treated with vitamin C (i.p.) and 3pRNA (i.t.) as indicated. mRNA expression of the differentiation antigens gp100 (A), TRP2 (B) and tyrosinase (C) was determined in tumor samples and normalized to actin. Mean and +/-SEM of three to five mice per group are shown. Statistical analysis was performed using student's *t*-test. * ($p < 0.05$), ** ($p < 0.01$). ns: not significant, w/o: without treatment, Vit C: vitamin C

Investigation of immune cell activity within B16 tumors firstly revealed an increase of MDSC upon 3pRNA treatment. This was indicated by a significant increase in Gr-1 mRNA expression in tumor samples (Figure 32A) and higher numbers of CD11b+ Gr-1+ NK1.1- CD3- cells as determined by flow cytometry (Figure 32B). On the one hand, this observation revealed a negative side effect of 3pRNA therapy as MDSC are known to suppress anti-tumor immunity [115]. On the other hand, 3pRNA treatment was able to strongly induce NK cell activation in tumor-draining lymph nodes as shown by upregulation of the activation markers CD69 and CD11c (Figure 32C). Both, MDSC infiltration and NK cell activation were not significantly influenced by addition of vitamin C to 3pRNA therapy. In contrast, solely the combination of both compounds enabled NK cell infiltration into the tumors, a necessary prerequisite to exert their anti-tumor effects (Figure 32D).

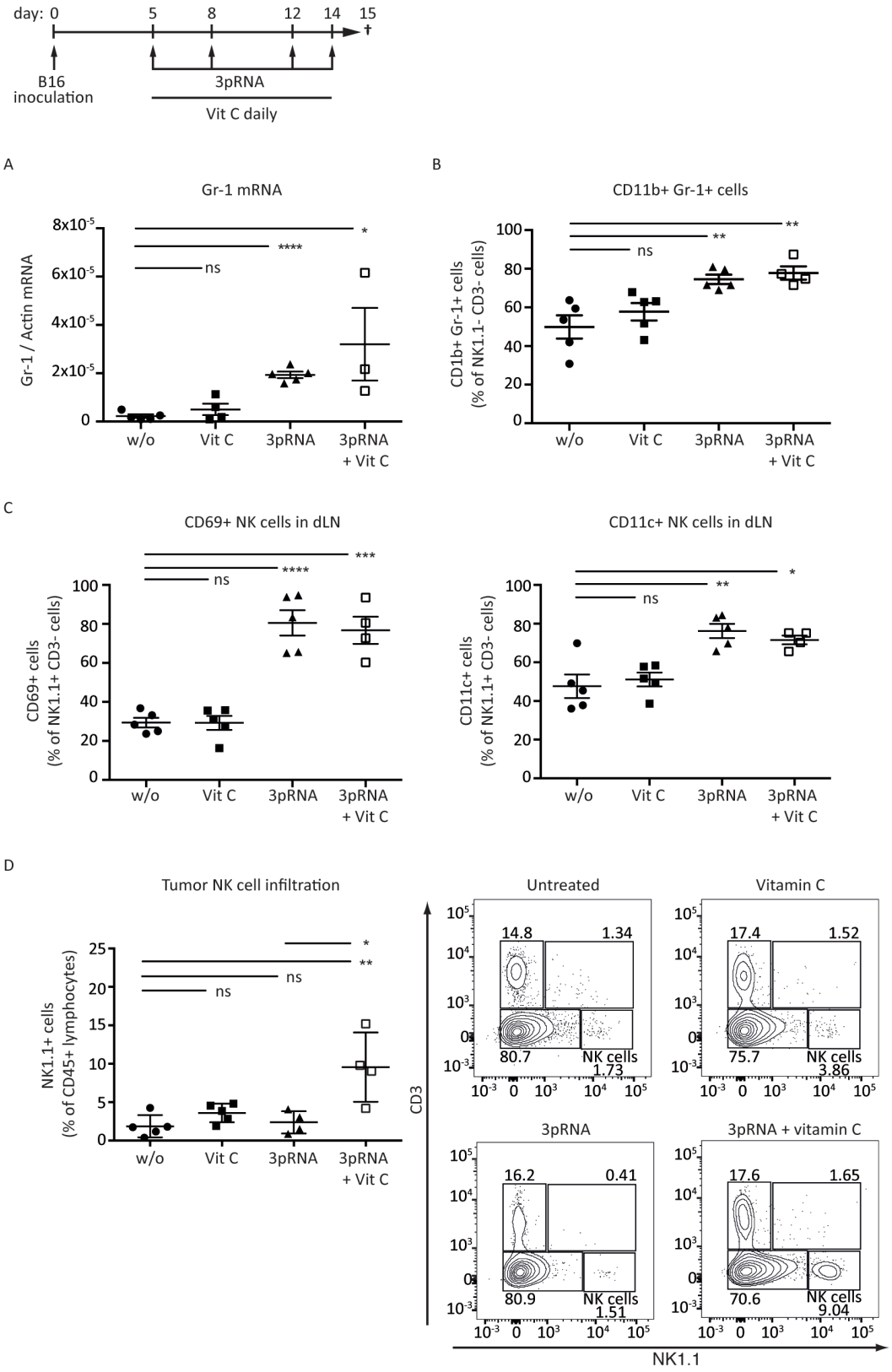

Figure 32: Effects of vitamin C-supported 3pRNA therapy on immune cell subsets. (A-D) Established subcutaneous tumors were treated as indicated. (A) Expression of Gr-1 mRNA in tumor samples as normalized to actin. (B) Quantification of CD11b+ Gr-1+ MDSC in tumors by FACS analysis. (C) Activation of NK cells in tumor-draining lymph nodes as determined by their CD69 (*left panel*) and CD11c (*right panel*) expression. Mean and +/-SEM of three to five mice are shown. (D) Amount of NK1.1+ cells in tumor samples. *Left panel:* Mean and +/-SEM of four to five mice. *Right panel:* A representative flow cytometry analysis. Statistical analysis was performed using student's *t*-test. * ($p < 0.05$), ** ($p < 0.01$), *** ($p < 0.001$), **** ($p < 0.0001$). ns: not significant, w/o: without treatment, Vit C: vitamin C, dLN: draining lymph node

The overall beneficial role of vitamin C addition to 3pRNA therapy was finally demonstrated by a more profound inhibition of tumor growth in comparison to 3pRNA alone (Figure 33A) and improved survival of mice treated with the combinatorial approach (Figure 33B).

In summary, vitamin C proved suitable for the re-establishment of 3pRNA-triggered RIG-I expression in hypoxic melanoma cell cultures and could enhance 3pRNA-induced anti-tumor immunity in a transplantable murine melanoma model.

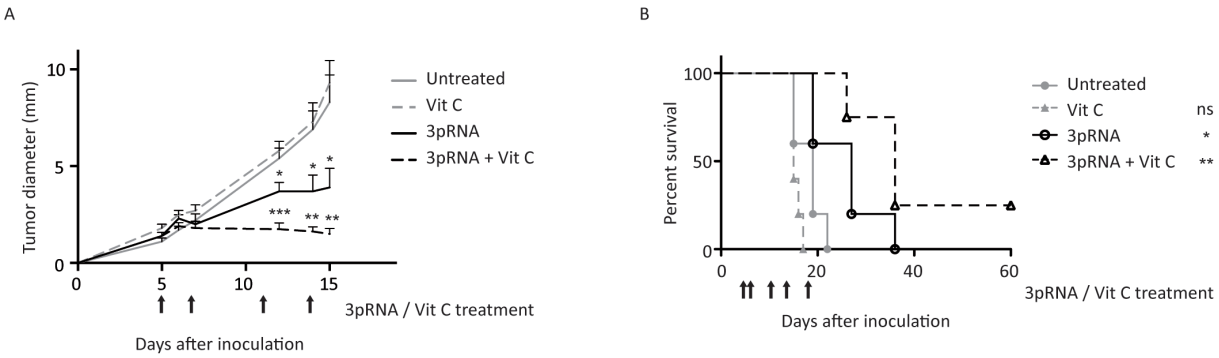

Figure 33: Improved 3pRNA-mediated inhibition of tumor growth by vitamin C supplementation. (A-B) Established subcutaneous tumors were treated with vitamin C (i.p.) and 3pRNA (i.t.) at the indicated time points. (A) Tumor growth as measured daily. Mean and +/-SEM of five mice per group are shown. (B) Survival curves using five mice per group. Statistical analysis was performed using student's *t*-test. * ($p < 0.05$), ** ($p < 0.01$), *** ($p < 0.001$). ns: not significant, Vit C: vitamin C

All in all, the here presented results establish that functional 3pRNA-triggered RIG-I signaling outcome is not substantially affected by hypoxia. This was demonstrated by unchanged ISG, MHC class-I and PDL-1 expression as well as functional T- and NK cell activation, although the cytokine expression of melanoma cells was modulated. Thus, 3pRNA-induced RIG-I signaling seems to resist the hypoxia-mediated attenuation of RLR protein upregulation and IFNα desensitization. Thereby 3pRNA is superior to IFNα regarding anti-tumor therapy of hypoxic melanoma cells. The results further suggest vitamin C is a suitable adjuvant to 3pRNA therapy as it allows restoration of RIG-I expression in hypoxic cells *in vitro* and boosts cytokine release and anti-tumor immunity *in vivo*.

6 Discussion

To ensure efficient and successful development of novel anti-cancer therapeutics it is fundamental to study the influence of tumor microenvironmental factors like hypoxia on drug function. This premise also holds true for the translation of RIG-I-activating 3pRNA compounds into the clinics, which have so far achieved encouraging pre-clinical results in immunotherapy of malignant melanoma, among other tumors. The present study therefore investigated the impact of oxygen deprivation on the RIG-I response in melanoma cells, finding RIG-I protein upregulation to be reduced under hypoxia. Intriguingly, major regulatory components of the RIG-I signaling pathway were not affected, just as the overall signaling outcome, comprising the induction of apoptosis, expression of ISGs, MHC class-I and PDL-1 as well as the activation of melanocyte antigen-specific CD8+ T-cells and NK cells. In contrast, recombinant IFNα lost its capacity to induce immune activation upon oxygen deprivation. Assuming that 3pRNA therapy could still benefit from reestablishment of RIG-I levels under hypoxia, ROS scavenging via vitamin C was discovered to reinstate protein expression *in vitro* and enhance intratumoral cytokine production and anti-tumor efficacy *in vivo*. These results shed light on the function of RIG-I under oxygen conditions likely encountered in many solid tumors, reasoning that 3pRNA-mediated immunotherapy is superior to IFNα treatment and offering additional combinatorial strategies to further improve anti-tumor reactivity.

6.1 Dissecting IFNα desensitization and differential RIG-I mRNA and protein levels

Since 1995 recombinant IFNα is an approved therapy for melanoma and other types of cancer. Therefore it was quite surprising to find that IFNα lost its potential to induce mRNA expression of the cytokine CXCL10 and different ISGs as well as to trigger upregulation of MHC class-I and PDL-1 under hypoxia, indicative for loss of its anti-tumor activity. Yet, these results can be explained by reduction of IFNαR expression on hypoxic melanoma cells, limiting initiation of the Jak/STAT signaling cascade. This is in line with previously described hypoxia-induced IFNαR1 downregulation in a PERK (PRKP-like endoplasmic reticulum kinase)- and eIF2α (eukaryotic translation initiation factor 2 alpha)-dependent manner, which resulted in reduced cancer cell sensitivity to IFNα and prevention of apoptosis [105]. Even much earlier Naldini *et al.* had also observed an inhibition of the anti-proliferative effect of interferons under hypoxia [116]. Of note, this observation was restricted to tumor cell lines showing increased proliferation upon reduction of oxygen tension. On the other hand the same group found hypoxia to enhance the antiviral activity of IFNα and IFNγ [117]. Importantly, the latter study was performed with those cells that did not lose their sensitivity to IFN in the proliferation study. These

findings indicate that the effect of hypoxia on the function of IFNα largely depends on the investigated cell lines as their differentiation, proliferation and metabolic behavior are differently influenced by oxygen deprivation. Altogether hypoxia-mediated desensitization to IFNα might explain the group of non-responders among patients receiving IFNα therapy. As part of future personalized cancer treatment it might thus be worthwhile to assess the hypoxic status of individual tumors and deduce their IFNα sensitivity.

In contrast to IFNα, the 3pRNA-induced mRNA expression and overall RIG-I signaling outcome was not suppressed upon oxygen deprivation. How is this possible taking into account that RIG-I protein amounts were significantly reduced and that proper RIG-I signaling function relies on an intact IFN-mediated feed-forward loop [30]? Firstly, remaining RIG-I and IFNαR expression levels might still be high enough to enable the establishment of a complete response to 3pRNA transfection. Secondly, the function of signaling molecules downstream of the IFNαR, for example of the transcriptional activators STAT1, STAT2 or STAT5, might be enhanced and thus compensate for reduced receptor expression. While studies on STAT1 reported hypoxia-mediated repression of transcription on the one hand and enhanced activation through phosphorylation on the other hand, STAT5 is consistently found to be activated upon oxygen deprivation in different cell types [118–120]. These two hypotheses would further include the assumption that IFN, which is produced as a secondary signaling molecule upon RIG-I activation (and that is actually increased under hypoxia), holds a stronger potential to initiate transcription of ISGs than recombinant IFN, that is added to cell culture medium and functions as the first and only signal. Alternatively and more simple, this might also be a matter of IFNα concentrations produced upon RIG-I activation versus direct treatment. Lastly, mRNA expression of the investigated targets might not exclusively rely on IFN signaling, but could also be induced directly by RIG-I-dependent IRF3/IRF7 and NFκB activation. Transcription of CXCL10 for example can be elicited by both transcription factors and a NFκB binding site is predicted for the RIG-I promoter [121,122]. This hypothesis is further supported by an observation of Ellermeier *et al.* who found functional 3pRNA-stimulated RIG-I signaling, including CXCL10 and MHC class-I upregulation, in a pancreatic cancer cell line that lacked IFNβ production due to a deletion in the respective gene [68].

Interestingly, hypoxia has been found to decrease expression of another PRR, namely TLR4, in endothelial cells in a ROS dependent manner [123]. This process relied on attenuation of the transcriptional activity of activator protein 1 (AP-1) and a respective binding site is predicted to exist also in the RIG-I promoter. Still, it is unlikely that a similar mechanism prevents RIG-I expression in hypoxic melanoma cells, since 3pRNA-induced RIG-I mRNA upregulation was unaffected by oxygen deprivation. In contrast, RIG-I and CXCL10 expression was solely reduced on the protein level. Such

differences can be either caused by posttranscriptional mechanisms, translational regulation or protein turnover. While the latter could be largely ruled out, as inhibition of protein degradation by proteasome-blockade did not reinstate hypoxic RIG-I levels to normoxic amounts, changes in translational regulation definitely play an important role during cellular adaptation to hypoxic microenvironments. Although translation can be regulated within every step of the translation process, that is initiation, elongation and termination, hypoxia generally causes a switch from cap-dependent to cap-independent translation [124]. As a result, a global reduction of translational activity is induced [125], whereas protein synthesis of certain mRNA transcripts is enhanced. This can be mediated for example by inhibitory upstream open reading frames, that are translated under normoxic, but ignored under hypoxic conditions, depending on eIF2α phosphorylation [126]. Furthermore, internal ribosomal entry sites, like within the 5'-untranslated region of VEGF mRNA, enable cap-independent initiation of translation upon oxygen deprivation [127]. Such modulation of translational activity might well be involved in the observed differential expression of RIG-I and CXCL10 mRNA and protein amounts. It is additionally tempting to speculate on a role for microRNAs (miRNA) in this process, as these short, endogenous, non-coding RNAs mediate degradation or translational suppression of their specific target mRNAs. Not very surprisingly, hypoxia possesses a very specific miRNA signature, with some of the transcripts being directly induced by HIF1α [128]. Among these hypoxia-regulated miRNAs miR-210 is the only one consistently upregulated in both healthy and cancerous hypoxic cells and thus is considered a master regulator of the hypoxic response [129]. Interestingly, miR-210 has been found to inhibit the LPS-induced production of proinflammatory cytokines by targeting NFκB1 in murine macrophages [130]. This links hypoxia-dependent miRNA upregulation with reduced expression of inflammatory proteins following PRR activation. Although degradation of RIG-I and CXCL10 mRNA was not enhanced in hypoxic, 3pRNA-transfected cells in this study, a miRNA-mediated inhibition of translation is conceivable and deserves further investigation.

Translational regulation, including the switch from cap-dependent to cap-independent protein synthesis, likewise plays an important role in the process of EMT, which is characterized by a shift of the protein expression profile from a proliferative, epithelial-like to a motile, mesenchymal-like state [131]. Hence, inhibition of RIG-I upregulation might be a direct consequence of hypoxia itself or result from hypoxia-induced EMT. A relation between RIG-I and the differentiation status of cells is not very farfetched, since RIG-I was originally identified as being induced in retinoic acid-mediated cell differentiation [15]. Moreover, within this thesis prevention of EMT through the treatment of cells with NFκB inhibitors allowed partial reestablishment of 3pRNA-triggered RIG-I expression under hypoxia. Together, this argues for an involvement of EMT in the attenuation of RIG-I translation and

suggests a consecutive process of hypoxia, EMT and 3pRNA-dependent RIG-I expression in murine melanoma cells.

6.2 Differential regulation of RIG-I and MDA5 under hypoxia

Even though 3pRNA-induced RIG-I protein upregulation was reduced under hypoxia as compared to normoxic conditions, protein levels were still increased above basal expression. In contrast, MDA5 expression, activated by its ligand poly-I:C or the induction of IFN-signaling by 3pRNA or recombinant IFNα, was not enhanced above basal levels upon oxygen deprivation. Consequently, RIG-I function not only seems superior to IFNα treatment but also provides advantages over MDA5 targeting in hypoxic tumor cells. The remaining question is how these closely related RIG-I like receptors, that employ identical signaling cascades and share a characteristic domain structure, can be differentially affected by oxygen deprivation. If attenuation of RIG-I as well as MDA5 protein upregulation relies on EMT-related modulation of translation, this observation might be explained by individual regulation of RIG-I- and MDA5 translation. This would consequently raise the question why such functionally similar proteins are regulated differentially. It might thus well be, that additional or alternative mechanisms are involved.

Initiation of downstream signaling involves the assembly of MDA5 into ATP-sensitive filaments using dsRNA as a scaffold. Thereby, several CARDs are brought into close proximity and subsequently stack with MAVS CARDs, which allows signalosome formation [132]. RIG-I can similarly form filaments upon activation, albeit these are shorter and less stable than those of MDA5 [133,134]. Alternatively, K63-polyubiquitin chains promote RIG-I tetramerization, leading to the assembly of MAVS into its active polymeric form [39]. Although polyubiquitin may also play a role in MDA5-signaling, its physiological role is less well understood and MDA5 is considered to have a higher propensity to form filaments than RIG-I [38,135]. Increased availability of K63-polyubiquitin under hypoxic conditions could thus favor RIG-I-mediated signaling, leaving MDA5 without any benefit. Yet, although recently peroxide was found to induce the accumulation of K63-polyubiquitin and the here applied hypoxia regimen enhanced the production of ROS in melanoma cells, differences in K63-polyubiquitination of whole cell lysates could not be observed between normoxic and hypoxic conditions [136].

Another potential mechanism that would allow sophisticated regulation of RIG-I and MDA5 signaling involves the third RLR family member LGP2, which is capable of binding dsRNA, but lacks any CARDs, therefore being unable to signal via MAVS. Instead, LGP2 represses RIG-I signaling potentially by competing for its ligand and on the contrary enhances MDA5 signaling via an as yet unknown mechanism [137,138]. Hypoxia-induced loss of LGP2 expression or function could hence free RIG-I from its inhibitory ties and at the same time withdraw a stimulating co-factor from MDA5

signaling. This hypothesis deserves closer investigation in the future and should help understanding the individual regulation of two closely related signaling pathways.

6.3 Cytokine expression patterns and cellular differentiation

Investigating the influence of oxygen deprivation on 3pRNA-induced cytokines revealed an increase of type-I IFN and TNFα, whereas CXCL10 was decreased and IL-6 remained stable. The fact that certain molecules are up- and others are downregulated argues for a distinct hypoxia-mediated modulation of cytokine expression, rather than a mere change of 3pRNA dose-sensitivity, which would equally reduce all 3pRNA-induced factors. Hypothetically, the enhanced type-I IFN production might at least in part compensate for loss of IFNαR expression in hypoxic cells and thereby contribute to the preservation of 3pRNA-induced signaling outcome in contrast to direct IFNα treatment (see above).

3pRNA-induced expression of selected cytokines, namely CXCL10 and IL-6, exhibited variable sensitivity towards oxygen deprivation in different cell lines. Additionally, attenuation of RIG-I protein upregulation was restricted to malignant melanoma cells and did not occur in the melanocyte cell line Melan-A and keratinocyte cell line Kera-308. It is not surprising that cell lines react differently to environmental stress factors depending on their tissue of origin and variations in their differentiation status. For example, Melan-A is a cell line of non-tumorigenic pigmented melanocytes that require a tumor promoter for growth [139]. Together with Kera-308, which were generated from DMBA (7,12-Dimethylbenzo(a)anthracen)-initiated mouse skin and resemble normal epidermal basal cells, Melan-A rank among the differentiated cells of the investigated panel [140]. HCmel17 and HCmel23 that derive from the HGF-Cdk4^{R24C} model of spontaneous autochthonous melanoma [110] are characterized by their chemoresistance and ability to metastasize and represent the most dedifferentiated cells (unpublished data, T. Tüting). The obtained results suggest a stepwise modification of the 3pRNA-induced RIG-I and cytokine pattern from unaffected RIG-I and reduced CXCL10 and IL-6 expression in differentiated cell lines to attenuated RIG-I and CXCL10 and unaffected IL-6 expression in dedifferentiated cells, when comparing hypoxic to normoxic incubation. HCmel3 cells, which have an intermediate differentiation status, exhibited diminished RIG-I upregulation alike dedifferentiated cells, but cytokine expression resembled differentiated cells. Together these observations strengthen evidence for a relation of EMT and RIG-I protein expression.

Like the other non-malignant cell lines (Melan-A, Kera 308) primary murine splenocytes induced RIG-I protein levels equally well under both oxygen conditions. The finding that attenuation of RIG-I upregulation was restricted to malignant cell lines raises the question of how cancer cells might benefit from a reduction of their RIG-I translation under hypoxia. Protein translation is a major

ATP-consumer [141], hence limiting RIG-I upregulation in hypoxic cancer cells might save much-needed energy, while maintaining sufficient anti-viral immunity with residual RIG-I expression. Yet, tumor cell growth is not necessarily limited by its energy demands, as the ATP amount required for proliferation may not exceed that for cellular maintenance [142]. Alternatively, one might envision the existence of an evolutionary pressure that favors survival of those tumor cells, which do not increase their RIG-I expression upon 3pRNA detection under hypoxia. This hypothesis is based on the assumption that very low cytosolic concentrations of RIG-I ligands might not be able to elicit a fully functional RIG-I response under hypoxia, other than the here investigated 3pRNA amounts. Genetic instability, a well-established trait of cancer cells describing elevated levels of mutations, chromosomal aberrations and epigenetic alterations, can be fostered by oxygen deprivation and might lead to accumulation of misplaced or aberrant nucleic acids [143,144]. Thus, in hypoxic cancer cells endogenous RIG-I ligands may be generated, driving immunity and apoptosis, although eukaryotic mRNA normally does not activate the receptor due to its 5'-cap structure and 2'-O-methylation of the terminal nucleotide [23]. Therefore, those cancer cells within the heterogeneous tumor cell population that are inert to unmodified self-RNAs by being unable to upregulate RIG-I may have a growth advantage and are evolutionary selected.

In summary, malignant melanoma cells attenuate 3pRNA-induced RIG-I protein expression upon oxygen deprivation in relation to EMT. This possibly provides cancer cells with survival-advantages in a hypoxic environment such as energy-savings or resistance to enhanced immune activation by self-RNA.

6.4 Mechanisms of sustained 3pRNA-dependent immune cell activation

The functional activation of immune effector cells by melanoma cells during hypoxia is fundamental to establish 3pRNA-mediated therapy against hypoxic solid tumors. Therefore, a very important finding of this study is the unaltered activation of CD8+ T- and NK cells in response to hypoxic, 3pRNA-treated B16F10 and HCmel3 melanoma cells. At the same time this observation is quite surprising, taking into account the hypoxia-induced loss of melanocyte differentiation antigen expression and a number of previous studies that rather point towards hypoxia-mediated tumor immune escape.

Since T-cell receptors of Pmel-1 CD8+ T-cells are genetically manipulated to recognize the $gp100_{25\text{-}33}$ antigen [145], a strong reduction in gp100 expression, as observed for hypoxic B16F10 and HCmel3 cells, would argue for diminished receptor – antigen interaction and less T-cell activation. Yet, attenuation of the protein's expression does not instantly have to result in reduced antigen presentation, for the respective processing machinery might still be saturated with gp100 peptides. Moreover, a genome-wide mRNA expression analysis in human umbilical vein endothelial cells

showed upregulation of the antigen processing and presentation pathway upon cobalt chloride-induced hypoxia [146]. Such mechanism could allow for more efficient processing and MHC loading of residual gp100 antigen stably present in the melanosome pigment granules. Additionally, hypoxia has been shown to augment the capacity of DCs and macrophages to present antigen, for example by likewise enhanced expression of the antigen processing machinery or via upregulation of co-stimulatory molecules [147–149]. Utilizing an *in vivo* model Calzascia *et al.* reported that TNFα and its respective receptors are required for effective T-cell priming, proliferation and optimal cytokine production in a situation where other immunostimulatory components are limited, like within the tumor microenvironment [150]. Since 3pRNA-induced TNFα expression was enhanced in hypoxic B16F10 cells, this cytokine could be additionally responsible for sustained T-cell activation in co-culture experiments.

Importantly, several studies have found impaired cancer cell susceptibility to NK cell and CTL-mediated lysis under hypoxia. One of the underlying mechanisms is the hypoxia-induced, HIF1α-dependent upregulation of PDL-1 leading to increased apoptosis of CTLs [103]. In contrast to this latter report, PDL-1 expression on the here-investigated B16F10 cells was not intensified under hypoxia and could thus not reduce numbers of activated CD8+ T-cells. Secondly, concomitant phosphorylation of STAT3 and stabilization of HIF1α as well as the hypoxia-inducible miR-210 have been ascribed a role in the impairment of cancer cell susceptibility to CTL-mediated lysis [151,152]. Yet, these studies did not observe an alteration of CTL reactivity, which is in concordance with the here presented results. Similarly, hypoxic tumor cells can escape NK cell-mediated killing through autophagic degradation of NK cell-derived cytotoxic granzyme B, a mechanism that does not argue against functional initial activation of NK cells [101]. On the other hand, autophagy has been shown to enhance the presentation of endogenous viral antigens via an alternative MHC class-I loading pathway [153,154]. Taking into account that hypoxia can induce autophagy in a HIF-dependent and -independent manner, this mechanism possibly contributes to sustained T-cell activation by melanoma cells with reduced gp100 expression by elevating their autophagy of melanosome pigment granules stably containing structural gp100 proteins [155]. To conclude, as tumor cells have different options to escape immune cell-mediated killing without directly acting on the effector cells themselves, it is feasible that 3pRNA-treated melanoma cells are destroyed less efficiently under hypoxia although activation of CD8+ T- and NK cells is not reduced.

Co-culture experiments with melanoma cells and splenocytes also revealed superior function of 3pRNA to IFNα therapy even under normoxic conditions. This is because high doses of recombinant IFNα only marginally induced immune cell activation in contrast to 3pRNA transfection, although both treatments significantly enhanced MHC class-I expression. Of note, standard IFNα therapy is administered systemically, also acting directly on immune cells, which was not the case in

the present experimental setup. Still, in terms of intratumoral application, the anti-tumor immune response initiated by RIG-I targeting can be considered more versatile than by direct IFNα treatment, including activation of CD8+ T- and NK cells.

6.5 Modulation of regulatory components in hypoxic RIG-I signaling

Although attenuation of 3pRNA-induced RIG-I protein expression under hypoxia could be largely attributed to posttranscriptional or translational effects, the investigation of regulatory components of the RIG-I signaling pathway revealed some interesting hypoxia-related changes.

Firstly, inhibition of the proteasome led to a reduction of 3pRNA-triggered RIG-I expression particularly in hypoxic cells. This argues against increased RIG-I protein degradation under hypoxia being responsible for diminished protein upregulation as discussed above. Instead, proteasomal degradation of some other factor seems to be necessary to maintain residual RIG-I expression, leaving the question for the identity of this molecule. Since LGP2 can repress RIG-I signaling potentially by competing for its ligand, maintained LGP2 degradation might be required for 3pRNA-induced RIG-I protein expression [137]. Also, according to findings of Castanier and colleagues proteasomal cleavage of MAVS is necessary to liberate the assembled signaling complex into the cytosol, which then allows IRF3 phosphorylation [156]. Additionally, functional protein degradation is essential for the release of NFκB from its inhibitory partner IκB and its subsequent nuclear translocation. Consequently, clearance of the competitive receptor LGP2, direct RIG-I induction by putative NFκB binding sites as well as IFN-dependent feed-forward signaling is hampered upon proteasome-blockade. Under hypoxia this could add to translational repression by EMT and be responsible for absent RIG-I protein upregulation.

Secondly, the expression of the peroxisomal marker protein PMP70 was found to be decreased in hypoxic melanoma cells, indicating reduced peroxisome abundance. This is in concordance with previous results showing hypoxia-mediated induction of autophagy and HIF2α-dependent pexophagy (autophagy of peroxisomes), aiming at a reduction of those highly oxygen consuming organelles [113,157]. Intriguingly, although hypoxia likewise induces mitophagy (autophagy of mitochondria) and both organelles are platforms for MAVS signalosome formation, the overall amount of MAVS was not significantly altered upon oxygen deprivation [158]. Of note, the performed western blot analysis indicated total MAVS protein amounts in whole cell lysates without providing information of its intracellular localization. Thus, it cannot be excluded that the adaptor protein is retained within autophagosomes not being accessible for RIG-I binding under hypoxia. Still, as the reduction of PMP70 expression was moderate and RIG-I signaling remained functional, it is more likely that the extent of pexophagy and mitophagy remained low upon oxygen deprivation so that sufficient signaling platforms could be provided. Moreover, autophagic sequestration of MAVS could

be compensated for by enhanced MAVS mRNA expression, for example induced by NOX2-derived ROS as shown by Soucy-faulkner *et al.* [114].

Lastly, when expression of the RIG-I signaling component and mitochondrial import receptor subunit TOM70 was investigated, an additional protein of reduced size appeared to be detected by the TOM70 specific antibody exclusively in hypoxic cells. To date, no splice variants of TOM70 are known that might be activated upon oxygen deprivation and could account for the respective western blot band. Furthermore, TOM70 assembles with at least six other proteins to make up the TOM complex, which functions in the import of mitochondrial precursor proteins. Yet, all of these related proteins are smaller than the observed 55 kDa (TOM5, TOM6, TOM7, TOM20, TOM22, TOM40) and even though some of them can be posttranslationally modified, their effective position after electrophoretic separation is below 55 kDa [159]. Therefore, either a so far unknown splice variant of TOM70 is expressed under hypoxia or the utilized antibody cross-reacts with an unrelated protein that is specifically induced upon oxygen deprivation. Since the nature and function of such a potential splice variant is highly interesting, this finding longs for more detailed investigation.

In summary, these observations indicate that many metabolic mechanisms influenced by hypoxia overlap with the RIG-I signaling pathway and presumably do not leave immune signaling unaffected. While autophagy and proteasomal function can influence the RIG-I response as discussed above, also the unfolded-protein response (UPR), that is primarily activated upon ER stress, is involved in innate immune activation via RIG-I as recently shown by Cho and colleagues [160]. In this process the UPR constituent inositol-requiring-1α (IREα) binds bacterial cholera toxin in the ER lumen and thereupon degrades endogenous mRNAs that subsequently function as RIG-I ligands in the cytosol. Alike autophagy, the UPR can be induced by hypoxia [161]. Lastly, also ROS can have different effects on RIG-I signaling, which is explicitly discussed below.

6.6 The two-sided role of ROS

Assuming that hypoxia-induced RIG-I attenuation related to EMT, it was hypothesized that prevention of EMT by ROS scavenging could reinstate RIG-I levels and further enhance RIG-I signaling in hypoxic tumor cells. This strategy is supported by studies reporting the involvement of ROS in hypoxic stabilization of HIF1α and the induction of EMT via HIF1α and TGFβ following H_2O_2 treatment [162–164]. Additionally, Shimojo *et al.* have successfully deployed ROS scavengers to suppress hypoxia-induced EMT in pancreatic cancer cells [94]. Moreover, ROS scavenging could prevent HIF1α- and HIF2α-induced mitophagy and pexophagy, thereby allowing longer interaction of RIG-I with MAVS, augmenting its upregulation and function.

On the contrary, ROS have been assigned important stimulatory functions for RLR signaling by being critical for MAVS expression and efficient IRF3 activation as well as by enhancing IFN

production and resistance to viral infection [42,114]. That is why in parallel, a project evolved around the targeted inhibition of the antioxidant transcription factor Nrf2 in combination with RIG-I stimulation using a bi-functional 3p-siRNA. Intriguingly, both approaches were successful: ROS scavenging reinstated RIG-I levels under hypoxia on the one hand and ROS increase by Nrf2 silencing enhanced 3pRNA-triggered cytokine production and apoptosis under normoxia on the other hand. This raises the question how inhibition of ROS or their amplification can both positively affect RIG-I signaling.

For a long time ROS were solely known as destructive by-products that confer damage to DNA, lipids and proteins. Yet, at the end of the last century, it became more and more appreciated that ROS additionally function as distinct signaling molecules. For example, ROS are involved in the activation of the NLRP3 (NACHT, LRR and PYD domains-containing protein 3) inflammasome leading to the secretion of proinflammatory IL-1β and IL-18 [165]. Furthermore, they function as second messengers in signal transduction from activated cytokine receptors to effector proteins, like in TNFα- and IL-1-induced activation of c-Jun NH2-terminal kinase (JNK) [166]. In hypoxic human umbilical vein endothelial cells ROS have been found to regulate the secretion of IL-6 and thereby influence endothelial permeability [167]. The multitude of ROS-mediated signaling events is further illustrated by a number of different transcription factors that can be activated by ROS, including HIF1α, NFκB and AP-1 [168,169]. The different types of ROS, mainly superoxide anion ($O_2^{\cdot-}$), hydrogen peroxide (H_2O_2) and the hydroxyl radical ($OH^{\cdot}$), can be generated enzymatically or non-enzymatically at different intracellular locations. Thus, hypoxia-induced ROS are produced at mitochondria, whereas the antioxidant targets of Nrf2 regulate ROS made at mitochondria as well as in the cytosol [170,171]. Taking all these observations into account, it is likely that under normoxic conditions a specific ROS composition generated by Nrf2 knockdown favors enhanced RIG-I signaling, while under hypoxia a different ROS composition induces EMT and concomitant RIG-I attenuation. Within the hypoxia setting investigated here, it was hence reasonable to pursue the strategy of ROS scavenging *in vivo*.

Vitamin C is a commonly known antioxidant that has the potential to detoxify ROS by donation of one or two electrons [172]. Since vitamin C is also safe and would be readily applicable for clinical usage, it was here considered to be the most suitable ROS scavenger in a model of transplantable B16 melanoma. Intriguingly, the additional application of vitamin C improved 3pRNA function *in vivo,* as indicated by enhanced CXCL10 cytokine production, ameliorated tumor growth-inhibition and prolonged animal survival, although intratumoral RIG-I expression was not increased as compared to 3pRNA alone. Whereas, vitamin C efficiently restored diminished RIG-I upregulation in hypoxic cells *in vitro*. Consideration of technical limitations can provide a clue for this observation. Increased CXCL10 production was demonstrated by immunohistochemistry of fixed tumor slices, thus providing spatial information, showing areas of low as well as very high cytokine abundance. In contrast, RIG-I

expression was determined by western blot analysis of whole tumor lysates, containing hypoxic and normoxic regions, and thus reflects the average intratumoral RIG-I expression. Immunohistochemical staining of RIG-I can provide the yet missing information whether regions of increased CXCL10 production also exhibit enhanced RIG-I expression.

In case RIG-I expression remains to be unaffected by supportive vitamin C treatment upon elimination of these technical limitations, vitamin C might actually function differently as expected from the *in vitro* situation. Cellular vitamin C uptake is mediated by two transmembrane transporter systems: Sodium vitamin C co-transporters (SVCTs) import reduced vitamin C that is able to donate electrons and thus eliminate ROS intracellularly [173]. Glucose transporters (mainly GLUT1) take up the oxidized form of vitamin C, which is then converted into the reduced state in a process that depletes the antioxidant protein glutathione [174]. This in turn causes the accumulation of ROS, ultimately leading to inhibition of glycolysis, ATP-depletion and death of KRAS- and BRAF-mutated cancer cells, as recently demonstrated by Yun *et al*. [175]. Accordingly, it is conceivable that such ROS increase is responsible for enhanced RLR signaling as discussed above. Yet, the effects shown by Yun *et al.* were restricted to KRAS- and BRAF-mutated cancer cells due to their increased GLUT1 expression and oncogene-induced dependency on glycolysis, whereas B16F10 cells do not possess these mutations [176]. Together with the remark that plasma levels of oxidized vitamin C are very low, as measured in healthy human beings, this argues against a similar ROS increase upon vitamin C application in the here investigated mouse model [177].

The use of vitamin C in combination with immunotherapy would add a new chapter to the long-standing history of vitamin C in anti-cancer therapy, which started in the mid 1970s when double Nobel Prize laureate Linus Pauling first claimed anti-cancer efficacy of high-dose vitamin C [178,179]. Together with Ewan Cameron he showed that supplemental vitamin C therapy in addition to routine treatment significantly prolonged survival of patients with terminal cancer, as 22% of patients receiving vitamin C were still alive one year after date of untreatability in contrast to 0.4% of the control group. While these promising studies failed to be reproduced by two clinical trials in the beginning, these discrepancies could now be ascribed to the different application routes of vitamin C (intravenous vs. oral) resulting in different plasma levels [180,181]. Moreover, recent publications elucidating the mechanisms of anti-tumorigenic effects have reactivated interest in vitamin C as anti-cancer agent, in particular against KRAS- and BRAF-mutated tumors, which could be effectively treated in the applied mouse model of colorectal cancer [175]. Mechanistically vitamin C induces inhibition of glycolysis resulting in ATP depletion and tumor cell death [175,182]. Interestingly, a key role of vitamin C treatment could also be attributed to a diminished expression and activation of HIF1 [183,184]. Therefore, a combinatorial therapy of RIG-I ligand and vitamin C might not only benefit from an enhanced immunostimulatory microenvironment, but also from the inhibition of metabolic

changes. An additional advantage is the established safety profile of vitamin C, which makes it readily applicable for 3pRNA combination therapy. In conclusion, the ROS scavenging activity of vitamin C presumably mediated its positive effects on 3pRNA-mediated RIG-I upregulation *in vitro* and anti-tumor function *in vivo,* rendering vitamin C a promising adjuvant for RIG-I-targeted cancer immunotherapy.

6.7 3pRNA-triggered modulation of tumor differentiation, MDSC and NK cells *in vivo*

To unravel the mechanism of vitamin C-boosted, 3pRNA-mediated anti-tumor immunity in the transplantable melanoma model in more detail, tumor cell differentiation and alterations of immune cell populations were thoroughly investigated. In concordance with *in vitro* findings the mRNA expression of melanocytic differentiation antigens within tumors was hardly affected by vitamin C treatment, but interestingly was increased upon 3pRNA stimulation, again suggesting a relationship between RIG-I and differentiation. This work thus provides evidence for hypoxia-induced EMT being accompanied by reduced 3pRNA-triggered RIG-I upregulation as well as a direct role for RIG-I-activation in stimulation of differentiation antigen expression in melanoma cells. Studies performed on acute promyelocytic leukemia cells indeed established a function of RIG-I in all-trans retinoic acid-induced cellular differentiation already before its anti-viral properties were uncovered [15]. One underlying mechanism was recently described by Li and colleagues who showed that RIG-I prevents the activation of AKT (RAC-alpha serine/threonine protein kinase) - mTOR (mammalian target of rapamycin) signaling, which otherwise inhibits differentiation [185]. This process at least partly involved activation of autophagy, which is likewise regulated by mTOR. Enhanced autophagic degradation of melanosomes, containing melanoma differentiation antigens, might provide a stimulus for short-term increase of differentiation antigen transcription to maintain sufficient expression levels. Yet, the effect of RIG-I activation on autophagy still is a matter of debate, due to contradictory observations. While Tormo *et al.* found that the RLR family member MDA5 induces autophagy upon stimulation with poly-I:C, RIG-I activation has been shown to block autophagic degradation of mitochondria by Meng and colleagues [186,187]. Furthermore, autophagy proteins ATG5-ATG12 complexes associate with RIG-I, thereby inhibiting its antiviral activity [188]. This association might then again also prevent the autophagy-promoting function of ATG5-ATG12. In summary, involvement of RIG-I in cellular differentiation is supported by several studies, however the underlying mechanism and the role of autophagy remains unclear. Furthermore, the rather small changes in differentiation antigen mRNA expression induced by 3pRNA treatment possibly do not translate into an overall profoundly differentiated tumor phenotype *in vivo*.

The ultimate goal of immunotherapy is the activation of immune effector cells against malignant cells in primary tumors and metastases. Therefore, modulations of immune cell behavior, initiated by 3pRNA alone or in combination with vitamin C, in the transplantable melanoma model deserve close examination and discussion. As indicated by increased Gr-1 mRNA expression and enhanced tumor infiltration of CD11b+ Gr-1+ cells, intratumoral application of 3pRNA caused an accumulation of MDSC, which could not be prevented by vitamin C supplementation. These results contradict previous findings of Ellermeier *et al.* who found reduced frequencies of MDSC upon RIG-I activation by a bi-functional 3p-siRNA [68]. Notably, in this report a large part of MDSC loss was attributable to the siRNA function and a pure 3pRNA control was missing. Interestingly, Zoglmeier and colleagues observed an expansion of CD11b+ Gr-1+ cells following TLR9 stimulation with CpG, but at the same time the immunosuppressive potential of these MDSC was reduced owing to their IFNα-dependent maturation [69]. Thus, a similar mechanism very probably is induced by 3pRNA-triggered IFN production. It is likely that tumor type and 3pRNA dosage can easily tip the balance towards MDSC support or inhibition, taking into account that 3pRNA-induced cytokines can do both, suppress MDSC (via IFN) or stimulate MDSC (via IL-6) [115,189]. In this regard it is noteworthy that hypoxia enhanced 3pRNA-induced IFN production in cell culture, but IL-6 was not influenced by oxygen deprivation, arguing for a cytokine milieu that favors suppression of MDSC function in hypoxic, 3pRNA-treated tumors. To ensure MDSC do not annihilate the immune stimulatory effects achieved by RIG-I activation, 3pRNA therapy can be combined with antibody-mediated blockade of IL-6 or CD40 agonists, the latter of which is involved in the induction of apoptosis in MDSC [190,191]. For example, Scarlett and colleagues already established anti-tumor immunity in an ovarian cancer model using CD40 agonist in combination with TLR3 stimulation [192].

Addressing the question for the major immune cell players in RIG-I-induced tumor eradication, this study found 3pRNA therapy to enhance the percentage of activated NK cells within tumor-draining lymph nodes, whereas no significant effects on CD8+ T-cell activation could be observed. This is in line with findings of Poeck *et al.* demonstrating NK cell dependent anti-tumor activity of RIG-I ligands in a B16 melanoma lung metastasis model [67]. In contrast, another report showed that therapeutic effects against pancreatic cancer completely relied on CD8+ T-cells without any involvement of NK cells [68]. The activation of CD8+ T-cells and NK cells both requires the expression of specific 'kill me' signals by their target cells. These include tumor antigens presented on MHC class-I to activate CD8+ T-cells, whereas NK cells typically react to cells missing MHC molecules, however can also respond to expressed ligands for activating receptors like the NKG2D receptor. The availability of such signals varies between tumor types and can be influenced by 3pRNA treatment. B16 melanoma cells are characterized by lacking NKG2D ligands and a very low MHC class-I expression, making them poorly immunogenic to CD8+ T-cells but prone to NK cell

attack [193,194]. Since it has been shown that NK cells can reject tumors even in the presence of MHC class-I when these tumor cells express the activating ligand retinoic acid early-inducible protein 1 (RAE-1), it is likely that RIG-I activation within B16 cells increases NK cell ligand expression to an extent that outrivals MHC class-I induction [195]. Taken together, the type of malignancy likely plays a decisive role in shaping the 3pRNA-elicited anti-tumor immune response by providing different 'kill me' signals.

Other than expected from the study of Poeck and colleagues, an increase in tumor NK cell infiltration was not observed in the context of 3pRNA treatment in the here-applied model of subcutaneous B16 melanoma [67]. This might hint at technical limitations of the performed FACS analysis. Possibly, NK cells irregularly infiltrated tumors upon 3pRNA application, but this spatial information was lost after single cell suspensions were generated from whole tumors and stained for NK cell markers amongst others. If this is not the case, the inhibition of tumor outgrowth and prolonged survival in this model must result from the direct tumoricidal function of 3pRNA. Of note, in this thesis *in vivo* experiments were conducted by intratumoral application of *in vitro*-generated 3pRNA, in contrast to Poeck *et al.* who utilized a bi-functional 3p-siRNA.BCL2 construct via intravenous injection. Together with diverse tumor locations (local disease vs. metastases) these technical variations can contribute to differences in tumor NK cell infiltration. Interestingly, supplementation of 3pRNA therapy with vitamin C enhanced NK cell numbers within the tumor, although it did not have an effect on their 3pRNA-mediated activation in the draining lymph nodes. This observation might relate to the anti-angiogenic function of vitamin C. On the one hand it prevents VEGF expression in B16 melanoma cells via the inhibition of p42/44 MAPK and downregulation of cyclooxygenase-2 [196]. On the other hand vitamin C suppresses HIF1α, which is the major transcription factor for VEGF mRNA expression [183,184]. Thus, similar to low-dose anti-VEGF receptor 2 antibody therapy that normalizes tumor vasculature resulting in a more homogeneous distribution of functional tumor vessels, vitamin C treatment might improve tumor NK cell infiltration by VEGF downregulation [197].

In summary, the combination of 3pRNA with vitamin C exerted its improved anti-tumoral function against subcutaneous B16 melanoma through the tumoricidal activity of the RIG-I ligand and possibly also vitamin C, 3pRNA-mediated NK cell activation and facilitated tumor infiltration by vitamin C-dependent stabilization of tumor vasculature.

6.8 Evolving combinatorial treatment strategies

Hypoxia has long been known to induce resistance to chemo- and irradiation therapy of cancer and accumulating data points towards the existence of multiple hypoxia-dependent immune escape mechanisms of tumor cells [101–104,198]. To counteract these detrimental effects, two different strategies

can be pursued. Firstly, tumor oxygenation can be improved before or during treatment to overcome hypoxia-related restrictions. This can be achieved for example by breathing 100% oxygen under increased atmospheric pressure, a method called *hyperbaric oxygen therapy*, which can improve the response to radiation and chemotherapy of many solid tumors [199]. Recently Hatfield *et al.* demonstrated that respiratory hyperoxia (breathing 60% oxygen) significantly improves tumor regression by reversing immunosuppression in the tumor microenvironment [200]. Mechanistically, increased oxygen pressure prevents the hypoxia-dependent accumulation of extracellular adenosine that activates A2A adenosine receptors, causing the establishment of an immunosuppressive milieu. Alternatively, restoring healthy vasculature within the tumor using inositol trispyrophosphate or low-dose anti-VEGF receptor 2 antibody, enhances the activity of chemotherapeutic drugs and cancer vaccines by improving drug delivery and reducing the expression of multi-drug efflux pumps or reprogramming the immunosuppressive tumor microenvironment, respectively [197,201]. The latter thereby involves a reduction of MDSC, polarization of tumor infiltrating macrophages from an immunosuppressive M2 to an immunostimulatory M1 phenotype and facilitated infiltration of immune effector cells.

The second approach to overcome hypoxia-induced resistance rather exploits the low oxygen tension in hypoxic tissues for selectively targeting tumor cells, leaving healthy cells unaffected. For instance by utilizing pro-drugs that only become activated within the reducing microenvironment of hypoxic tumors. Exemplarily, TH-302, a pro-drug that releases the cytotoxic DNA alkylator bromo-isophosphoramide nitrogen mustard upon activation, significantly improved progression-free survival and tumor responses in a phase II clinical trial in combination with the cytostatic compound gemcitabine against metastatic pancreatic cancer [202]. Another DNA alkylating pro-drug, apaziquone, is tested in several ongoing phase III trials to prevent recurrence of non-muscle invasive bladder cancer following tumor resection (NCT01410565, NCT01469221, NCT02563561). Moreover, also gene therapy can harness tumor hypoxia by inserting HIF binding sites into the promoter of expression plasmids, thereby restricting target gene expression to HIF-enriched areas. Fukui *et al*. for example deployed an IFNα2b gene construct with repetitive HIF binding sites in renal cancer cells, showing enhanced expression upon application of a hypoxia-mimicking agent and resulting in suppressed cell viability [203]. Although no negative influence of hypoxia on 3pRNA treatment was detected in this study, combinatorial strategies might still improve RIG-I-targeted immunotherapy. Such can involve the simultaneous administration of hypoxia-activated pro-drugs, which enhance the release of tumor antigens and immune stimulating danger signals through their cytotoxic function. Alternatively, a combination with respiratory hyperoxia could free hypoxic tumor cells from the immunosuppressive microenvironment of extracellular adenosine and thus enhance 3pRNA-mediated immune activation.

Considering the observation that 3pRNA transfection elicited a strong upregulation of PDL-1 on melanoma cells, that was maintained under hypoxic conditions, a simultaneous blockade of the respective immune checkpoint might release the brakes from the immune system, allowing even more efficient and prolonged anti-tumor immunity. Since anti-PD1 antibodies nivolumab and pembrolizumab are already approved for melanoma treatment and several anti-PDL-1 compounds have completed phase I clinical trials with encouraging results, this approach offers a fast and easy-to-apply possibility to further improve the therapeutic potential of RIG-I ligands [204]. In summary, immune checkpoint-inhibition as well as vitamin C supplementation can be realized most rapidly for combined 3pRNA therapy and represent very promising strategies to gain highest benefit of future RIG-I-targeted immunotherapy for patients suffering from malignant melanoma.

6.9 Conclusion

A reduction in oxygen supply has repeatedly been shown to affect immune cell functions during inflammation as well as to enable tumor immune escape, thus indicating the (currently largely unmet) importance of taking into account the correct tissue-representative oxygen tension in *in vitro* experiments when investigating anti-tumor immunity. In this regard, this thesis studied the effect of hypoxia on the innate immune receptor RIG-I in murine melanoma cells, demonstrating inhibition of the 3pRNA-induced RIG-I protein upregulation upon oxygen deprivation. On the contrary, RIG-I mRNA expression was not affected. Furthermore, RIG-I signaling outcome remained uninvolved as MHC class-I and PDL-1 increase, induction of ISGs as well as CD8+ T-cell and NK cell activation in 3pRNA-treated melanoma cell co-cultures worked equally well under normoxia and hypoxia. Instead, IFNα lost its capacity to induce an immune response altogether. Thus, while hypoxia-dependent downregulation of IFNαR expression desensitized cells to treatment with recombinant IFNα, remaining RIG-I and IFNαR levels were sufficient to establish a complete and functional RIG-I response to 3pRNA stimulation. Still it remains possible that RIG-I signaling outcome becomes restricted at very low 3pRNA concentrations. Figure 34 summarizes different cellular processes that are influenced by hypoxia and can contribute to altered protein translation of RIG-I, including EMT, mTOR inhibition, miRNA expression and activation of the unfolded protein response. The involvement of ROS and NFκB-dependent EMT in RIG-I attenuation was demonstrated by reestablishment of RIG-I protein expression upon NFκB inhibition or antioxidant treatment *in vitro*. Moreover, vitamin C as ROS scavenger also enhanced intratumoral proinflammatory CXCL10 production and anti-tumor efficacy in a subcutaneous melanoma model *in vivo*.

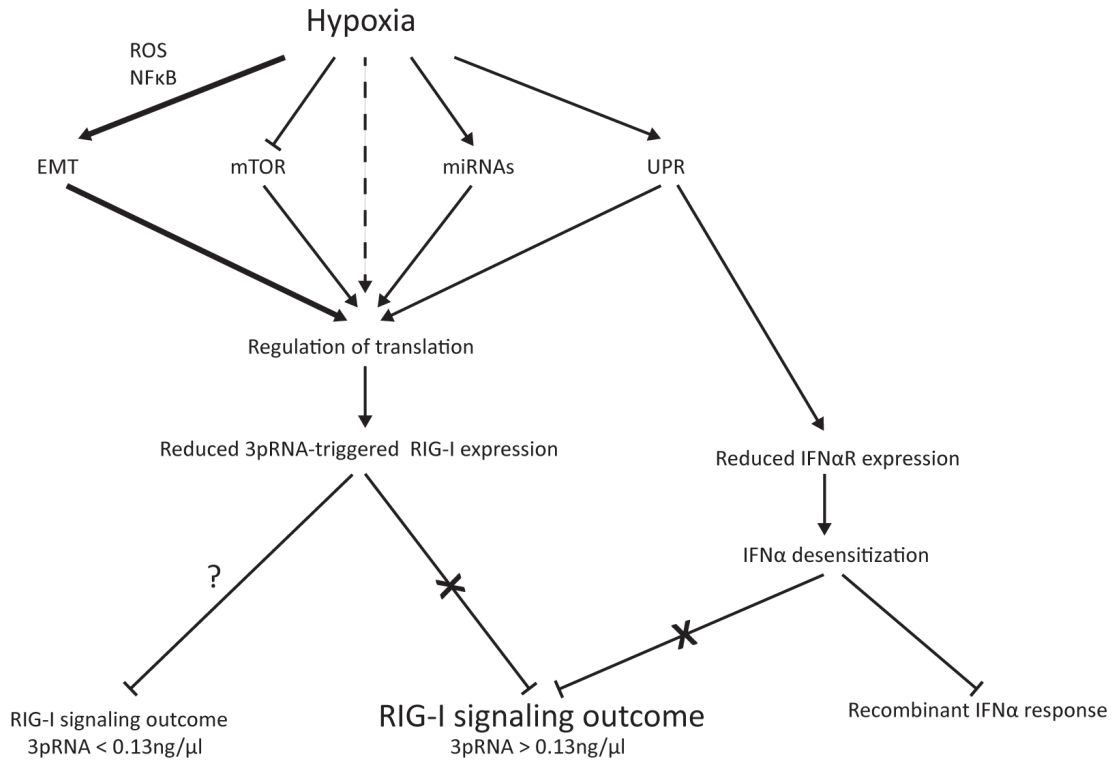

Figure 34: Cellular pathways that regulate translation under hypoxia and their influence on RIG-I signaling. Production of reactive oxygen species (ROS) and activation of NFκB are involved in hypoxia-induced epithelial-to-mesenchymal-transition (EMT) of cancer cells, which affects regulation of translation. Contribution of this process to attenuated 3pRNA-triggered RIG-I expression was shown by reestablishment of RIG-I upregulation upon NFκB inhibition and ROS scavenging. Besides, translation can be modulated by inhibition of mammalian target of rapamycin (mTOR) signaling, induced miRNA expression and activation of the unfolded protein response (UPR). While mTOR inhibition is also responsible for the induction of autophagy, the UPR results in reduced IFNαR expression. A dashed line indicates the existence of even more mechanisms that regulate translation under hypoxia. The here presented results show that reduced 3pRNA-tiggered RIG-I expression under hypoxia does not repress the RIG-I signaling outcome. Still it remains possible that the RIG-I response becomes restricted at very low 3pRNA concentrations. IFNα desensitization does likewise not affect RIG-I signaling outcome, but inhibits immune activation in response to recombinant IFNα.

Taken together, this thesis provides evidence for functional RIG-I activation in hypoxic tumor cells that resists attenuation of RIG-I protein expression and IFNα desensitization, rendering 3pRNA-mediated immunotherapy a very encouraging treatment also for tumors lacking sufficient oxygen supply. To become fully devoid of other hypoxia-induced inhibiting mechanisms on anti-tumor effector functions, it is advisable to combine 3pRNA treatment with additional immune activating therapies. These may include antibody-mediated depletion of MDSC, inhibition of the PD-1/PDL-1 immune checkpoint or blockade of the immunosuppressive pathway of extracellular adenosine. Yet, when excessively boosting the immune system, one has to be well aware of the risk to cause an overshooting immune response, which may cause severe adverse effects. Therefore, vitamin C might bring the advantage of indirectly enhancing RIG-I therapy by primarily acting on ROS. Altogether, these findings cover a fundamental part in the development of RIG-I ligands into successful immunotherapeutics to improve prognosis of melanoma patients.

7 References

1. Murphy, K. Janeway's Immunobiology. (*Garland Science*, 2012).
2. Topham, N. J. & Hewitt, E. W. Natural killer cell cytotoxicity: how do they pull the trigger? *Immunology* 128**,** 7–15 (2009).
3. Chaplin, D. D. Overview of the Immune Response. *J. Allergy Clin. Immunol.* 125**,** S3–23 (2010).
4. Medzhitov, R. Toll-like receptors and innate immunity. *Nat Rev Immunol* 1**,** 135–145 (2001).
5. Duewell, P. *et al.* RIG-I-like helicases induce immunogenic cell death of pancreatic cancer cells and sensitize tumors toward killing by CD8+ T cells. *Cell Death Differ* 21**,** 1825–1837 (2014).
6. Blank, C. *et al.* Blockade of PD-L1 (B7-H1) augments human tumor-specific T cell responses in vitro. *Int J Cancer* 119**,** 317–327 (2006).
7. McCoy, K. D. & Le Gros, G. The role of CTLA-4 in the regulation of T cell immune responses. *Immunol. Cell Biol.* 77**,** 1–10 (1999).
8. Youn, J.-I. & Gabrilovich, D. I. The biology of myeloid-derived suppressor cells: The blessing and the curse of morphological and functional heterogeneity. *European Journal of Immunology* 40**,** 2969–2975
9. Willment, J. A. & Brown, G. D. C-type lectin receptors in antifungal immunity. *Trends Microbiol.* 16**,** 27–32 (2008).
10. Kawai, T. & Akira, S. Toll-like receptors and their crosstalk with other innate receptors in infection and immunity. *Immunity* 34**,** 637–50 (2011).
11. Wu, J. *et al.* Cyclic GMP-AMP is an endogenous second messenger in innate immune signaling by cytosolic DNA. *Science* 339**,** 826–830 (2013).
12. Chen, G., Shaw, M. H., Kim, Y.-G. & Nunez, G. NOD-like receptors: role in innate immunity and inflammatory disease. *Annu. Rev. Pathol.* 4**,** 365–398 (2009).
13. Ng, C. S., Kato, H. & Fujita, T. Recognition of viruses in the cytoplasm by RLRs and other helicases--how conformational changes, mitochondrial dynamics and ubiquitination control innate immune responses. *Int Immunol* 24**,** 739–749 (2012).
14. Kato, H. *et al.* Length-dependent recognition of double-stranded ribonucleic acids by retinoic acid-inducible gene-I and melanoma differentiation-associated gene 5. *J. Exp. Med.* 205**,** 1601–1610 (2008).
15. Sun, Y.-W. RIG-I, a human homolog gene of RNA helicase, is induced by retinoic acid during the differentiation of acute promyelocytic leukemia cell. (*Shanghai second Medical University*, 1997).
16. Yoneyama, M. *et al.* The RNA helicase RIG-I has an essential function in double-stranded RNA-induced innate antiviral responses. *Nat. Immunol.* 5**,** 730–737 (2004).
17. Ablasser, A. *et al.* RIG-I-dependent sensing of poly(dA:dT) through the induction of an RNA polymerase III-transcribed RNA intermediate. *Nat Immunol* 10**,** 1065–1072 (2009).
18. Chiu, Y.-H., MacMillan, J. B. & Chen, Z. J. RNA Polymerase III Detects Cytosolic DNA and Induces Type I Interferons through the RIG-I Pathway. *Cell* 138**,** 576–591 (2015).
19. Pichlmair, A. *et al.* RIG-I-mediated antiviral responses to single-stranded RNA bearing 5'-phosphates. *Science (80-.).* 314**,** 997–1001 (2006).

20. Hornung, V. *et al.* 5'-Triphosphate RNA is the ligand for RIG-I. *Science* 314**,** 994–7 (2006).

21. Schlee, M. *et al.* Recognition of 5' Triphosphate by RIG-I Helicase Requires Short Blunt Double-Stranded RNA as Contained in Panhandle of Negative-Strand Virus. *Immunity* 31**,** 25–34 (2009).

22. Goubau, D. *et al.* Antiviral immunity via RIG-I-mediated recognition of RNA bearing 5[prime]-diphosphates. *Nature* 514**,** 372–375 (2014).

23. Devarkar, S. C. *et al.* Structural basis for m7G recognition and 2'-O-methyl discrimination in capped RNAs by the innate immune receptor RIG-I. *Proceedings of the National Academy of Sciences of the United States of America* 113**,** 596–601

24. Goldeck, M., Tuschl, T., Hartmann, G. & Ludwig, J. Efficient solid-phase synthesis of pppRNA by using product-specific labeling. *Angew. Chem. Int. Ed. Engl.* 53**,** 4694–4698 (2014).

25. Kowalinski, E. *et al.* Structural basis for the activation of innate immune pattern-recognition receptor RIG-I by viral RNA. *Cell* 147**,** 423–35 (2011).

26. Hou, F. *et al.* MAVS forms functional prion-like aggregates to activate and propagate antiviral innate immune response. *Cell* 146**,** 448–461 (2011).

27. Seth, R. B., Sun, L., Ea, C.-K. & Chen, Z. J. Identification and characterization of MAVS, a mitochondrial antiviral signaling protein that activates NF-kappaB and IRF 3. *Cell* 122**,** 669–682 (2005).

28. Dixit, E. *et al.* Peroxisomes Are Signaling Platforms for Antiviral Innate Immunity. *Cell* 141**,** 668–681 (2010).

29. Matsumiya, T. & Stafforini, D. M. Function and regulation of retinoic acid-inducible gene-I. *Crit Rev Immunol* 30**,** 489–513

30. Yoneyama, M. & Fujita, T. RNA recognition and signal transduction by RIG-I-like receptors. 54–65 (2009).

31. Nistal-Villan, E. *et al.* Negative role of RIG-I serine 8 phosphorylation in the regulation of interferon-beta production. *J Biol Chem* 285**,** 20252–20261

32. Sun, Z., Ren, H., Liu, Y., Teeling, J. L. & Gu, J. Phosphorylation of RIG-I by casein kinase II inhibits its antiviral response. *J. Virol.* 85**,** 1036–1047 (2011).

33. Kim, M.-J., Hwang, S.-Y., Imaizumi, T. & Yoo, J.-Y. Negative feedback regulation of RIG-I-mediated antiviral signaling by interferon-induced ISG15 conjugation. *J. Virol.* 82**,** 1474–1483 (2008).

34. Mi, Z., Fu, J., Xiong, Y. & Tang, H. SUMOylation of RIG-I positively regulates the type I interferon signaling. *Protein Cell* 1**,** 275–283

35. Arimoto, K. *et al.* Negative regulation of the RIG-I signaling by the ubiquitin ligase RNF125. *Proc. Natl. Acad. Sci. U. S. A.* 104**,** 7500–7505 (2007).

36. Gack, M. U. *et al.* TRIM25 RING-finger E3 ubiquitin ligase is essential for RIG-I-mediated antiviral activity. *Nature* 446**,** 916–920 England. .

37. Oshiumi, H., Matsumoto, M., Hatakeyama, S. & Seya, T. Riplet/RNF135, a RING finger protein, ubiquitinates RIG-I to promote interferon-beta induction during the early phase of viral infection. *J. Biol. Chem.* 284**,** 807–817 (2009).

38. Jiang, X. *et al.* Ubiquitin-induced oligomerization of the RNA sensors RIG-I and MDA5 activates antiviral innate immune response. *Immunity* 36**,** 959–973

39. Zeng, W. *et al.* Reconstitution of the RIG-I pathway reveals a signaling role of unanchored polyubiquitin chains in innate immunity. *Cell* 141**,** 315–330 (2010).

40. Matsumiya, T. *et al.* The levels of retinoic acid-inducible gene I are regulated by heat shock protein 90-alpha. *J Immunol* 182**,** 2717–2725 (2009).

41. Liu, X.-Y., Wei, B., Shi, H.-X., Shan, Y.-F. & Wang, C. Tom70 mediates activation of interferon regulatory factor 3 on mitochondria. *Cell Res.* 20**,** 994–1011 (2010).

42. Tal, M. C. *et al.* Absence of autophagy results in reactive oxygen species-dependent amplification of RLR signaling. *Proc Natl Acad Sci U S A* 106**,** 2770–2775 (2009).

43. Belardelli, F., Ferrantini, M., Proietti, E. & Kirkwood, J. M. Interferon-alpha in tumor immunity and immunotherapy. *Cytokine Growth Factor Rev.* 13**,** 119–134 (2002).

44. Bachmann, M. F. & Oxenius, A. Interleukin 2: from immunostimulation to immunoregulation and back again. *EMBO Reports* 8**,** 1142–1148

45. Alexandrescu, D. T. *et al.* Immunotherapy for melanoma: current status and perspectives. *J. Immunother.* 33**,** 570–90 (2010).

46. Gleason, M. K. *et al.* Bispecific and trispecific killer cell engagers directly activate human NK cells through CD16 signaling and induce cytotoxicity and cytokine production. *Molecular cancer therapeutics* 11**,** 2674–2684

47. Wu, J., Fu, J., Zhang, M. & Liu, D. Blinatumomab: a bispecific T cell engager (BiTE) antibody against CD19/CD3 for refractory acute lymphoid leukemia. *J. Hematol. Oncol.* 8**,** 104 (2015).

48. Hodi, F. S. *et al.* Improved survival with ipilimumab in patients with metastatic melanoma. *N Engl J Med* 363**,** 711–723

49. Topalian, S. L. *et al.* Survival, Durable Tumor Remission, and Long-Term Safety in Patients With Advanced Melanoma Receiving Nivolumab. *J. Clin. Oncol.* (2014). doi:10.1200/JCO.2013.53.0105

50. Garon, E. B. *et al.* Pembrolizumab for the treatment of non-small-cell lung cancer. *N. Engl. J. Med.* 372**,** 2018–2028 (2015).

51. Topalian, S. L. *et al.* Safety, Activity, and Immune Correlates of Anti–PD-1 Antibody in Cancer. *N. Engl. J. Med.* 366**,** 2443–2454 (2012).

52. Wolchok, J. D. *et al.* Nivolumab plus ipilimumab in advanced melanoma. *N Engl J Med* 369**,** 122–133

53. Welters, M. J. P. *et al.* Induction of tumor-specific CD4+ and CD8+ T-cell immunity in cervical cancer patients by a human papillomavirus type 16 E6 and E7 long peptides vaccine. *Clin. Cancer Res.* 14**,** 178–187 (2008).

54. Kenter, G. G. *et al.* Vaccination against HPV-16 oncoproteins for vulvar intraepithelial neoplasia. *N. Engl. J. Med.* 361**,** 1838–1847 (2009).

55. Gardner, T., Elzey, B. & Hahn, N. M. Sipuleucel-T (Provenge) autologous vaccine approved for treatment of men with asymptomatic or minimally symptomatic castrate-resistant metastatic prostate cancer. *Hum. Vaccin. Immunother.* 8**,** 534–539 (2012).

56. Aranda, F. *et al.* Trial Watch: Adoptive cell transfer for oncological indications. *Oncoimmunology* 4**,** e1046673 (2015).

57. Kochenderfer, J. N. *et al.* Chemotherapy-refractory diffuse large B-cell lymphoma and indolent B-cell malignancies can be effectively treated with autologous T cells expressing an anti-CD19 chimeric antigen receptor. *J. Clin. Oncol.* 33**,** 540–549 (2015).

58. Maude, S. L. *et al.* Chimeric antigen receptor T cells for sustained remissions in leukemia. *N. Engl. J. Med.* 371**,** 1507–1517 (2014).

59. Louis, C. U. *et al.* Antitumor activity and long-term fate of chimeric antigen receptor–positive

T cells in patients with neuroblastoma. *Blood* 118**,** 6050–6056 (2011).

60. Ahmed, N. *et al.* Human Epidermal Growth Factor Receptor 2 (HER2) -Specific Chimeric Antigen Receptor-Modified T Cells for the Immunotherapy of HER2-Positive Sarcoma. *J. Clin. Oncol.* 33**,** 1688–1696 (2015).

61. Gosu, V., Basith, S., Kwon, O.-P. & Choi, S. Therapeutic applications of nucleic acids and their analogues in Toll-like receptor signaling. *Molecules* 17**,** 13503–13529 (2012).

62. Adams, S. *et al.* Topical TLR7 agonist imiquimod can induce immune-mediated rejection of skin metastases in patients with breast cancer. *Clin. Cancer Res.* 18**,** 6748–6757 (2012).

63. Baumgaertner, P. *et al.* Vaccination-induced functional competence of circulating human tumor-specific CD8 T-cells. *Int. J. Cancer* 130**,** 2607–2617 (2012).

64. Tarhini, A. A. *et al.* Safety and immunogenicity of vaccination with MART-1 (26-35, 27L), gp100 (209-217, 210M), and tyrosinase (368-376, 370D) in adjuvant with PF-3512676 and GM-CSF in metastatic melanoma. *J. Immunother.* 35**,** 359–366 (2012).

65. Besch, R. *et al.* Proapoptotic signaling induced by RIG-I and MDA-5 results in type I interferon-independent apoptosis in human melanoma cells. *J Clin Invest* 119**,** 2399–2411 (2009).

66. Kubler, K. *et al.* Targeted activation of RNA helicase retinoic acid-inducible gene-I induces proimmunogenic apoptosis of human ovarian cancer cells. *Cancer Res* 70**,** 5293–5304 (2010).

67. Poeck, H. *et al.* 5'-Triphosphate-siRNA: turning gene silencing and Rig-I activation against melanoma. *Nat. Med.* 14**,** 1256–1263 (2008).

68. Ellermeier, J. *et al.* Therapeutic efficacy of bifunctional siRNA combining TGF-beta1 silencing with RIG-I activation in pancreatic cancer. *Cancer Res.* 73**,** 1709–1720 (2013).

69. Zoglmeier, C. *et al.* CpG blocks immunosuppression by myeloid-derived suppressor cells in tumor-bearing mice. *Clin. Cancer Res.* 17**,** 1765–1775 (2011).

70. Anz, D. *et al.* Suppression of Intratumoral CCL22 by Type I Interferon Inhibits Migration of Regulatory T Cells and Blocks Cancer Progression. *Cancer Res.* (2015). doi:10.1158/0008-5472.CAN-14-3499

71. Howlader, N. *et al.* SEER Cancer Statistics Review, 1975-2012. *National Cancer Institute*. Bethesda, MD. http://seer.cancer.gov/csr/1975_2012/, based on November 2014 SEER data submission, posted to the SEER web site April 2015.

72. American Cancer Society. Cancer Facts & Figures 2015. Atlanta: *American Cancer Society* (2015).

73. Davies, M. A. & Samuels, Y. Analysis of the genome to personalize therapy for melanoma. *Oncogene* 29**,** 5545–5555 (2010).

74. Chapman, P. B. *et al.* Improved survival with vemurafenib in melanoma with BRAF V600E mutation. *N. Engl. J. Med.* 364**,** 2507–2516 (2011).

75. Flaherty, K. T. *et al.* Improved survival with MEK inhibition in BRAF-mutated melanoma. *N. Engl. J. Med.* 367**,** 107–114 (2012).

76. Hauschild, A. *et al.* Dabrafenib in BRAF-mutated metastatic melanoma: a multicentre, open-label, phase 3 randomised controlled trial. *Lancet (London, England)* 380**,** 358–365 (2012).

77. Schadendorf, D. *et al.* Pooled Analysis of Long-Term Survival Data From Phase II and Phase III Trials of Ipilimumab in Unresectable or Metastatic Melanoma. *J. Clin. Oncol.* 33**,** 1889–1894 (2015).

78. Postow, M. A., Callahan, M. K. & Wolchok, J. D. Immune Checkpoint Blockade in Cancer Therapy. *Journal of clinical oncology : official journal of the American Society of Clinical*

Oncology doi:10.1200/JCO.2014.59.4358

79. Tchekmedyian, N. *et al.* Propelling Immunotherapy Combinations Into the Clinic. *Oncology (Williston Park).* 29**,** (2015).

80. Hockel, M. & Vaupel, P. Tumor hypoxia: definitions and current clinical, biologic, and molecular aspects. *J Natl Cancer Inst* 93**,** 266–276 (2001).

81. Carreau, A., El Hafny-Rahbi, B., Matejuk, A., Grillon, C. & Kieda, C. Why is the partial oxygen pressure of human tissues a crucial parameter? Small molecules and hypoxia. *J. Cell. Mol. Med.* 15**,** 1239–53 (2011).

82. Lartigau, E. *et al.* Intratumoral oxygen tension in metastatic melanoma. *Melanoma Res* 7**,** 400–406 (1997).

83. Vaupel, P., Kallinowski, F. & Okunieff, P. Blood flow, oxygen and nutrient supply, and metabolic microenvironment of human tumors: a review. *Cancer Res* 49**,** 6449–6465 (1989).

84. Koong, A. C., Chen, E. Y. & Giaccia, A. J. Hypoxia causes the activation of nuclear factor kappa B through the phosphorylation of I kappa B alpha on tyrosine residues. *Cancer Res.* 54**,** 1425–1430 (1994).

85. Semenza, G. L. & Wang, G. L. A nuclear factor induced by hypoxia via de novo protein synthesis binds to the human erythropoietin gene enhancer at a site required for transcriptional activation. *Mol. Cell. Biol.* 12**,** 5447–54 (1992).

86. Byrne, A. M., Bouchier-Hayes, D. J. & Harmey, J. H. Angiogenic and cell survival functions of vascular endothelial growth factor (VEGF). *J. Cell. Mol. Med.* 9**,** 777–794 (2005).

87. Gray, L. H., Conger, A. D., Ebert, M., Hornsey, S. & Scott, O. C. The concentration of oxygen dissolved in tissues at the time of irradiation as a factor in radiotherapy. *Br J Radiol* 26**,** 638–648 (1953).

88. Hall, E. J. H. Radiobiology for the radiologist. (*Harper & Row*, 1978).

89. Brahimi-Horn, C. & Pouyssegur, J. The role of the hypoxia-inducible factor in tumor metabolism growth and invasion. *Bull Cancer* 93**,** E73–80 (2006).

90. Kondo, A. *et al.* Hypoxia-induced enrichment and mutagenesis of cells that have lost DNA mismatch repair. *Cancer Res.* 61**,** 7603–7607 (2001).

91. Mitrus, I. *et al.* Properties of B16-F10 murine melanoma cells subjected to metabolic stress conditions. *Acta Biochim Pol* 59**,** 363–366 (2012).

92. Kalluri, R. & Weinberg, R. a. Review series The basics of epithelial-mesenchymal transition. *J. Clin. Invest.* 119**,** 1420–1428 (2009).

93. Schäfer, M. & Werner, S. Cancer as an overhealing wound: an old hypothesis revisited. *Nat. Rev. Mol. Cell Biol.* 9**,** 628–638 (2008).

94. Shimojo, Y. *et al.* Attenuation of reactive oxygen species by antioxidants suppresses hypoxia-induced epithelial-mesenchymal transition and metastasis of pancreatic cancer cells. *Clin Exp Metastasis* 30**,** 143–154 (2013).

95. Cheng, Z. X. *et al.* Nuclear factor-kappaB-dependent epithelial to mesenchymal transition induced by HIF-1alpha activation in pancreatic cancer cells under hypoxic conditions. *PLoS One* 6**,** e23752 (2011).

96. Holzel, M., Bovier, A. & Tuting, T. Plasticity of tumour and immune cells: a source of heterogeneity and a cause for therapy resistance? *Nat Rev Cancer* 13**,** 365–376 (2013).

97. Landsberg, J. *et al.* Melanomas resist T-cell therapy through inflammation-induced reversible dedifferentiation. *Nature* 490**,** 412–416 (2012).

98. Shehade, H., Acolty, V., Moser, M. & Oldenhove, G. Cutting Edge: Hypoxia-Inducible Factor 1 Negatively Regulates Th1 Function. *J. Immunol.* 195**,** 1372–1376 (2015).

99. Gaber, T. & Tran, C. Pathophysiological hypoxia affects the redox state and IL-2 signalling of human CD4+ T cells and concomitantly impairs survival and proliferation. *Eur. J. Immunol.* 43**,** 1588–97 (2013).

100. Mancino, A. *et al.* Divergent effects of hypoxia on dendritic cell functions. *Blood* 112**,** 3723–3734 (2008).

101. Baginska, J. *et al.* Granzyme B degradation by autophagy decreases tumor cell susceptibility to natural killer-mediated lysis under hypoxia. *Proc. Natl. Acad. Sci. U. S. A.* 110**,** 17450–5 (2013).

102. Noman, M. Z. *et al.* Blocking hypoxia-induced autophagy in tumors restores cytotoxic T-cell activity and promotes regression. *Cancer Res* 71**,** 5976–5986 (2011).

103. Barsoum, I. B., Smallwood, C. A., Siemens, D. R. & Graham, C. H. A mechanism of hypoxia-mediated escape from adaptive immunity in cancer cells. *Cancer Res* 74**,** 665–674 (2014).

104. Siemens, D. R. *et al.* Hypoxia increases tumor cell shedding of MHC class I chain-related molecule: role of nitric oxide. *Cancer Res* 68**,** 4746–4753 (2008).

105. Bhattacharya, S. *et al.* Anti-tumorigenic effects of Type 1 interferon are subdued by integrated stress responses. *Oncogene* 32**,** 4214–21 (2013).

106. Bradford, M. M. A rapid and sensitive method for the quantitation of microgram quantities of protein utilizing the principle of protein-dye binding. *Anal. Biochem.* 72**,** 248–254 (1976).

107. Vaupel, P. The role of hypoxia-induced factors in tumor progression. *Oncologist* 9**,** 10–17 (2004).

108. Kang, D.-C. *et al.* Expression analysis and genomic characterization of human melanoma differentiation associated gene-5, mda-5: a novel type I interferon-responsive apoptosis-inducing gene. *Oncogene* 23**,** 1789–1800 (2004).

109. Yoneyama, M. *et al.* Shared and unique functions of the DExD/H-box helicases RIG-I, MDA5, and LGP2 in antiviral innate immunity. *J. Immunol.* 175**,** 2851–2858 (2005).

110. Landsberg, J. *et al.* Autochthonous primary and metastatic melanomas in Hgf-Cdk4R24C mice evade T-cell-mediated immune surveillance. *Pigment Cell Melanoma Res.* 23**,** 649–660 (2010).

111. Freeman, G. J. Engagement of the PD-1 Immunoinhibitory Receptor by a Novel B7 Family Member Leads to Negative Regulation of Lymphocyte Activation. *J. Exp. Med.* 192**,** 1027–1034 (2000).

112. Baird, N. a, Turnbull, D. W. & Johnson, E. a. Induction of the heat shock pathway during hypoxia requires regulation of heat shock factor by hypoxia-inducible factor-1. *J. Biol. Chem.* 281**,** 38675–81 (2006).

113. Walter, K. M. *et al.* Hif-2α Promotes Degradation of Mammalian Peroxisomes by Selective Autophagy. *Cell Metab.* 20**,** 882–897 (2015).

114. Soucy-faulkner, A., Mukawera, E., Fink, K., Martel, A. & Jouan, L. Requirement of NOX2 and Reactive Oxygen Species for Efficient RIG-I-Mediated Antiviral Response through Regulation of MAVS Expression. 6**,** (2010).

115. van den Boorn, J. G. & Hartmann, G. Turning tumors into vaccines: co-opting the innate immune system. *Immunity* 39**,** 27–37 (2013).

116. Naldini, A., Carraro, F. & Bocci, V. Effects of hypoxia on the antiproliferative activity of human interferons. *J. Interferon Cytokine Res.* 15**,** 137–142 (1995).

117. Naldini, A., Carraro, F., Fleischmann, W. R. J. & Bocci, V. Hypoxia enhances the antiviral

activity of interferons. *J. Interferon Res.* 13**,** 127–132 (1993).

118. Joung, Y.-H. *et al.* Hypoxia activates signal transducers and activators of transcription 5 (STAT5) and increases its binding activity to the GAS element in mammary epithelial cells. *Exp. Mol. Med.* 35**,** 350–357 (2003).

119. Ivanov, S. V, Salnikow, K., Ivanova, A. V, Bai, L. & Lerman, M. I. Hypoxic repression of STAT1 and its downstream genes by a pVHL/HIF-1 target DEC1/STRA13. *Oncogene* 26**,** 802–812 (2007).

120. Lee, M. Y. *et al.* Phosphorylation and activation of STAT proteins by hypoxia in breast cancer cells. *Breast* 15**,** 187–195 (2006).

121. Brownell, J. *et al.* Direct, interferon-independent activation of the CXCL10 promoter by NF-kappaB and interferon regulatory factor 3 during hepatitis C virus infection. *J. Virol.* 88**,** 1582–1590 (2014).

122. Search result: NF-kappaB binding sites in DDX58 gene promoter. Available at: http://www.sabiosciences.com/chipqpcrsearch.php?species_id=1&factor=NF-kappaB&gene=DDX58&nfactor=n&ninfo=n&ngene=n&B2=Search. (Accessed: 13th April 2016)

123. Ishida, I. *et al.* Hypoxia Diminishes Toll-Like Receptor 4 Expression Through Reactive Oxygen Species Generated by Mitochondria in Endothelial Cells. *J. Immunol.* 169**,** 2069–2075 (2002).

124. Spriggs, K. A., Bushell, M. & Willis, A. E. Translational regulation of gene expression during conditions of cell stress. *Mol. Cell* 40**,** 228–37 (2010).

125. Thomas, J. D. & Johannes, G. J. Identification of mRNAs that continue to associate with polysomes during hypoxia. *RNA* 13**,** 1116–1131 (2007).

126. Vattem, K. M. & Wek, R. C. Reinitiation involving upstream ORFs regulates ATF4 mRNA translation in mammalian cells. *Proc. Natl. Acad. Sci. U. S. A.* 101**,** 11269–11274 (2004).

127. Huez, I. *et al.* Two independent internal ribosome entry sites are involved in translation initiation of vascular endothelial growth factor mRNA. *Mol. Cell. Biol.* 18**,** 6178–6190 (1998).

128. Kulshreshtha, R. *et al.* A MicroRNA Signature of Hypoxia . *Molecular and Cellular Biology* 27**,** 1859–1867

129. Noman, M. Z., Janji, B., Berchem, G. & Chouaib, S. miR-210 and hypoxic microvesicles: Two critical components of hypoxia involved in the regulation of killer cells function. *Cancer Lett.* (2015). doi:10.1016/j.canlet.2015.10.026

130. Qi, J. *et al.* microRNA-210 negatively regulates LPS-induced production of proinflammatory cytokines by targeting NF-kappaB1 in murine macrophages. *FEBS Lett.* 586**,** 1201–1207 (2012).

131. Evdokimova, V., Tognon, C. E. & Sorensen, P. H. B. On translational regulation and EMT. *Semin. Cancer Biol.* 22**,** 437–445 (2012).

132. Peisley, A. *et al.* Cooperative assembly and dynamic disassembly of MDA5 filaments for viral dsRNA recognition. *Proc. Natl. Acad. Sci. U. S. A.* 108**,** 21010–21015 (2011).

133. Patel, J. R. *et al.* ATPase-driven oligomerization of RIG-I on RNA allows optimal activation of type-I interferon. *EMBO Rep.* 14**,** 780–787 (2013).

134. Peisley, A., Wu, B., Yao, H., Walz, T. & Hur, S. RIG-I forms signaling-competent filaments in an ATP-dependent, ubiquitin-independent manner. *Mol. Cell* 51**,** 573–583 (2013).

135. Reikine, S., Nguyen, J. B. & Modis, Y. Pattern Recognition and Signaling Mechanisms of RIG-I and MDA5. *Front. Immunol.* 5**,** 342 (2014).

136. Silva, G. M., Finley, D. & Vogel, C. K63 polyubiquitination is a new modulator of the oxidative stress response. *Nat. Struct. Mol. Biol.* 22**,** 116–123 (2015).

137. Rothenfusser, S. *et al.* The RNA helicase Lgp2 inhibits TLR-independent sensing of viral replication by retinoic acid-inducible gene-I. *J. Immunol.* 175**,** 5260–5268 (2005).

138. Childs, K. S., Randall, R. E. & Goodbourn, S. LGP2 plays a critical role in sensitizing mda-5 to activation by double-stranded RNA. *PLoS One* 8**,** e64202 (2013).

139. Bennett, D. C., Cooper, P. J. & Hart, I. R. A line of non-tumorigenic mouse melanocytes, syngeneic with the B16 melanoma and requiring a tumour promoter for growth. *Int. J. Cancer* 39**,** 414–418 (1987).

140. Strickland, J. E. *et al.* Development of murine epidermal cell lines which contain an activated rasHa oncogene and form papillomas in skin grafts on athymic nude mouse hosts. *Cancer Res.* 48**,** 165–169 (1988).

141. Buttgereit, F. & Brand, M. D. A hierarchy of ATP-consuming processes in mammalian cells. *Biochem. J.* 312 (Pt 1**,** 163–167 (1995).

142. Locasale, J. W. & Cantley, L. C. Metabolic flux and the regulation of mammalian cell growth. *Cell Metab.* 14**,** 443–451 (2011).

143. Yuan, J., Narayanan, L., Rockwell, S. & Glazer, P. M. Diminished DNA repair and elevated mutagenesis in mammalian cells exposed to hypoxia and low pH. *Cancer Res.* 60**,** 4372–4376 (2000).

144. Reynolds, T. Y., Rockwell, S. & Glazer, P. M. Genetic instability induced by the tumor microenvironment. *Cancer Res.* 56**,** 5754–5757 (1996).

145. Overwijk, W. W. *et al.* Tumor regression and autoimmunity after reversal of a functionally tolerant state of self-reactive CD8+ T cells. *J Exp Med* 198**,** 569–580 (2003).

146. Hang, X. *et al.* Transcription and splicing regulation in human umbilical vein endothelial cells under hypoxic stress conditions by exon array. *BMC Genomics* 10**,** 1–14 (2009).

147. Acosta-Iborra, B. *et al.* Macrophage oxygen sensing modulates antigen presentation and phagocytic functions involving IFN-gamma production through the HIF-1 alpha transcription factor. *J. Immunol.* 182**,** 3155–3164 (2009).

148. Aiello, S. *et al.* Hypoxia directly enhances dendritic cell antigen presentation. in *Frontiers in Immunology Conference Abstract*

http://www.frontiersin.org/Journal/FullText.aspx?f=35&name=immunology&ART_DOI=10.3389/conf.fimmu.2013.02.00620, . doi:10.3389/conf.fimmu.2013.02.00620

149. Ricciardi, A. *et al.* Transcriptome of hypoxic immature dendritic cells: modulation of chemokine/receptor expression. *Mol. Cancer Res.* 6**,** 175–185 (2008).

150. Calzascia, T. *et al.* TNF-alpha is critical for antitumor but not antiviral T cell immunity in mice. *J. Clin. Invest.* 117**,** 3833–3845 (2007).

151. Noman, M. Z. *et al.* Hypoxia-inducible miR-210 regulates the susceptibility of tumor cells to lysis by cytotoxic T cells. *Cancer Res.* 72**,** 4629–4641 (2012).

152. Noman, M. Z. *et al.* The cooperative induction of hypoxia-inducible factor-1 alpha and STAT3 during hypoxia induced an impairment of tumor susceptibility to CTL-mediated cell lysis. *J. Immunol.* 182**,** 3510–3521 (2009).

153. Tey, S.-K. & Khanna, R. Autophagy mediates transporter associated with antigen processing-independent presentation of viral epitopes through MHC class I pathway. *Blood* 120**,** 994–1004 (2012).

154. English, L. *et al.* Autophagy enhances the presentation of endogenous viral antigens on MHC class I molecules during HSV-1 infection. *Nat. Immunol.* 10**,** 480–487 (2009).

155. Mazure, N. M. & Pouysségur, J. Hypoxia-induced autophagy: cell death or cell survival? *Curr. Opin. Cell Biol.* 22**,** 177–80 (2010).

156. Castanier, C. *et al.* MAVS ubiquitination by the E3 ligase TRIM25 and degradation by the proteasome is involved in type I interferon production after activation of the antiviral RIG-I-like receptors. *BMC Biol.* 10**,** 44 (2012).

157. Viry, E. *et al.* Autophagy: an adaptive metabolic response to stress shaping the antitumor immunity. *Biochem. Pharmacol.* 92**,** 31–42 (2014).

158. Schonenberger, M. J. & Kovacs, W. J. Hypoxia signaling pathways: modulators of oxygen-related organelles. *Front. cell Dev. Biol.* 3**,** 42 (2015).

159. Becker, T. *et al.* Biogenesis of the mitochondrial TOM complex: Mim1 promotes insertion and assembly of signal-anchored receptors. *J. Biol. Chem.* 283**,** 120–127 (2008).

160. Cho, J. A. *et al.* The unfolded protein response element IRE1alpha senses bacterial proteins invading the ER to activate RIG-I and innate immune signaling. *Cell Host Microbe* 13**,** 558–569

161. Wouters, B. G. & Koritzinsky, M. Hypoxia signalling through mTOR and the unfolded protein response in cancer. *Nat Rev Cancer* 8**,** 851–864 (2008).

162. Brunelle, J. K. *et al.* Oxygen sensing requires mitochondrial ROS but not oxidative phosphorylation. *Cell Metab.* 1**,** 409–14 (2005).

163. Guzy, R. D. *et al.* Mitochondrial complex III is required for hypoxia-induced ROS production and cellular oxygen sensing. *Cell Metab.* 1**,** 401–8 (2005).

164. Kim, M. C., Cui, F. J. & Kim, Y. Hydrogen peroxide promotes epithelial to mesenchymal transition and stemness in human malignant mesothelioma cells. *Asian Pac J Cancer Prev* 14**,** 3625–3630 (2013).

165. Zhou, R., Tardivel, A., Thorens, B., Choi, I. & Tschopp, J. Thioredoxin-interacting protein links oxidative stress to inflammasome activation. *Nat. Immunol.* 11**,** 136–140 (2010).

166. Lo, Y. Y., Wong, J. M. & Cruz, T. F. Reactive oxygen species mediate cytokine activation of c-Jun NH2-terminal kinases. *J. Biol. Chem.* 271**,** 15703–15707 (1996).

167. Ali, M. H. *et al.* Endothelial permeability and IL-6 production during hypoxia: role of ROS in signal transduction. *Am J Physiol* 277**,** L1057–65 (1999).

168. Nakajima, S. & Kitamura, M. Bidirectional regulation of NF-kappaB by reactive oxygen species: A role of unfolded protein response. *Free Radic Biol Med* 65C**,** 162–174

169. Puri, P. L. *et al.* Reactive oxygen intermediates mediate angiotensin II-induced c-Jun.c-Fos heterodimer DNA binding activity and proliferative hypertrophic responses in myogenic cells. *J. Biol. Chem.* 270**,** 22129–22134 (1995).

170. Chandel, N. S. *et al.* Mitochondrial reactive oxygen species trigger hypoxia-induced transcription. *Proc Natl Acad Sci U S A* 95**,** 11715–11720 (1998).

171. Kovac, S. *et al.* Nrf2 regulates ROS production by mitochondria and NADPH oxidase. *Biochim. Biophys. Acta* 1850**,** 794–801 (2015).

172. Du, J., Cullen, J. J. & Buettner, G. R. Ascorbic acid: chemistry, biology and the treatment of cancer. *Biochim. Biophys. Acta* 1826**,** 443–57 (2012).

173. Tsukaguchi, H. *et al.* A family of mammalian Na+-dependent L-ascorbic acid transporters. *Nature* 399**,** 70–75 (1999).

174. Vera, J. C., Rivas, C. I., Fischbarg, J. & Golde, D. W. Mammalian facilitative hexose transporters mediate the transport of dehydroascorbic acid. *Nature* 364**,** 79–82 (1993).

175. Yun, J. *et al.* Vitamin C selectively kills KRAS and BRAF mutant colorectal cancer cells by

targeting GAPDH. 1–10 (2015).

176. Castle, J. C. *et al.* Exploiting the mutanome for tumor vaccination. *Cancer Res.* 72**,** 1081–1091 (2012).

177. Dhariwal, K. R., Hartzell, W. O. & Levine, M. Ascorbic acid and dehydroascorbic acid measurements in human plasma and serum. *Am. J. Clin. Nutr.* 54**,** 712–716 (1991).

178. Cameron, E. & Pauling, L. Supplemental ascorbate in the supportive treatment of cancer: Prolongation of survival times in terminal human cancer. *Proc. Natl. Acad. Sci. U. S. A.* 73**,** 3685–3689 (1976).

179. Cameron, E. & Pauling, L. Supplemental ascorbate in the supportive treatment of cancer: reevaluation of prolongation of survival times in terminal human cancer. *Proc. Natl. Acad. Sci. U. S. A.* 75**,** 4538–4542 (1978).

180. Creagan, E. T. *et al.* Failure of high-dose vitamin C (ascorbic acid) therapy to benefit patients with advanced cancer. A controlled trial. *N. Engl. J. Med.* 301**,** 687–690 (1979).

181. Moertel, C. G. *et al.* High-dose vitamin C versus placebo in the treatment of patients with advanced cancer who have had no prior chemotherapy. A randomized double-blind comparison. *N. Engl. J. Med.* 312**,** 137–141 (1985).

182. Tian, W. *et al.* The Hypoxia-inducible factor renders cancer cells more sensitive to Vitamin C-induced toxicity. *J. Biol. Chem.* 289**,** 3339–3351 (2014).

183. Miles, S. L., Fischer, A. P., Joshi, S. J. & Niles, R. M. Ascorbic acid and ascorbate-2-phosphate decrease HIF activity and malignant properties of human melanoma cells. *BMC Cancer* 1–12 (2015). doi:10.1186/s12885-015-1878-5

184. Gao, P. *et al.* HIF-dependent antitumorigenic effect of antioxidants in vivo. *Cancer Cell* 12**,** 230–8 (2007).

185. Li, X.-Y. *et al.* RIG-I modulates Src-mediated AKT activation to restrain leukemic stemness. *Mol. Cell* 53**,** 407–19 (2014).

186. Tormo, D. *et al.* Targeted Activation of Innate Immunity for Therapeutic Induction of Autophagy and Apoptosis in Melanoma Cells. *Cancer Cell* 16**,** 103–114 (2009).

187. Meng, G. *et al.* Multifunctional antitumor molecule 5'-triphosphate siRNA combining glutaminase silencing and RIG-I activation. *Int. J. Cancer* 134**,** 1958–1971 (2014).

188. Jounai, N. *et al.* The Atg5 Atg12 conjugate associates with innate antiviral immune responses. *Proc. Natl. Acad. Sci. U. S. A.* 104**,** 14050–5 (2007).

189. Chen, M.-F. *et al.* IL-6-stimulated CD11b+ CD14+ HLA-DR- myeloid-derived suppressor cells, are associated with progression and poor prognosis in squamous cell carcinoma of the esophagus. *Oncotarget* 5**,** 8716–8728 (2014).

190. Shen, J., Chen, X., Wang, Z., Zhang, G. & Chen, W. Downregulation of CD40 expression contributes to the accumulation of myeloid-derived suppressor cells in gastric tumors. *Oncol. Lett.* 8**,** 775–780 (2014).

191. Weiss, J. M. *et al.* Regulatory T cells and myeloid-derived suppressor cells in the tumor microenvironment undergo Fas-dependent cell death during IL-2/alphaCD40 therapy. *J. Immunol.* 192**,** 5821–5829 (2014).

192. Scarlett, U. K. *et al.* In situ stimulation of CD40 and Toll-like receptor 3 transforms ovarian cancer-infiltrating dendritic cells from immunosuppressive to immunostimulatory cells. *Cancer Res.* 69**,** 7329–7337 (2009).

193. Seliger, B., Wollscheid, U., Momburg, F., Blankenstein, T. & Huber, C. Characterization of the major histocompatibility complex class I deficiencies in B16 melanoma cells. *Cancer Res.* 61**,**

1095–1099 (2001).

194. Nausch, N. & Cerwenka, A. NKG2D ligands in tumor immunity. *Oncogene* 27**,** 5944–5958 (2008).

195. Cerwenka, A., Baron, J. L. & Lanier, L. L. Ectopic expression of retinoic acid early inducible-1 gene (RAE-1) permits natural killer cell-mediated rejection of a MHC class I-bearing tumor in vivo. *Proc. Natl. Acad. Sci. U. S. A.* 98**,** 11521–11526 (2001).

196. Kim, H. N. *et al.* Vitamin C down-regulates VEGF production in B16F10 murine melanoma cells via the suppression of p42/44 MAPK activation. *J. Cell. Biochem.* 112**,** 894–901 (2011).

197. Huang, Y. *et al.* Vascular normalizing doses of antiangiogenic treatment reprogram the immunosuppressive tumor microenvironment and enhance immunotherapy. *Proc. Natl. Acad. Sci.* 109**,** 17561–17566 (2012).

198. Ohta, A. *et al.* A2A adenosine receptor protects tumors from antitumor T cells. *Proc. Natl. Acad. Sci.* 103**,** 13132–13137 (2006).

199. Al-Waili, N. S. *et al.* Hyperbaric oxygen and malignancies: a potential role in radiotherapy, chemotherapy, tumor surgery and phototherapy. *Med Sci Monit* 11**,** 279–289 (2005).

200. Hatfield, S. M. *et al.* Immunological mechanisms of the antitumor effects of supplemental oxygenation. *Sci. Transl. Med.* 7**,** 277ra30 (2015).

201. Kieda, C. *et al.* Stable tumor vessel normalization with pO2 increase and endothelial PTEN activation by inositol trispyrophosphate brings novel tumor treatment. *J. Mol. Med.* 91**,** 883–899 (2013).

202. Borad, M. J. *et al.* Randomized Phase II Trial of Gemcitabine Plus TH-302 Versus Gemcitabine in Patients With Advanced Pancreatic Cancer. *J. Clin. Oncol.* 33**,** 1–8 (2014).

203. Fukui, N. *et al.* Development of a novel interferon-alpha2b gene construct with a repetitive hypoxia-inducible factor binding site and its suppressive effects on human renal cell carcinoma cell lines in vitro. *Int. J. Clin. Oncol.* 19**,** 497–504 (2014).

204. Philips, G. K. & Atkins, M. Therapeutic uses of anti-PD-1 and anti-PD-L1 antibodies. *Int. Immunol.* 27**,** 39–46 (2015).

8 Appendix

8.1 Abbreviations

3pRNA	5’-triphosphate RNA
ACT	adoptive cell transfer
AKT	RAC-alpha serine/threonine protein kinase
AP-1	activator protein 1
APC	allophycocyanin
ATG	autophagy protein
ATP	adenosine triphosphate
BiKE	bispecific killer cell engager
BiTE	bispecific T cell engager
BPB	bromphenolblue
BRAF	serine/threonine-protein kinase B-raf
BSA	bovine serum albumin
CAR	chimeric antigen receptor
CARD	caspase activation and recruitment domain
CCL22	C-C motif chemokine 22
CD	cluster of differentiation
cDNA	complementary DNA
cGAS	cyclic GMP-AMP synthase
CLR	C-type lectin receptor
CpG	cytosine-guanine oligodeoxynucleotide
CTD	C-terminal domain
CTL	cytotoxic T-lymphocyte
CTLA-4	cytotoxic T-lymphocyte-associated protein 4
CTP	cytidine triphosphate
CXCL10	interferon-dependent lymphocyte-attracting chemokine 10
Cy	cyanines
DC	dentritic cell
DMEM	dulbecco’s modified eagle medium
DMSO	dimethylsulfoxide
DTT	dithiotreitol
EDTA	ethylenediaminetetraacetic acid
eIF2α	eukaryotic translation initiation factor 2 alpha
ELISA	enzyme-linked immunosorbent assay
EMT	epithelial-mesenchymal-transition
FACS	fluorescence-activated cell sorting
Fam	fluorescein amidite
FCS	fetal calve serum
FDA	U.S. food and drug administration
FITC	fluorescein isothiocyanate
GFP	green fluorescent protein
GLUT1	glucose transporter 1

GM-CSF	granulocyte macrophage colony-stimulating factor
Gr-1	glutathione reductase 1
GTP	guanosine triphosphate
H&E	hematoxylin and eosin
HER2	human epidermal growth factor receptor 2
HIF	hyopoxia inducible factor
HMGB1	high mobility group protein B1
HRP	horseradish peroxidase
HSP90	heat shock protein 90
i.p.	intraperitoneal
i.t.	intratumoral
i.v.	intravenous
IFIT1	interferon-induced protein with tetratricopeptide repeats 1
IFN	interferon
IFNαR	IFNα receptor
IHC	immunohistochemistry
IKK	IκB kinase
IL	interleukin
IRF	interferon-regulatory factor
ISG	IFN-stimulated gene
IVT4	*in vitro* transcript 4
IκB	inhibitor of NFκB
Jak	janus kinase
JNK	c-Jun NH2-terminal kinase
LGP2	laboratory of genetics and physiology 2
LPS	lipopolysaccharide
MACS	magnetic cell separation
MAPK	mitogen-activated protein kinase
MAVS	mitochondrial antiviral signaling protein
MBL	mannose-binding lectin
MDA5	melanoma differentiation associated factor 5
MDSC	myeloid-derived suppressor cells
MEK	MAPK kinase
MHC	major histocompatibility complex
MIC	MHC class-I chain-related molecule
miRNA	microRNA
mRNA	messenger RNA
mTOR	mammalian target of rapamycin
NEAA	non-essential amino acids
NEMO	NFκB essential modulator
NFκB	nuclear factor-κB
NK	natural killer
NLR	NOD-like receptor
NLRP3	NACHT, LRR and PYD domains-containing protein 3
NOD	nucleotide-binding domain
NOX2	NADPH oxidase 2
Nrf2	nuclear factor erythroid 2-related factor 2
ODN	oligodeoxynucleotide

PAMP	pathogen associated molecular pattern
PBS	phosphate-buffered saline
PD-1	programmed cell death protein 1
PDL-1	programmed cell death ligand 1
PE	phycoerythrin
PEI	polyethylenimine
PerCP	peridinin chlorophyll protein complex
PERK	PRKP-like endoplasmic rediculum kinase
PMA	phorbol 12-myristate 13-acetate
PMP70	peroxisomal membrane protein 70
pO_2	partial oxygen pressure
polyI:C	polyinosinic:polycytidylic acid
PRR	pattern recognition receptor
qPCR	quantitative polymerase chain reaction
RAE-1	retinoic acid early-inducible protein 1
RIG-I	retinoic acid-inducible gene I
RLR	RIG-I-like receptor
RNAi	RNA interference
RNF	ring-finger protein
ROS	reactive oxygen species
RPMI	roswell park memorial institute medium
RT	room temperature
SDS	sodiumdodecylsulfate
SEM	standard error of mean
SLP	synthetic long peptide
STAT	signal transducer activator of transcription
SUMO	small ubiquitin-like modifier-1
SVCT	sodium vitamin C co-transporter
TAA	tumor-associated antigen
TBK1	TANK-binding kinase 1
TBP	TATA-box binding protein
TBS	tris-buffered saline
TCR	T-cell receptor
TGFβ	transforming growth factor beta
TLR	Toll-like receptor
TNFα	tumor necrosis factor alpha
TOM	translocase of outer membrane
Treg	regulatory T-cells
TriKE	trispecific killer cell engager
TRIM	tripartite motif protein
TRP2	tyrosinase-related protein 2
Ub	ubiquitin
UTP	uridine triphosphate
VEGF	vascular endothelial growth factor

8.2 List of figures

Figure 1: Pattern recognition receptors and their cellular localizations. 6
Figure 2: The RIG-I signaling pathway. 8
Figure 3: Different cancer immunotherapy approaches. 10
Figure 4: Correlation of tumor growth and hypoxia. 16
Figure 5: Hypoxia in B16F10 cells. 36
Figure 6: Hypoxia induces epithelial-to-mesenchymal transition (EMT) via reactive oxygen species (ROS)-production and NFκB activation. 37
Figure 7: Reduced interferon α receptor (IFNαR) expression under hypoxia. 37
Figure 8: Hypoxia attenuates RIG-I protein upregulation. 38
Figure 9: RIG-I expression kinetics upon 3pRNA stimulation. 39
Figure 10: Attenuation of RIG-I upregulation is not aggravated by increased hypoxia. 39
Figure 11: Transfection efficiency is not affected by hypoxia. 40
Figure 12: Hypoxia differentially influences 3pRNA- or IFNα-induced RIG-I mRNA expression. 40
Figure 13: Hypoxia prevents MDA5 protein upregulation upon stimulation. 41
Figure 14: Hypoxia does not influence 3pRNA-induced apoptosis. 42
Figure 15: 3pRNA- and IFNα-induced interferon-stimulated gene (ISG) mRNA expression and -stability. 43
Figure 16: Hypoxia modulates the 3pRNA-induced cytokine pattern. 44
Figure 17: Hypoxia influences the 3pRNA-triggered RIG-I response in various melanoma cell lines. 45
Figure 18: Hypoxia-mediated effects on the 3pRNA-induced RIG-I response in non-malignant cells. 46
Figure 19: Hypoxia-mediated effects on the 3pRNA-induced RIG-I response in murine splenocytes. 46
Figure 20: Hypoxia abrogates IFNα- but not 3pRNA-induced MHC class-I and PDL-1 expression. 47
Figure 21: *In vitro* CD8+ T- and NK cell activation through 3pRNA-treated melanoma cells remains fully functional under hypoxia. 49
Figure 22: Hypoxia does not affect the capability of cytotoxic effector cells to become activated. 50
Figure 23: HSP90 expression is not affected by hypoxia. 51

Figure 24: Effects of hypoxia on K63-ubiquitin expression and RIG-I expression upon proteasome inhibition. 51
Figure 25: Influence of hypoxia on the protein expression of RIG-I signaling components. 52
Figure 26: Rescue of melanocyte differentiation antigen expression under hypoxia. 53
Figure 27: NFκB inhibition and vitamin C treatment partially restore 3pRNA-induced RIG-I upregulation under hypoxia. 54
Figure 28: Superior cytokine release and tumor cell toxicity of bi-functional 3p-siNrf2 over 3pRNA alone. 55
Figure 29: 3pRNA therapy enhances RIG-I expression in B16 tumors. 56
Figure 30: Vitamin C enhances 3pRNA-induced CXCL10 release in B16 tumors. 58
Figure 31: Differentiation antigen expression in vitamin C- and 3pRNA-treated B16 tumors. 58
Figure 32: Effects of vitamin C-supported 3pRNA therapy on immune cell subsets. 59
Figure 33: Improved 3pRNA-mediated inhibition of tumor growth by vitamin C supplementation. 60
Figure 34: Cellular pathways that regulate translation under hypoxia and their influence on RIG-I signaling. 77

8.3 List of tables

Table 1: Cultivation of cell lines. 26
Table 2: Cell numbers according to cell line and sizes of tissue culture test plates. 27
Table 3: Composition of transfection mixes using Lipofectamine2000. 27
Table 4: Composition of transfection mixes using Lipofectamine RNAiMAX. 27
Table 5: Dilutions of primary antibodies for western blot application. 32

9 Acknowledgments

I would like to express my sincere gratitude to Prof. Gunther Hartmann for giving me the opportunity to conduct this interesting and sophisticated project in such an excellent working environment. Additionally, I deeply acknowledge his supervision and review of my thesis.

I am also indebted to my supervisor Dr. Jasper van den Boorn whose guidance helped me throughout the entire time as PhD student. I cannot thank enough for his scientific advice, revision of this thesis, constant encouragement and unlimited optimism!

My sincere thanks goes to all members of the supervising committee, namely Prof. Sven Burgdorf, Prof. Waldemar Kolanus and Prof. Ute Nöthlings for spending some of their precious time and examining my thesis.

I wish to cordially thank Christian Hagen, Silke Lambing and Dorottya Horváth for performing some experiments within the framework of this thesis. Moreover, it is a pleasure to thank all other members of the AG van den Boorn, AG Schlee and AG Coch for always providing a helping hand, for scientific discussions as well as entertaining coffee breaks and for experimental advice as well as Tuesdays climbing sessions.

Furthermore, I am thankful to Dr. Daniela Wenzel who made this whole project possible by replying to my request and sharing the hypoxic incubator. In addition, I would like to thank her colleagues from the Institute of Physiology I for not getting tired of opening the entrance door for me and sharing their equipment.

Last but not least, I am grateful to my family, who supported me during ups and downs. I greatly appreciate their interest in my work and their constant encouragement. I wish to especially thank Christian for his support, his patience, his motivation and love.